TECHNISCHE UNIVERSITÄT WIEN
Vienna University of Technology

Energy Economics Group

Influence of zero-emission mobility on the residual load

DIPLOMARBEIT

Ausgeführt zum Zwecke der Erlangung des akademischen Grades eines
Diplom-Ingenieurs (Dipl.-Ing.)

unter der Leitung von

Assoc.-Prof. Dipl.-Ing. Dr. Johann Auer
Dipl-Ing. Christoph Loschan

eingereicht an der
Technischen Universität Wien
Fakultät für Elektrotechnik und Informationstechnik
Institut für Energiesysteme und Elektrische Antriebe

von

Deivis Shomo BSc.
[redacted]

Wien, im März 2023

Energy Economics Group
Gußhausstraße 27-29, A-1040 Wien

Acknowledgement

I would like to thank all the individuals who have contributed to the successful completion of my diploma thesis through their personal and professional support. Special gratitudes go to Assoc.-Prof. Dipl.-Ing. Dr. Johann Auer and Dipl.-Ing. Christoph Loschan for their exceptional guidance and patient supervision. Their expertise and dedicated support not only aided me in resolving technical issues, but also with important decisions during the execution of my thesis.

I would especially like to thank my parents and sister for their unwavering support and encouragement throughout my academic journey. With the completition of my Master's degree, I am proud to carry forward the long-standing tradition of numerous engineers in my family.

Abstract

The penetration of electric vehicles (EVs) and fuel cell electric vehicles (FCEVs) is expected to accelerate in the coming years due to increasingly stringent regulations on emissions from the transportation sector. EV charging and the generation of green hydrogen for FCEVs represent a flexible load, offering the potential to align charging or refueling processes with specific goals such as reducing peak loads. The lack of charging coordination can result in a substantial increase in peak load demands and a need for additional peak load capacity. This thesis investigated the impact of EV and FCEV on regional residual load from the perspective of a grid operator, using a mixed-integer linear optimization model (MILP) to minimize total energy procurement costs. The model considered various charging scenarios that meet local power demand while taking into account the main grid connection, photovoltaic generation and local battery storage. Two use cases have been examined, with each one having various charging optimisation scenarios based on the EV and FCEV penetration rate. To assess charging method impact, three approaches were examined: instantaneous or uncontrolled charging, cost-based smart charging, and smart charging with parallel charging constraints. Results indicated that instant charging incured the highest energy procurement costs while both smart charging methods yielded notable cost reduction. Nevertheless, exclusively prioritizing cost optimization led to extreme peak loads, that can be mitigated by adding several parallel charging constraints at a marginally increased charging cost. Notably, the charging power supply played a crucial role, as the additional tariff for DC charging contributed substantially to the overall costs. The combination of EVs and fuel cell electric trucks and buses proved to be the most cost-optimal solution, mainly due to the absence of DC charging tariffs for the hydrogen production as the electrolysers are connected in AC mode. Additionally, hydrogen production did not trigger a surge in peak loads, as the load demand was spread over the day and during periods of high PV generation. Continued advancements in modelling techniques could entail the incorporation of a greater range of specific driving profiles and vehicle-to-grid (V2G) functionalities. By incorporating a broader spectrum of driving patterns, the forecasting accuracy of mobility demand could be enhanced, and the modelling precision could be improved. Additionally, leveraging the V2G potential can bolster grid flexibility and mitigate grid stress. As a prospective strategy, the deployment of a dynamic power-based pricing scheme at DC fast charging stations and the rollout of an incentive program to align the EV charging load with the instantaneous grid demand could expedite the adoption of EVs.

Zusammenfassung

Die Durchdringung von Elektrofahrzeugen (EVs) und Brennstoffzellen-Elektrofahrzeugen (FCEVs) wird sich in den kommenden Jahren aufgrund immer strengerer Emissionsvorschriften für den Verkehrssektor voraussichtlich beschleunigen. Das Laden von EVs und die Erzeugung von grünem Wasserstoff für FCEVs stellen eine flexible Last für das Stromnetz dar und bieten das Potenzial, die Lade- oder Betankungsprozesse auf bestimmte Ziele wie die Reduzierung von Lastspitzen abzustimmen. In dieser Diplomarbeit wurde die Auswirkung des Ladens von Elektrofahrzeugen auf die regionale Residuallast aus der Sicht eines Netzbetreibers untersucht, wobei ein gemischt-ganzzahliges lineares Optimierungsmodell (MILP) zur Minimierung der gesamten Energieversorgungskosten verwendet wurde. Das Modell berücksichtigt verschiedene Ladeszenarien zur Deckung des lokalen Strombedarfs unter Einbeziehung von Netzanschluss, Photovoltaik und lokaler Batteriespeicherung. Es wurden zwei verschiedene Anwendungsfälle untersucht, wobei für jeden Fall verschiedene Ladeoptimierungsszenarien basierend auf der EV- und FCEV-Durchdringungsrate entwickelt wurden. Um die Auswirkungen der Ladeverfahren zu bewerten, wurden drei Ansätze untersucht: ungesteuertes Laden, kostenbasiertes intelligentes Laden und intelligentes Laden mit parallelen Ladebeschränkungen. Die Ergebnisse zeigten, dass der ungesteuerte Laden die höchsten Stromkosten verursachte, während beide intelligenten Ladeverfahren eine deutliche Kostenreduzierung bewirkten. Die reine Kostenoptimierung führte jedoch zu extremen Lastspitzen, die durch zusätzliche parallele Ladebedingungen mit leicht erhöhten Ladekosten verringert werden können. Die Ladeleistung spielte eine große Rolle, da der Zusatztarif für das DC-Laden einen großen Teil der Gesamtkosten ausmachte. Die Kombination aus EVs und FCEVs erwies sich als die kostenoptimalste Lösung, hauptsächlich aufgrund des nicht vorhandenen Gleichstromladetarifs für die Wasserstofferzeugung, da die Elektrolyseure im Wechselstrombetrieb angeschlossen sind. Die Wasserstoffproduktion führte zu keiner erhöhten Spitzenlast, da der Lastbedarf über den Tag verteilt ist und in Zeiten mit hoher PV-Erzeugung anfällt. Weitere Verbesserung der Modellierung können insbesondere den Einsatz von ein größeres Spektrum an Fahrprofilen und Vehicle-to-Grid Konzept beinhalten. Durch die Berücksichtigung eines breiteren Spektrums von Fahrprofilen könnte die Vorhersage der Mobilitätslast verbessert und die Modellgenauigkeit erhöht werden. Das V2G-Potenzial könnte die Flexibilität und Stabilität des Netzes erhöhen. Eine dynamische, ladungsbasierte Tarifstruktur an Gleichstrom-Schnellladestationen sowie ein Anreizprogramm zur Abstimmung der Ladeleistung von Elektrofahrzeugen auf die aktuelle Netzlast könnten die Einführung von E-Fahrzeugen beschleunigen.

Contents

Abbreviations

AC	Alternating current
BEV	Battery electric vehicle
CCS	Combined charging system
CO_2	Carbon dioxide
DC	Direct current
DSO	Distribution system operator
ENTSO-E	European association of transmission system operators for electricity
EV	Electric vehicle
FCEV	Fuel cell electric vehicle
H2G	Hydrogen-to-Grid
H_2	Hydrogen
ICE	Internal combustion engine
IEC	International Electrotechnical Commission
MILP	Mixed Integer Linear Programming
OpEx	Operational Expenditures
PEM	Proton exchange membrane
PV	Photovoltaic
SAE	Society of Automotive Engineers
SoC	State of Charge
TSO	Transmission system operator
V2G	Vehicle-to-Grid

CHAPTER 1

Introduction

1.1 Motivation

Electric vehicles (EVs) and fuel cell electric vehicles (FCEVs) are expected to become increasingly widespread in the coming years as emissions standards for the transportation sector become stricter in accordance with the European Union's 2030 climate and energy goals. EVs and FCEVs are gaining popularity as a clean and efficient alternative to traditional gasoline-powered vehicles. One of the main motivations for increasing the use of EVs in transportation systems is to reduce greenhouse gas emissions, as transportation is a significant contributor to global greenhouse gas emissions. In addition to the environmental benefits, the increasing adoption of EVs can also have economic benefits. As the technology continues to improve and costs continue to decline, it is becoming increasingly cost-effective to own and operate an EV. In addition, the use of EVs can help support the development of new technologies and industries, creating new jobs and economic opportunities.

As the use of electric vehicles (EVs) and fuel cell electric vehicles (FCEVs) continues to grow, there is increasing interest in the potential impact of zero-emission mobility on the residual load of the grid. Direct charging of EVs and the production of green hydrogen for FCEVs can provide a flexible load on the electricity system that can be adjusted to meet specific objectives, such as reducing load peaks. However, without an effective charging strategy, there may be an increase in residual load and a need for additional peak load capacity. A Stanford study showed that by continuing to charge the cars only in the evenings or overnight, the grid will experience significant stress without added investments [1]. On the other hand, an optimized charging strategy can provide additional flexibility for the electricity system and facilitate the integration of renewable energy sources, ultimately leading to lower electricity generation costs.

Smart charging technologies allow for the control and optimization of EV charging based on factors such as the availability of renewable energy sources, grid conditions,

and the needs of the vehicle owner. By optimizing the charging of EVs based on the availability of renewable energy sources and grid conditions, we can help reduce the total cost of electricity and improve the overall performance of the grid. This can have technical benefits such as reduced power losses, improved voltage and frequency stability, and reduced wear and tear on grid infrastructure.

Green hydrogen production, through electrolysis, is also an important aspect of the transition to a low-carbon future. Electrolysis involves using electricity to split water into hydrogen and oxygen, with the hydrogen being used as a fuel. One of the key advantages of green hydrogen is its potential to help balance the grid. When renewable energy sources, such as solar and wind, are producing more electricity than needed, the excess energy can be used to produce hydrogen through electrolysis. This means that the charging of FCEVs can be scheduled to occur during times when there is excess renewable energy available, or when demand for electricity is low. Green hydrogen production does not produce any greenhouse gas emissions, and FCEVs emit only water vapor as a by-product of their operation.

1.2 Research question and method

The primary objective of this thesis is to identify the impact of the growing adoption of electric vehicles and fuel cell electric vehicles on local residual load. To achieve this, the factors related to EV and FCEV demand in transportation sector such as energy consumption, vehicle inventory, driving behavior and many more are examined. The parameters needed to calculate local residual load, including residential load, renewable electricity generation and battery storage capabilities are also quantified. A linear optimization model is programmed from the perspective of a grid operator that minimizes the electricity costs associated with charging the EV fleet and producing green hydrogen for the FCEV fleet, while still meeting mobility requirements and technical constraints. Another area of research is to more thoroughly understand the different effects of various charging methods on the residual load and analyze the grid stability. Furthermore, these charging methods are further associated with power-based tariff premiums and the influence of such added costs on the total energy procurement costs is examined. Therefore, this thesis also investigates the sensitivity of EV and FCEV penetration rate and charging mode to further examine the influence of the EV and FCEV fleet on residual load.

The developed linear optimization model is implemented in Python, using the Pyomo framework [2, 3]. The objective function minimises the total energy procurements costs of the grid operator using different charging scenarios, while fulfilling the power demand of local area. The power supply is mainly provided by the main grid connection but decentralized energy resources like PV supply are also included. Furthermore, local battery storage is integrated in the model that is charged mainly in times of excessive PV generation but nonetheless, can be also charged directly from the grid in case of low electricity prices. The electricity prices are taken from ENTSO-E (European association for the cooperation of transmission system operators for electricity) database. The power demand includes the residential demand extracted from E-Control, that is

considered non-flexible in the model. In addition to that, the flexible mobility demand originates from the battery electric vehicles and the green hydrogen production for fuel cell vehicles. The mobility demand has a specific set of parameters regarding driving behavior, plug-in time periods and vehicle types and based on these mobility requirements, the most cost-optimal charging profiles are generated. Based on these optimized charging profiles, the respective energy procurement costs are calculated and the load profiles together with peak loads are plotted. The model is solved with the Gurobi solver, and the visualizations are done with Matlab [4, 5].

1.3 Structure of the thesis

After a short introduction to the topic, Chapter 2 of this work provides a review of existing papers and studies that have addressed smart charging methods for large fleets of electric vehicles in relation to cost optimization and grid stability as well as studies focused on fuel cell electric vehicles and green hydrogen production through electrolysis. In Chapter 3 the methods of the thesis and the mathematical formulation of the optimisation model are outlined, together with the respective flowchart and function diagram. The other part of this chapter focuses on the different use cases that are considered in this work and the various charging optimization scenarios. Chapter 4 presents the results of the two use cases in technical terms such as load profile or peak load as well as in economic terms like energy procurement costs. Chapter 5 offers a discussion of these results, highlighting important observations and comparing the different use cases and charging scenarios. In Chapter 6, the outcomes of the research are emphasized, and conclusions are drawn regarding the research question. Furthermore, thoughts on potential future studies and research are provided.

CHAPTER 2

State-of-the-Art and progress beyond

In this section, some of the existing research and studies are shown, which are mainly related to the research questions. These are divided into two main parts that are also comprised in this thesis. First, there is the implementation of an optimization model for the charging strategies of the electric vehicle's fleets based on load profiles and energy procurement costs. The second part includes the integration of hydrogen vehicles in the optimization model and the respective effects in the grid optimization. The own contribution of this work is stated in the last section.

2.1 Electric vehicle charging strategies

With the increasing trend of electric vehicles usage in different areas of the transport sector, there is also an increased incentive to carry out deepened research and studies related to electric vehicles. These studies usually include optimization models that are however very different in objectives and problem statements.

In this paper, only battery electric vehicles and fuel cell electric vehicles are considered. As for the charging of electric vehicles, IEC 62196 has determined four standardized charging modes. Modes 1 to 3 are related to charging with alternating current (AC) while Mode 4 refers to electric vehicle charging with direct current (DC) [6]. In terms of AC charging, European countries have adopted IEC 62196 Type 2 connector and based on the distribution system operators (DSOs) guidelines, the AC charging power is capped at 22 kW [7]. In case of one-phase operation, the maximum current is limited to 16 Arms so that the charging power is capped at 3,6 kW. In other parts of the world, there are different charging power limits based on their voltage levels and allowed peak currents, however not higher than the 22 kW charging limit set in Europe. As for the DC charging, there are different protocols and connectors being placed in different parts of the world. Europe and North America have settled mainly for the SAE Combined Charging System (CCS1/CCS2), which is a more developed version of AC Type 2. The

maximum power output is limited at 900 kW; however, the most usual DC charging stations provide charging possibilities between 50 - 350 kW.

The increasing demand and penetration rate of EVs is subsequently having a higher effect in the power grid, and it is challenging the grid operators. On the other hand, the integration of these electric vehicles may give an added flexibility to the grid operators, to flatten the load profile as well as manage supply costs [8]. Nevertheless, this growing demand should be associated with the appropriate charging strategies to avoid unnecessary peak loads and high energy costs. In the last years, plug-in electric vehicle charging has typically begun in the moment that the driver arrives home and plugs in the vehicle [9, 10]. This added load usually corresponds with the daily peak demand in the evening hours and it consequently can change the aggregated residential demand and increases grid costs overall. The uncoordinated charging of a high number of EVs impacts the power grid in terms of greater peak load, affecting voltage and frequency, reducing overall stability and straining transmission lines [11].

In most charging sessions, the amount of time it takes an electric vehicle to achieve the desired charging demand is much less than the connection time to a charging station [12, 13]. Thus, there is opportunity to optimize the whole aggregated charging process by shifting this load in more advantageous time periods. Smart charging, coordinated charging or also controlled charging are some of the terms to explain this optimization process. For example, when the solar PV supply is at highest during lunch time, the EV charging load can be shifted, and this reduces the evening peak [14]. Many types of algorithms with different objectives have been presented, ranging from cost optimization of large-scale EV charging to minimization of CO_2 emissions or also to maximization renewable energy resources [13, 15, 16]. One study has shown that by integrating smart charging, electric vehicles can mitigate increasing peak loads as well as contribute to more integration of renewable energy sources [17]. In one residential use case, smart charging could increase the share of EVs from 10 % to 52 % without any need to invest in grid reinforcements [18]. Furthermore, more studies have shown that smart charging is economically advantageous in various electricity markets, with possible financial gains ranging from 106 to 1008 EUR/year per EV [10, 19]. In the case that 50 % of electric vehicles participate in coordinated charging, the power supply costs are reduced by approximately 17 % compared to uncoordinated charging [20]. A more advanced step towards smart charging is to include vehicle-to-grid (V2G) power exchange, which brings higher flexibility but contains increased battery degradation costs. This bidirectional power exchange has shown good early results; however, this part is not included in the scope of this thesis.

To address the EV charging scheduling problem, different dispatch methods have been used that can be categorized in two main groups. Decentralized charging methods include day-ahead pricing patterns to change charging behaviors and lower energy costs [21, 22]. Such approach can ease the load demand in peak hours but on the other side it can lead to new peak loads in other parts of the day when the electricity price is very beneficial [23]. Another requirement for this approach to be successful is the prerequisite of knowing the price information beforehand, which may not always be

possible. The other method is a more centralized approach, where the EV aggregator can gather data on the EV's charging demands and then centrally schedule the EV's charging intervals. One study has shown that EV charging scheduling in a centralized manner can assure the utilization of surplus power during the valley periods [24].

2.2 Inclusion of fuel cell vehicles

One way to decarbonize the transport sector is through electric vehicles and this has caught the most intention in the last 10 - 20 years. However, hydrogen can play a significant role in the future of transportation as well [25]. In comparison to traditional internal combustion engines (ICEs), fuel cell electric vehicles (FCEVs) have a much higher energy conversion efficiency and produce zero tailpipe air pollutant emissions [26]. A FCEV comprises of six main components: (1) Hydrogen storage tank, (2) air intake system, (3) fuel cell system, (4) power control unit, (5) battery, and (6) electric motor. The H_2 from the storage tank is combined with the oxygen from the air intake system to generate electricity through an electrochemical process in the fuel cell system. The only by-product is water vapor, thus there are no tailpipe emissions from the FCEVs. As of end of 2020, there were three fuel cell passenger cars available on the market in Europe and the US [27]. In addition, heavy-duty FCEVs are being developed increasingly because of the advantages in high specific energy density and fast refueling.

The further development of FCEVs is very much dependent on the implementation and construction of energy supply facilities that support such vehicles. The sustainable production of hydrogen without any emissions will be significant to decreasing the emissions from transportation sector. The most future-prone solution for no emission hydrogen production is through water electrolysis, that is however very dependent on the electricity generation mix of each country [27]. There are different electrolysis technologies, with proton exchange membrane (PEM) and alkaline electrolysis being the most developed [28]. When compared to alkaline electrolysis, PEM technology provides more flexible operation as it requires less than 1 minute for start-up and only second for ramp up from idle state to maximum power, which makes is more suitable for intermittent power inputs [29]. On the other hand, PEM membrane lifetime is less than half of alkaline membrane lifetime, and it reflects key drawbacks that prevent the widespread use of PEM technology. The competitiveness of renewable-produced hydrogen is highly conditioned to investment costs, which are currently still quite high. However, the OpEx costs also have a major impact, and the main operating costs of an electrolyser is the electricity purchase price [30]. Regarding the tradeoff between investment and operating costs, one study showed that increasing hydrogen production flexibility lowers grid operation costs and CO_2 emissions, but the optimal least-cost point comes with an annual capacity factor between 80 % and 90 % [27].

The storage of hydrogen for FCEVs is simpler than that of electricity, and the production of hydrogen from fewer facilities is more flexible and easier to operate without affecting driver's behaviour. Hydrogen production through electrolysis can operate as a buffer for the power grid, by helping to maintain grid stability and enabling load shifting while also allowing more renewable generation that would be curtailed otherwise. When

compared to plug-in electric vehicles, the electrolysers load is a more flexible grid asset (i.e., systems are at the MW-scale) that can ramp up quickly and does not depend on a huge number of single-agent (sometimes irrational) decision makers as in the decentralized charging approach [31]. One study concluded that 8 hours of hydrogen storage is fully sufficient to optimally operate the model and that the use of hydrogen to reproduce electricity and fed it back to the grid (H2G) can improve peak shaving [32]. The findings also demonstrated that oversizing electrolyzers can significantly reduce renewable energy's intermittent nature. A few studies have explored the hydrogen production from excess electricity (mainly wind energy) and have highlighted that low electricity costs combined with high hydrogen prices are requirements for the profitability of electrolysers [33, 34]. Hydrogen production plant localization is also analyzed and the findings showed that in the case of non-dispatchable wind energy, the transmission problems can be solved only by building electrolysers very near to the wind farms [35].

2.3 Own Contribution

While the literature presented above focuses mostly on one type of electric vehicle (either plug-in battery or fuel cell), the aim of this work is to better understand the effects of the combined increasing penetration of EVs and FCEVs on the regional residual load. In particular, the thesis includes a mixed-integer linear programming (MILP) model that optimizes the energy costs of two real use cases (suburban and rural) combined with various EV penetration rates and different charging strategies. In order to converge to more realistic results, an additional contribution of this work is the optimization model with the objective of cost minimization as well as grid stability. On the contrary, previous works have been focused in one main objective and not regarding consequent problems. With this work, the reader is given an insight into the main differences between the rural and suburban use cases and how different charging scenarios and EV penetration rates affect the energy procurement costs and peak loads of a region. Therefore, the results of this thesis shall help decisionmakers such as DSOs, TSOs and municipalities to rethink their investment strategies and push forward those mobility scenarios with the highest overall benefits.

CHAPTER 3

Methodology

In this chapter, the developed methodology is explained in more details. First, Section 3.1 presents the mathematical formulation together with the respective flowchart, objectives and constraints. Then, Section 3.2 provides an overview of use cases that are taken into consideration in this work. Building upon, Section 3.3 describes the charging scenarios for each use case. To better understand the context of the formulations, the nomenclature can be found in the end of the thesis.

3.1 Mathematical formulation

The core objective of the proposed optimization model is to better understand the effects of increasing penetration of EVs and FCEVs on the local residual load of two regions (suburban and rural use case) and minimize the energy procurement costs.

3.1.1 Function diagram and flowchart

Firstly, the function diagram of the optimization model is shown in Figure 3.1. The diagram represents the local grid with the respective power supplies and loads. The main power supply occurs from the main grid P_{grid} associated with distributed energy resources like solar PV P_{PV}. There is also a battery reserve $P_{batteries}$ assisting with added flexibility in the grid operations. Regarding the loads in this representation of the local grid, the residential demand $P_{residential}$ describes the aggregated load of all households included in chosen district. Furthermore, the aggregated load of electric vehicle charging demand $P_{charging}$ is divided into two main charging modes, AC level 2 charging mode with power outputs up to 22 kW and DC fast charging mode with 50 kW power output. On the other hand, the mobility load coming from the FCEVs is expressed in the energy demand required to produce and store the hydrogen needed for such vehicles. The main contributor to the hydrogen production is the electrolyser $P_{electrolysis}$ connected with the required compressor and cooler, which then is stored at

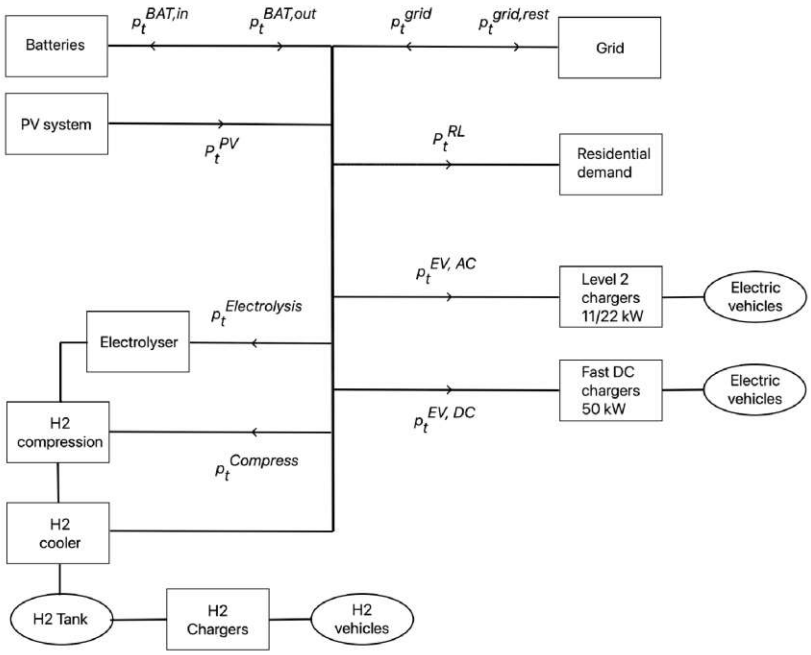

Figure 3.1: Function diagram

the hydrogen tank to be at disposal for refueling.

Secondly, the flowchart of the optimization model is shown in Figure 3.2 below. It begins with preparing the necessary input data and finishes with a final set of load profiles and cost estimations. The model is built to calculate the minimal energy costs for each 15 minute timestep during a whole year. The whole procedure can be explained in the following steps:

- Import of the electricity prices and respective tariffs that are taken as equal in both use cases.
- Import of all other input variables that differ in each use case: aggregated residential load profile, PV supply profile, battery reserve specification, details of each car bundle regarding quantity, type, driving behavior, plug-in timeslots and charging station specifications.
- Optimization of the local energy grid with the goal of a cost-effective energy supply using a python-based library Pyomo.
- Variation to the next charging scenario for a comparison analysis of the results and graphs.
- Extraction of the energy procurement costs and visualization of load profiles.

3.1.2 Objective function

The scope of the optimization model is to decrease the electricity costs incurred by charging the EV fleet and producing green hydrogen for the FCEV fleet. The mixed-

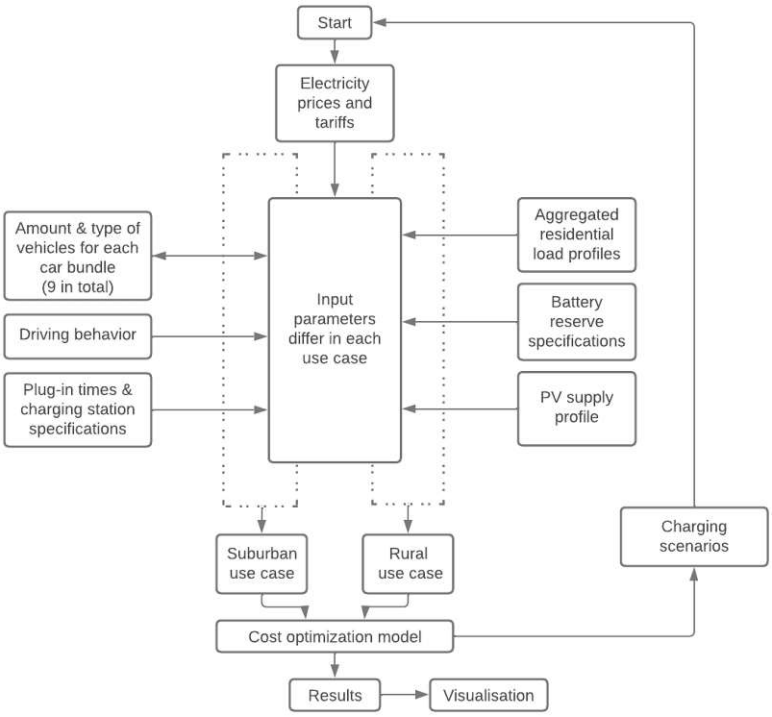

Figure 3.2: Flowchart

integer linear programming model is developed in Python using the Pyomo library, which is applied to solve optimization problems. Furthermore, matplotlib library is used to plot 2D graphs and numpy is utilized for working with arrays [36, 37]. In the following sections, the decision variables are continuously written in lower letters while the model's input parameters are marked with capital letters.

The objective fuction of the model minimzes the costs of the energy procurement from the main grid p_{grid} multiplied with the electricity costs C_{elec} and the respective grid tariffs C_{grid} and an additional sum function of the load demand from the vehicles charging in DC fast charging $P_{EV,DC}$ multiplied with an added DC tariff $C_{DC,charging}$. The reason of the DC tariff is to incentivize the further development of DC fast charging network through contributions from drivers that benefit from this premium service. The electricity costs are based on the electricity spot market price while the grid tariffs include the electricity tax, the transmission tariffs as well as the CO_2 emission tariff or also called carbon tax. The symbol x expresses the decision variable vector and includes all decision variables of the model. The total sum iterates over a year for every 15-min timestep. The iteration parameter is defined with i and scales from 0 to 35039, which describes the amount of 15-min timesteps in a whole calendar year. The objective function is shown in the equation as follows:

$$\min_{x} \sum_{t=0}^{T} (p_t^{grid} * (C^{elec} + C^{grid}) + \sum_{\theta=\theta_0}^{\theta_\Gamma} p_{\theta,t}^{EV,DC} * C^{DC,charging}) \tag{3.1}$$
$$\forall t \in (0,T), \forall \theta \in (0,\Theta)$$

The symbol x is used as decision variable vector and encompasses all decision variables of the model. The objective function above ensures the lowest energy procurements costs by optimizing the aggregated power demand in the timesteps with the lowest prices while meeting all the required constraints. The end results provide the minimized total energy costs of a specific region (district, village or similar) in the perspective of the distribution network operator.

The decision variable vector x is defined as below,

$$\begin{aligned} x^T = & (p_t^{grid}, p_t^{grid,rest}, p_t^{Bat,in}, p_t^{Bat,out}, soc_t^{Bat}, p_{\theta,t}^{EV,AC}, p_{\theta,t}^{EV,DC}, \\ & soc_{\theta,t}^{EV}, p_t^{Electrolysis}, soc_{S,t}^{H_2}, soc_{\phi,t}^{H_2}, p_{\phi,t}^{H_2,charge}) \\ & \forall t \in (0,T), \forall \theta \in \Theta, \forall \phi \in \Phi \end{aligned} \tag{3.2}$$

$p_{grid,t}$ represents the power supply originating from the main grid, $p_{grid,rest}$ indicates the power supply flowing back to the grid in cases of overproduction from the distributed energy resources, $p_{bat,in/out}$ correspond to the charging and discharging power of the battery reserve together with the soc_{bat} representing the state of charge of the battery reserve. $p_{EV,AC}$ and $p_{EV,DC}$ stand for the load coming from the Level 2 charging demand and DC fast charging demand while $soc_{bat,\theta}$ represents the state of charge for each electric vehicle θ. The last part includes the decision variables of the hydrogen production and storage. $p_{electrolysis}$ corresponds to the electrolyser load while $p_{H_2,charge}$, charge indicates the mobility load coming from the fuel cell vehicles. soc_S and soc_ϕ represent the state of charge of the large hydrogen storage tank and the state of charge of each fuel cell vehicle bundle ϕ respectively. It is important to notice that all decision variables above are based on each 15-min timestep.

3.1.3 Constraints

Equilibrium

The main constraint of the optimization model is the power supply and demand equilibrium in each timestep. This constraint ensures that the non-flexible demand coming from the residential load and the required charging demand of plug-in electric vehicles and fuel cell electric vehicles is always fulfilled. Regarding the power supply, the model prioritizes decentralized energy resources such as PV in the region and the supply coming from the battery reserve, before drawing more power from the main grid. The optimization of the flexible charging demands from electric vehicles is done by the

model in timesteps where the electricity prices are lower.

$$p_t^{grid} - p_t^{grid,rest} = P_t^{RL} + p_t^{Bat,in} - p_t^{Bat,out} - P_t^{PV} + \sum_{\theta=\theta_0}^{\theta_\Gamma} p_{\theta,t}^{EV,AC} + \sum_{\theta=\theta_0}^{\theta_\Gamma} p_{\theta,t}^{EV,DC} + p_t^{Electrolysis} \quad \forall t \in (0,T), \forall \theta \in \Theta \tag{3.3}$$

The power supply includes the main grid supply P_{grid}, the intermittent solar PV supply P_{PV}, and the power originating from the discharge capacities of the battery reserve $P_{bat,out}$. The demand side is comprised of the non-flexible aggregated residential load P_{RL}, the charging demand from the battery reserve $P_{bat,in}$ usually in times of low electricity prices or high PV generation, the flexible charging demand of electric vehicles $P_{EV,AC}$ and $P_{EV,DC}$ in AC and DC charging stations with the respective charging constraints and lastly, the hydrogen production load $P_{electrolysis}$ needed to produce the hydrogen based on the refueling constraints of the fuel cell vehicles.

Residential load and PV supply

The aggregated residential load is based on the multiplication of a typical load profile of a median household with data coming from E-Control together with the number of households that each use case (suburban and rural) contains. This load is considered as non-flexible in the model and residential load shifting is not regarded in this work.

$$p_t^{RL} = p_t^{Loadprofile} + N_{residences} \quad \forall t \in (0,T) \tag{3.4}$$

The aggregated PV supply of the region is calculated by multiplying the power generating profile of the PV in the considered region with the installed PV capacity in each use case. It is important to note that the investment costs of the solar PV system are not included in this model and the power supply from the solar PV does not induce added costs.

$$p_t^{PV} = p_t^{PV,profile} + p_{installed}^{PV} \quad \forall t \in (0,T) \tag{3.5}$$

Battery reserve

Regarding the stationary battery reserve, the maximum powerflow P_{max}^{Bat} and the battery capacity soc_{max}^{Bat} are used in this model. The battery reserve can exclusively feed the loads in the considered region and is not bounded only to EVs. The main constraint of the battery reserve involves the energy capacity in each timestep as below

$$soc_t^{Bat} = soc_{t-1}^{Bat} * (1 - E^{Bat,standby}) + (p_t^{Bat,in} * \eta_t^{Bat,in} - \frac{p_t^{Bat,out}}{\eta_t^{Bat,out}}) * \Delta t \quad (3.6)$$
$$\forall t \in (0, T)$$

The state of charge in the current timestep soc_t^{Bat} is based on the value of the state of charge in the previous timestep soc_{t-1}^{Bat} and combining it with some stand-by or self-discharge losses that occur physically inside the battery. Afterwards, the current state of charge differs based on energy flows in and out, with the battery reserve being charged or discharged with $p_t^{Bat,in}$ and $p_t^{Bat,out}$ while also considering the respective efficiency $\eta_t^{Bat,in}$ or $\eta_t^{Bat,out}$.

The state of charge at each timestep is limited by the minimal and maximal capacity of the battery.

$$SoC_{min}^{Bat} < soc_t^{Bat} < SoC_{max}^{Bat} \quad (3.7)$$
$$\forall t \in (0, T)$$

The initial state of charge in the beginning of the optimization should be equal to the state of charge in the final timestep. This reflects the requirement that the model should have the same initial and end conditions.

$$soc_{last}^{Bat} = SoC_{end}^{Bat} = SoC_{init}^{Bat} \quad (3.8)$$

The powerflow out of the battery

$$p_t^{Bat,out} \leq P_{max}^{Bat} * (1 - powerdirection_t) \quad (3.9)$$
$$\forall t \in (0, T)$$

as well as into the battery cannot exceed the maximum powerflow of the battery

$$p_t^{Bat,in} \leq P_{max}^{Bat} * powerdirection_t \quad (3.10)$$
$$\forall t \in (0, T)$$

The term $powerdirection_t$ is a bool parameter of the model and it defines the orientation of the powerflow.

Electric vehicles

The constraints of electric vehicles apply for all electric vehicle bundles, whether it is charged in an AC or DC charging station. Based on the equilibrium constraint, the

total load of the EV is covered from various power supplies. However, the EV cannot feed back to the grid and vehicle-to-grid (V2G) technologies were not included in this work.

Similar to the stationary battery reserve, the state of charge of each electric vehicle bundle Θ is defined by the previous state of charge including the self-discharging losses and combined with energy flows in and out.

$$\begin{aligned} soc_{\theta,t}^{EV} =& soc_{\theta,t-1}^{EV} * (1 - E^{Bat,standby}) + (p_{\theta,t}^{EV,in} * \eta_t^{EV,in}) * \Delta t * \sigma_{\theta,t}^{EV,conn} \\ & - E_{\theta,t}^{EV,consumption} * (1 - \sigma_{\theta,t}^{EV,conn}) \\ & \forall t \in (0,T), \forall \theta \in \Theta \end{aligned} \tag{3.11}$$

Each vehicle bundle has a predefined driving behavior and the respective energy consumption $E_{\theta,t}^{EV,consumption}$, which is deducted from the battery in each timestep. The term $\sigma_{\theta,t}^{EV,conn}$ is a bool parameter that is based on the plug-in timeslots of each vehicle bundle and determines if the electric vehicle is connected to a charging station in each timestep.

The state of charge of each vehicle bundle at every timestep is limited to the minimal and maximal capacity of the battery

$$\begin{aligned} & SoC_{min}^{EV} < soc_{\theta,t}^{EV} < SoC_{max}^{EV} \\ & \forall t \in (0,T), \forall \theta \in \Theta \end{aligned} \tag{3.12}$$

It is important to note that in contrast to the minimal capacity of the battery reserve, the minimum state of charge recommended for electric vehicles SoC_{min}^{EV} is determined at approximately 20 % and lower values should be avoided [38]. This remaining capacity is used for necessary electrical functions and compensating the self-discharging effect of the battery when in idle mode.

The initial state of charge is equal to the final state of the charge in the last timestep, akin to the battery reserve.

$$soc_{last}^{EV} = SoC_{end}^{EV} = SoC_{init}^{EV} \tag{3.13}$$

The powerflow charging the electric vehicle battery is capped at the maximum power supply $P_{\theta,Max}^{EV}$ that is allowed by the respective charging station. Each of the vehicle bundles have their corresponding charging station in the mobility use cases. It should also be emphasized that each vehicle type also has a maximum power that can be allowed for charging, and this value should correspond with that of the charging station.

$$0 \leq p_{\theta,t}^{EV,in} \leq P_{\theta,max}^{EV} \quad \forall t \in (0,T), \forall \theta \in \Theta \tag{3.14}$$

Hydrogen production and fuel cell vehicles

Similar to the electric vehicle constraint above, also the constraints of the fuel cell vehicles apply to all vehicle bundles and these vehicles are not considered to be used as hydrogen storage for purposes of re-electrification to be fed back to the grid. The load originating from the processes of electrolysis, compression and cooling can be covered by various power supplies in the region.

Contrary to the electric vehicles, the fuel cell vehicles cannot be directly connected to the grid so there are some intermediate steps in between such as producing the hydrogen with the electrolysers and preparing it to be stored at large hydrogen tanks usually located in refueling stations. The load of the electrolyser is capped to its nominal power

$$0 \leq p_t^{Electrolysis} \leq P_{max}^{Electrolysis} \quad \forall t \in (0,T) \tag{3.15}$$

In this work, a PEM-based electrolyser has been chosen with the purpose of higher flexibility in grid operations. As mentioned in Section 2.2, this technology supports quick start-up time and can ramp up in second from idle mode to maximum power. Thus, the power constraint above allows the electrolyser $p_t^{Electrolysis}$ to ramp down up to standstill if needed.

The produced hydrogen is stored in a large hydrogen tank and the state of charge of this tank $soc_t^{H_2}$ is defined by the previous state of charge coupled with the energy flows in and out

$$soc_t^{H_2} = soc_{t-1}^{H_2} + (p_t^{Electrolysis} * \eta^{Electrolysis}) - p_{\phi,t}^{H_2,charge} \quad \forall t \in (0,T), \forall \phi \in \Phi \tag{3.16}$$

In contrast to electricity storage, there are no self-discharging losses in storing hydrogen. The constraint above also includes the system efficiency of hydrogen production $\eta_{Electrolysis}$, which is significantly lower than those of battery reserve.

The state of charge of the hydrogen tank is limited to the minimum and maximum capacity of this tank

$$SoC_{min}^{H_2,tank} < soc_t^{H_2} < SoC_{max}^{H_2,tank} \tag{3.17}$$

After the hydrogen is stored, the refueling process of fuel cell vehicles can begin and the state of charge of the hydrogen tank from each vehicle bundle $soc_{\phi,t}^{H_2}$ is determined by the previous state of charge combined with the hydrogen inflow and the consumption in each timestep

$$soc_{\phi,t}^{H_2} = soc_{\phi,t-1}^{H_2} + (h_{\phi,t}^{H_2,charge} * \rho_{\phi,t}^{H_2,conn}) - H_{\phi,t}^{H_2,consumption} * (1 - \rho_{\phi,t}^{H_2,conn}) \quad (3.18)$$
$$\forall t \in (0,T), \forall \phi \in \Phi$$

Similar to electric vehicles, a bool parameter $\rho_{\phi,t}^{H_2,conn}$ is included in order to define the timesteps in which the vehicle can be refueled.

The state of charge of each vehicle bundle at each timestep is restricted to the minimal and maximal capacity of the hydrogen tank inside the vehicle

$$SoC_{\phi,min}^{H_2,vehicle} < soc_{\phi,t}^{H_2} < SoC_{\phi,max}^{H_2,vehicle} \quad (3.19)$$
$$\forall t \in (0,T), \forall \phi \in \Phi$$

The hydrogen flow from the refueling station to the fuel cell vehicle is capped to the maximum hydrogen outflow that is supported by the station in combination with the maximum allowed hydrogen inflow allowed by the fuel cell vehicle itself.

$$0 \leq h_{\phi,t}^{H_2,charge} \leq H_{\phi}^{Max} \quad (3.20)$$
$$\forall t \in (0,T), \forall \phi \in \Phi$$

3.2 Definition of use cases

The following section describes the two use cases that are examined in this work in order to investigate the effects of higher penetration of EVs and FCEVs in the residual load of a suburban and a rural use case. Each of the use cases includes the residential load originating from the current households located in the respective area, the projected distributed energy resources in the form of solar PV and the associating battery reserve, and the estimated mobility load divided into EVS and FCEVs. The chosen areas can be seen in Figure 3.3 below.

3.2.1 Sub-urban use case

The first use case is a typical suburban area represented by the 21. district of Vienna. This district is considered as part of the outskirts of the city of Vienna and there are 165 673 residents living in this district as of year 2019 [39]. These residents are divided into 78 109 households, with an average of 2,12 people per apartment which is slightly

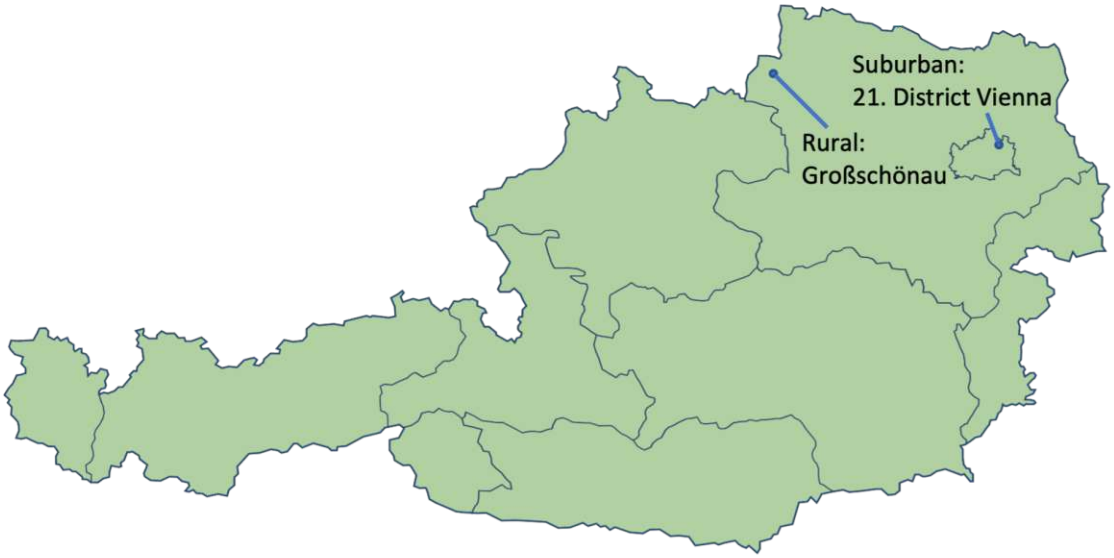

Figure 3.3: Map of Austria with location of use cases

higher than the average of the whole city of Vienna with 2,04 people per apartment. The majority of the households are with one or two tenants, which has a direct impact to the load demand of each household. Based on the E-control data for the year 2017, the annual energy consumption of an average household sums up to 4 440 kWh per year [40]. The respective energy consumption H0 profile is included into the model to find out the aggregated residential load of the whole area.

As for the solar PV supply, because of the households' arrangements into multi-party buildings, the solar PVs can be installed only in the roofs of the residential buildings. Until the year 2022, the largest energy provider in Austria called Wien Energie operates 23 community solar power plants in multi-apartments buildings with an average installed capacity of 130 kWp [41]. Furthermore, of the approximately 68 000 multi-family dwellings in Vienna, it is worth installing community generation systems on about 10 % of these sites [42]. Based on the data above, aggregated installed capacity of the 21. district sums up to 74,25 MWp, or at about 0,95 kWp per each household.

The investment costs of batteries have been decreasing steadily throughout the last decade and the trend is still continuing downwards. Thus, the option of using a battery reserve in case of high PV generation or low electricity prices is becoming much more viable. The optimal net storage capacity is up to 1 kWh for each kWp of installed PV [43]. Moreover, the maximum discharge power supply is also set at 1 kW [44]. Thus, the aggregated storage capacity sums up to 74,25 MW. Nevertheless, as battery storage systems have a minimum required capacity, the aggregated storage capacity can be divided either in thousands of distributed and small-scale battery systems of 10 - 15 kWh capacity or in tens of grid-scale battery systems with 2 - 4 MWh capacity.

In the 21. district of Vienna, there were 64 556 passenger cars and 4 530 light-to-medium duty trucks [45]. The largest bus garage Leopoldau is located in this district,

and it contains 177 buses that are parked there throughout parts of the day. Based on these data, this work comprises 13 different vehicle bundles with each one having a specific vehicle type, an individual driving behavior in terms of the number of annual kilometers driven and plug-in hours per week as well as the respective charging station. There are 3 different passenger electric vehicle types divided in 5 vehicle bundles in Table 3.1 as follows:

	Bundle 1	Bundle 2	Bundle 3	Bundle 4	Bundle 5
Share of total pass. EVs	30 %	20 %	20 %	15 %	15 %
Model	Smart EQ	VW ID.3	VW ID.3	Tesla Model 3	Tesla Model 3
Energy source	Electricity	Electricity	Electricity	Electricity	Electricity
Battery capacity	16,7 kWh	58 kWh	58 kWh	50 kWh	50 kWh
Annual driven distance	10 000 km	13 000 km	13 000 km	16 000 km	16 000 km
Plugged-in duration per week	36 hours	16 hours	7 hours	16,8 hours	8,4 hours
Charging time	Overnight	Overnight	Daytime	Overnight	Daytime
Charging power	Level 2 AC charging; 4,6 kW	Level 2 AC charging; 22 kW	Level 2 AC charging; 22 kW	DC fast charging; 50 kW	DC fast charging; 50 kW

Table 3.1: Passanger battery electric vehicle specifications in the different vehicle bundles

The vehicle data are based on the datasheets from each of the vehicle types [46, 47, 48]. The average passenger car user in Austria drives approximately 13 000 km each year [49]. It is important to note that in the case of vehicle bundle 1, the vehicle type (Smart EQ) does not support the full power output that the charging station offers. This vehicle type supports charging power up to 4,6 kW, so this is the upper limit considered in this work. For the rest of the vehicle bundles, they all support the maximum power output that the respective charging station offers.

One of the main factors that plays an important role in the final outcome of the residual load profile are the plug-in duration and time period throughout the day. In order to avoid high peak loads, electric vehicle charging should on one side be shifted towards day periods that do not have a high demand. On the other side, they should also be spread throughout parts of the day in order not to cause new peak loads originating only to additional electric vehicle charging. A Stanford study showed that by continuing to charge the cars in the evenings or overnight, the grid will experience

significant stress without added investments [1]. Moreover, another study found out that off-site parking access, especially in cities, is not available for all drivers. In the UK, this parking and charging availability in various cities ranges from 50 % up to 70 %. Thus, in this work, 65 % of passenger electric vehicles are charged typically overnight while 35 % use daytime charging, mostly during workhours at their work location. In more details, this second group can be represented at best from commuters.

	Bundle 6	Bundle 7	Bundle 8	Bundle 9
Share to total buses/trucks	86 %	14 %	70 %	30 %
Model	E-Citaro	E-Citaro	Volvo FL Electric	Volvo FL Electric
Energy source	Electricity	Electricity	Electricity	Electricity
Battery capacity	292 kWh	292 kWh	265 kWh	265 kWh
Annual driven distance	57 760 km	57 760 km	24 000 km	36 000 km
Plugged-in duration per week	84 hours	84 hours	30 hours	48 hours
Charging time	Overnight	Daytime	Overnight	Overnight
Charging power	DC fast charging; 50 kW	DC fast charging; 50 kW	DC fast charging; 50 kW	DC fast charging; 50 kW

Table 3.2: Electric bus and truck specifications in the different vehicle bundles

Light and medium duty trucks together with bus public transport constitute the next four vehicle bundles as shown in Table 3.2. They are represented by one vehicle type respectively, the E-Citaro bus for the public transport and Volvo FL Electric for the goods transport.

Similar to the Table 3.1, the vehicle data are based on the datasheets from each of the vehicle types [50, 51]. Regarding the annual driven distance for the busses in Vienna, the average distance of the bus lines is 6,6 km and the average speed 17,1 km/h [52]. Based on these data, each bus can cover 12 full round trips, or one round trip per hour. In case of the light and medium duty trucks, the average annual driven distance of truck drivers in Germany sums up at approximately 24 000 km [53]. The second truck bundle (Bundle 9) represents the use case of two work-shifts, thus assuming 50 % higher travelled kilometers. Due to large battery capacities, all these vehicle bundles have to be charged in DC fast charging stations in order to achieve the required plug-in time periods. These charging stations are thought to be located at the respective parking lots, where the vehicles can be charged overnight.

Regarding the fuel cell electric vehicles and the respective mobility load, an electrolyser, a storage tank, a hydrogen compressor, and cooler are required for the hydrogen production and storage. The selected proton exchange membrane (PEM) electrolyzer has a nominal power of 4 MW which corresponds to the maximum production of 1800 kg H_2 per day [54]. Thus, this electrolyzer has an energy consumption of 53,33 kWh

per kg of H_2 and a system efficiency of 74 %. As the highest H_2 output pressure from the electrolyzer is only 30 bar, it needs to be compressed to higher pressure values for better storage purposes. Some experts have shown that 500 bar is the optimal pressure for hydrogen storage, as it provides a good combination of volume-to-cost, and it can avoid short compressor operations in refueling processes [55]. Therefore, a hydrogen storage tank of 1000 kg at 500 bar has been selected in this work. Compressing the hydrogen coming out of the electrolysis to 500 bar requires 2,33 kWh of energy per each kg of H_2 [56]. Before storing it in the hydrogen tank, the hydrogen needs to be cooled to ideally -40 °C due to better refueling conditions and shorter refueling durations. This cooling process has an energy consumption of 0,15 kWh per kg of H_2. All the components above are included in a hydrogen refueling station, which in this work it is assumed to be placed next to the overnight parking lot of these vehicles. Depending on the penetration rate of fuel cell vehicles, the hydrogen refueling station components should be adapted with multiples of the defines parameters.

In this work, fuel cell electric vehicles include only buses for public transport and light-to-medium duty trucks for goods transport. The well-to-wheel efficiency of battery electric vehicles ranges between 75 - 85 % while for fuel cell vehicles, the efficiency drops to 35 % due to electrolysis losses [57]. Thus, passenger fuel cell electric vehicles were not taken into consideration because of their lack of overall benefits on short distances compared to battery electric vehicles. The last four vehicle bundles represent the fuel cell buses and trucks as shown in Table 3.3 below.

	Bundle 10	Bundle 11	Bundle 12	Bundle 13
Share to total buses/trucks	86 %	14 %	70 %	30 %
Model	Urbino 12	Urbino 12	Hyundai XCIENT	Hyundai XCIENT
Energy source	Hydrogen	Hydrogen	Hydrogen	Hydrogen
Hydrogen tank	37,5 kg H2 (1 237 kWh)	37,5 kg H2 (1 237 kWh)	31 kg H2 (1 033 kWh)	31 kg H2 (1 033 kWh)
Annual driven distance	57 760 km	57 760 km	24 000 km	36 000 km
Refueling time per week	84 hours	84 hours	45 hours	24 hours
Refueling time	Overnight	Daytime	Overnight	Overnight

Table 3.3: Fuel cell electric bus and truck specifications in the different vehicle bundles

Similar to the prior tables, the vehicles' data are in accordance with the datasheets of each vehicle type [58, 59]. These fuel cell vehicles contain hydrogen stored at 350 bar in the hydrogen tanks. For better comparative purposes, the annual driven distance is kept the same as in the battery electric buses and trucks. The refueling time in disposal represents the time period that the fuel cell vehicles are available to be refueled, however in contrast to battery electric vehicles, the fuel cell trucks, and buses have much shorter refueling times at approximately 15 - 20 minutes.

3.2.2 Rural use case

The second use case is a regular rural are represented by the town of Großschönau, which is located in the northwestern region of Lower Austria. This town holds 1 230 residents as of the year 2022 [60]. In the state of Lower Austria, there are on average 2,26 residents per household [61]. Therefore, there are approximately 545 households in the town of Großschönau with an emphasized majority being one-family houses. As for the local load profile, the annual energy consumption of an average household and the respective H0 profile is kept equal to the previous suburban use case.

In regard to solar PV supply, the state of Lower Austria has a renewable energy goal of 3 000 MWp of installed capacity until 2030 [62]. In this thesis, it is assumed that half of this installed capacity is targeted towards residential housing. By breaking it up to each household, it accounts to an average installed capacity of 2 kWp per household. Therefore, the aggregated installed capacity in this use case sums up to 1,1 MWp. By keeping the same ratio of installed PV to storage capacity as in suburban use case, the aggregated battery capacity adds up to 1,1 MWh with a power output of 1,1 MW. In this case, as the households are more separated and the aggregated battery capacity is smaller than previous use case, the distributed approach with hundreds of small-scale 10 kWh battery systems works better.

The car ownership rate in the state of Lower Austria was determined at 661 cars per 1000 residents [63]. Therefore, the amount of registered passenger cars in Großschönau is assumed at approximately 813 vehicles. Furthermore, considering the ratio of approximately 63 registered trucks per 1000 residents in the state of Lower Austria, the number of trucks located in this area is assumed at 77 [64].

In regard to the vehicle bundles that are taken into consideration in this use case, the bundles of passenger electric vehicles (Bundles 1 - 5) and those of light-to-medium duty trucks (Bundles 8, 9, 12, 13) are kept identical to suburban use case for better comparison. As there is no public transport available nor required within the town, the vehicle bundles of public transport are not considered.

The hydrogen production and storage are adapted to the lower number of fuel cell vehicles that need to be refueled in this area in order to maintain a good volume-to-cost ratio and high full load hours. Thus, the PEM electrolyzer has a 1 MW nominal power with a maximum hydrogen production of 450 kg H_2 per day. This is also regarded as one of the smallest electrolyzer of this technology. As for the hydrogen compression and cooling processes, there are no changes undertaken. Moreover, the hydrogen storage tank of 500 kg at 500 bar is further used for higher flexibility purposes.

3.3 Definition of charging optimisation scenarios

The following section describes the penetration rate of EVs and FCEVs in each of the prior use cases and the respective electric vehicle charging scenario. The penetration

rate of EVS and FCEVs is based on the current number of registered vehicles in each of the use cases and the assumption of converting the specific percentage of internal combustion engine vehicles into electric vehicles. So, the total number of vehicles will not change in the next years. For comparison purposes, the standard scenario is comprised of only the aggregated non-flexible residential load, without any distributed energy generation or storage and in the absence of any EVs or FCEVs in the transportation sector. Furthermore, there are three optimization scenarios that contain the residential load, PV supply and battery storage as well as solely battery electric vehicles with different penetration rates. The other three optimization scenarios are similar to the previous ones, however with the difference that there is a mobility mix between battery electric vehicles for passenger cars and fuel cell electric vehicles for the buses and light-to-medium duty trucks.

Battery electric vehicles

The first three scenarios differ based on the penetration rate of battery electric vehicles. In the first scenario, the residential load, PV supply and battery storage are subject to each use case while there is a 10 % penetration rate of battery electric vehicles for passenger cars and trucks. In addition, the road public transport represented by battery electric buses has a 100 % penetration rate as this share of the mobility mix can be converted in the early steps because of their predictable driving behavior. This scenario is clearly linked to the EU climate goals for 2030, in which is stated that 37,5 % of CO_2 emissions coming from passenger cars and light-to-medium duty trucks should be reduced and this translates into 590 000 electric vehicles being on the road by 2030 [65]. Another report forecasted the penetration of electric trucks into the global medium duty market to reach approximately 10 % by 2030 [66].

The second scenario contains the same charging methods but in contrast to the first scenario, the penetration rate of battery electric vehicles for passenger cars and trucks increases to 25 % while battery electric buses remain at 100 %. The third scenario represents the most optimistic scenario in terms of EVs share in the mobility mix, as the penetration rate of battery electric vehicles for passenger cars and trucks increases to 50 %. These three scenarios provide the necessary results in the next steps towards the end goal of climate-neutral mobility by 2040 [67].

Fuel cell electric vehicles

These next three optimization scenarios are similar to the previous scenarios regarding the residential load, PV supply and battery storage capacities. Nevertheless, the mobility mix in these scenarios is divided between battery electric vehicles for the passenger cars and fuel cell vehicles for the buses and light-to-medium duty trucks. This selection is based on the respective benefits of each technology and the added advantages of hydrogen vehicles in long-haul distance trips as well as fast refueling.

The fourth optimization scenario is similar to the first one, however the 10 % penetration rate of battery electric buses and the 100 % battery electric buses are replaced with

fuel cell vehicles. In this way, the mobility mix is comprised of 10 % battery electric vehicles, 10 % fuel cell trucks and 100 % fuel cell buses. Also, the next two scenarios are analogous to scenario 2 and 3, but in this case, there are 25 % and 50 % fuel cell trucks respectively instead of battery electric trucks, while the whole battery electric buses are also converted to fuel cell buses. A summary of all optimization scenarios can be found at Table 3.4.

	Standard	Scenario 1	Scenario 2	Scenario 3	Scenario 4	Scenario 5	Scenario 6
Residential Load	Yes	Yes	Yes	Yes	Yes	Yes	Yes
PV supply	No	Yes	Yes	Yes	Yes	Yes	Yes
Battery storage	No	Yes	Yes	Yes	Yes	Yes	Yes
Passenger vehicles	No	10 % (electric)	25 % (electric)	50 % (electric)	10 % (electric)	25 % (electric)	50 % (electric)
Buses	No	100 % (electric)	100 % (electric)	100 % (electric)	100 % (hydrogen)	100 % (hydrogen)	100 % (hydrogen)
Light-to-medium duty trucks	No	10 % (electric)	25 % (electric)	50 % (electric)	10 % (hydrogen)	25 % (hydrogen)	50 % (hydrogen)

Table 3.4: List of all optimisation scenarios and the respective loads

Charging methods

The optimization scenarios outlined above encompass three charging methodologies, determined by the input parameters. The first of these is instant or immediate charging, whereby the charging process for each electric vehicle commences as soon as it is plugged in. This mode of charging represents the current state of affairs in most charging stations, as smart charging solutions are still in their nascent stages and only exist in isolated instances. This study implements instant charging by limiting the plug-in duration to that required for full battery charge, which varies among vehicle bundles due to differing battery capacities.

As a secondary charging method, this work proposes cost-based smart charging, which only prioritizes cost optimization. This approach considers the duration of an electric vehicle's stay at a charging station as the plug-in time period. Research indicates that 65 % of battery electric vehicles are charged overnight, with the plug-in time period extending from the moment they are parked until the driver's departure the following morning. The remaining vehicles are charged during the day, with a shorter plug-in time period due to driving patterns such as commuters charging at their workplace. The model optimizes the charging transaction based on the specific plug-in duration to minimize charging costs, without any limitations imposed by the electrical grid other than the charging station power supply capabilities.

A third charging methodology is presented in which smart charging is combined with parallel charging restrictions of 20 % for passenger cars and 50 % for trucks. The plug-in duration remains unchanged from the previous cost-based smart charging methodology. These technical constraints simulate the finite number of charging stations and the limitations of the existing electrical grid infrastructure in terms of power supply. These additional charging constraints result in a solution that is more aligned with real-world conditions, as the power supply is limited and significant fluctuations are not technically feasible. Consequently, smart charging with parallel charging constraints represents a compromise between reducing charging costs and achieving regional load balancing.

CHAPTER 4

Results

The implementation of the previously introduced methodology with the goal of understanding the effects of additional EVs and FCEVs in the residual load of a region follows below. This chapter describes the most important results of the two use cases and the outlined optimization scenarios. The results of each use case (Section 4.1 and Section 4.2) include the technical findings in terms of load profile and peak load as well as economical outcomes relating to energy procurement costs. The discussion of the results is shown in Chapter 5.

4.1 Suburban use case

4.1.1 Load profiles and peak loads

Scenario 1 - 10 % EV penetration

In this section, the load profiles and the development of peak loads originating from the defined optimization scenarios are determined in different time periods. Starting with the first scenario and its comparison with the standard scenario, the results' graphs are shown below. The chosen timeframe is a two-day period during the wintertime, that represents the behavior of winter months. The main goal of these plots is to show the general differences between the load profiles of each charging scenario in a 48-hour time period. Figure 4.1a displays the typical aggregated residential load profile (blue) and the load profile resulting from the optimization scenario with instant charging method (orange). The standard load profile has a peak load of 82,35 MW during evening hours (18:45) while the peak load originating from instant charging load profile amounts to 157,26 MW, resulting in an 91 % increase in the peak load. In addition, the electricity price (yellow) is also included to gain a better understanding of the correlation between charging methods and electricity prices. Because of electricity price volatility, the generated load profile contains numerous fluctuations that correspond to high load peaks when charging the battery reserve in time periods of low prices and vice versa.

Furthermore, as the plug-in time periods begin from 15:00, the new peaks resulting from instant charging can be seen in the afternoon and evening hours.

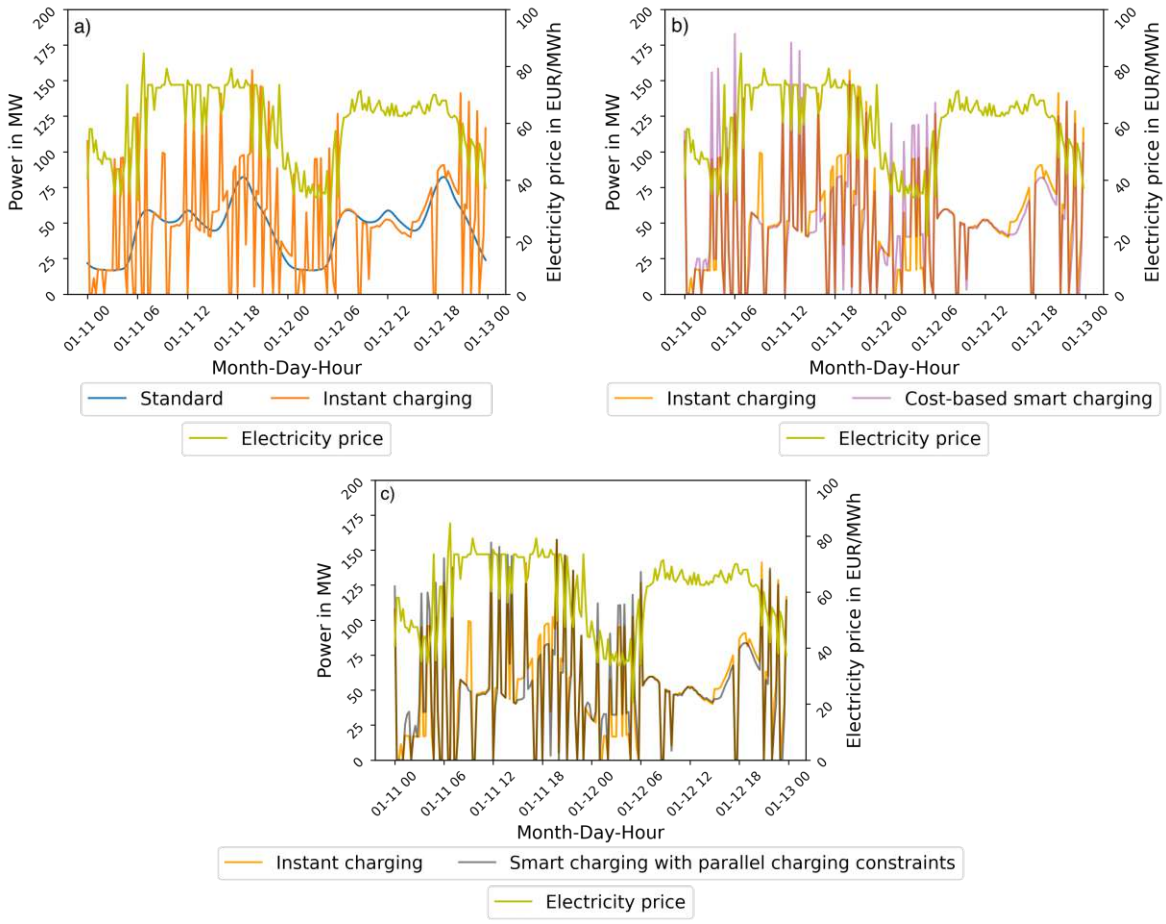

Figure 4.1: Load profiles of different charging methods; a) Standard scenario and Instant charging load profile; b) Instant charging and cost-based smart charging load profile; c) Instant charging and smart charging with parallel charging constraint method

Figure 4.1b shows the load profiles of the instant charging and smart charging methods. The graphs are plotted with a 50 % transparency in order to better notice the time periods with the same load profile. As shown, the smart charging approach contains peak loads of up to 182,85 MW during early morning hours (06:00) which results into 122 % higher peak loads compared to standard load profile and an increase of 16,3 % compared to instant charging. Furthermore, a certain level of load shifting is achieved as the highest peak loads appear during night hours. It is also important to notice that the smart charging approach generally delivers higher peak loads because of its objective function to find the most cost-optimal time periods to charge the electric vehicles. In Figure 4.1c, the smart charging approach with additional technical constraints in parallel charging can be found and its comparison to instant charging method. This approach delivers peak loads of up to 157,48 MW in evening hours (19:45), very similar to instant charging, while having a significantly lower costs. In contrast to smart

charging (purely cost-based charging), this approach delivers approximately 14 % lower peak loads, especially during night hours, while also achieving load shifting.

The next step is to extrapolate the previous short-term results for the full year of 2021, divided into months. Thus, the results are more generalized and comprehensive, while the effects of possible outliers are avoided. Figure 4.2 shows the monthly peak loads of each charging scenario for a whole year.

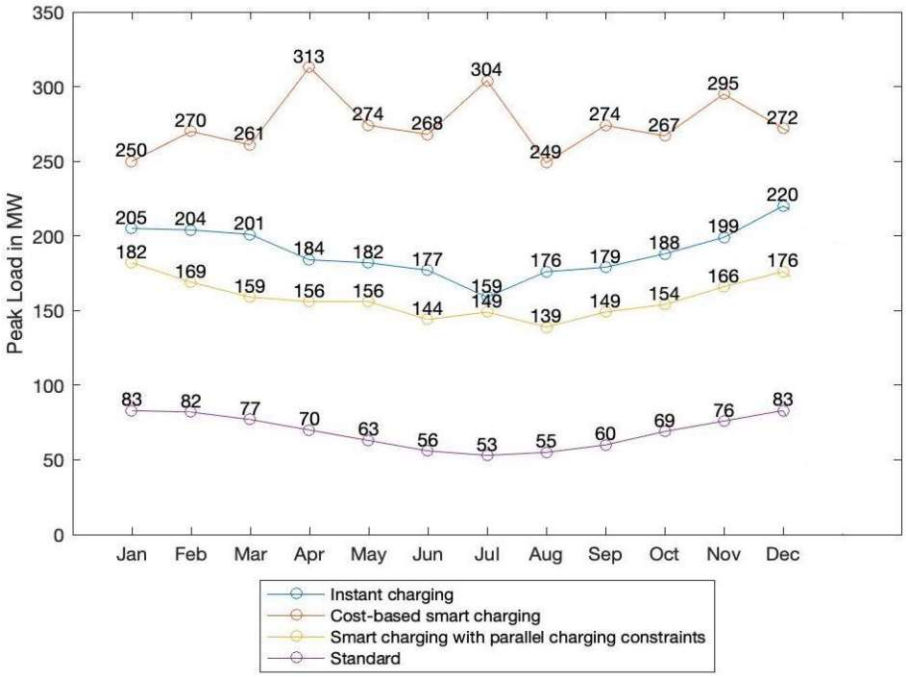

Figure 4.2: Monthly peak loads of all charging methods in scenario 1

As shown above, the standard load profile with solely aggregated residential load delivers the lowest peak loads as expected. By including the additional loads of charging scenario 1, all charging methods provide higher peak loads compared to standard scenario. Smart charging method delivers the highest peak loads throughout the whole year because of its goal to minimize costs and not focus on the peak load. It is important to note that high peak loads of higher than 200 MW happen sporadically 2 - 10 times a month in timeslots with very low electricity prices. During the absolute majority of the time (+95 %), smart charging approach resembles the other charging approaches. The results also show that the smart charging method has different behavior compared to other charging approaches (for example April and July), as it delivers higher peak loads compared to previous months while all other charging methods continue on a downwards trend mainly because of increasing weather temperatures. In the Figure 4.17 below, one month was chosen as a representation of each season and the peak load comparisons are shown.

Starting with January as a winter month, the instant charging method delivered a peak load 145 % higher than the standard scenario, while smart charging and smart charging

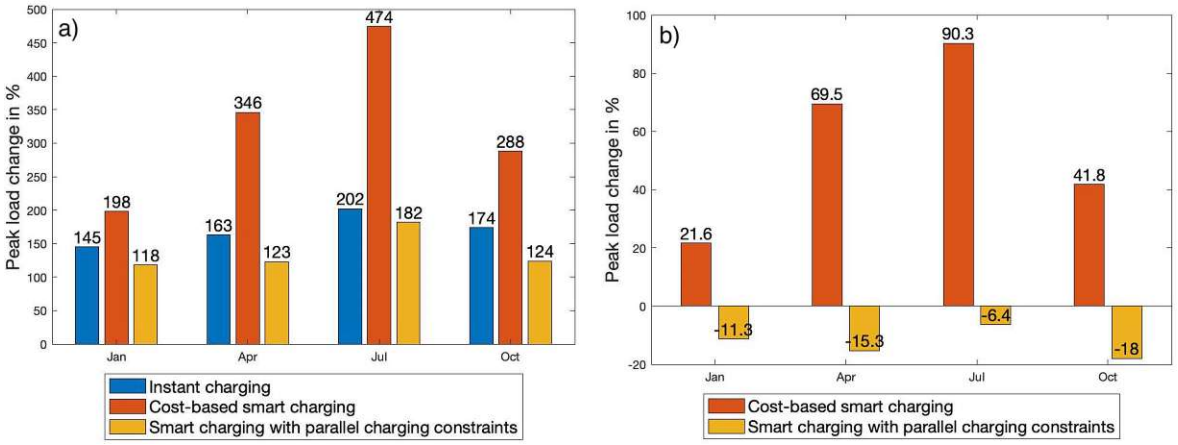

Figure 4.3: a) Comparison of the peak loads of each charging method with standard scenario and, b) comparison of the peak loads of the two smart charging methods with instant charging method in different months

with parallel charging constraint method's peak load amounted to an increase of 198 % and 118 % compared to standard scenario. The results of the other months and seasons show similar results in regards to instant charging and smart charging with parallel charging constraints, and the latter delivers the lowest peak loads throughout the whole year. On the other side, the smart charging approach delivers increased peak loads of up to 474 % higher compared to standard scneario.

Figure 4.3b shows the comparison of the two smart charging approaches with the instant charging approach in terms of peak load results. Smart charging delivers peak loads of up to 90,3 % higher than instant charging in summer months and the lowest differences with 21,6 % in winter months. On the other hand, smart charging with parallel charging constraints delivers consistantly lower peak loads throughout the year, with up to -18 % in October. This shows that smart charging with parallel charging constraint provides the best load profiles among the selected approaches.

Scenario 2 - 25 % EV penetration

The second scenario has an increased EV penetration from 10 % to 25 % as explained in Section 3.3. Similar to above, the Figure 4.4 presents the monthly peak loads of each charging scenario throughout the year. The results show resembling behavior to Scenario 1, as smart charging approach provides the highest peak loads, followed by instant charging method. It is again important to note that high peak loads of higher than 200 MW happen occasionally 2-10 times a month in timeslots with very low electricity prices. The smart charging with parallel charging constraints approach displays the lowest peak loads among the charging approaches. In comparison to Scenario 1, the peak loads have an increase of 27 % in the case of smart charging with parallel charging constraints and an increase of up to 85 % in the case of smart charging method, as the EV penetration increases from 10 % to 25 %.

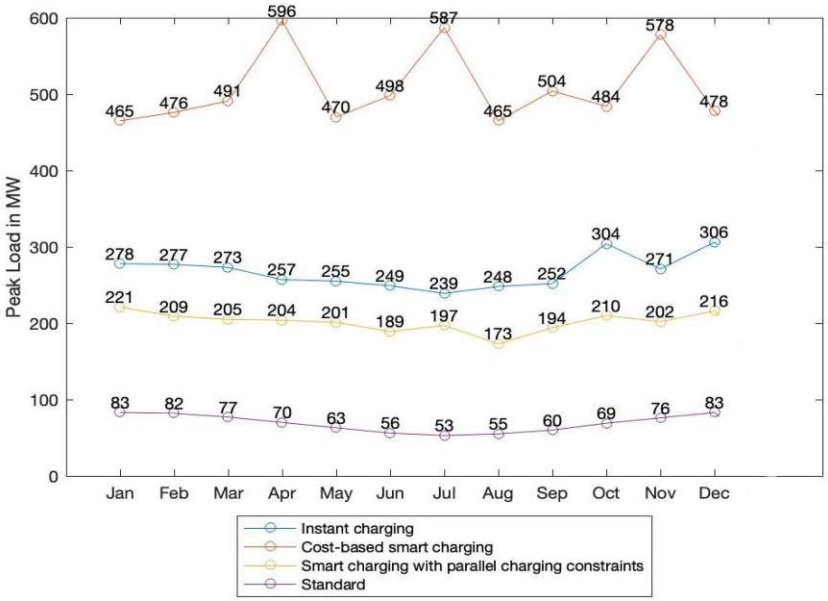

Figure 4.4: Monthly peak loads of all charging methods in scenario 2

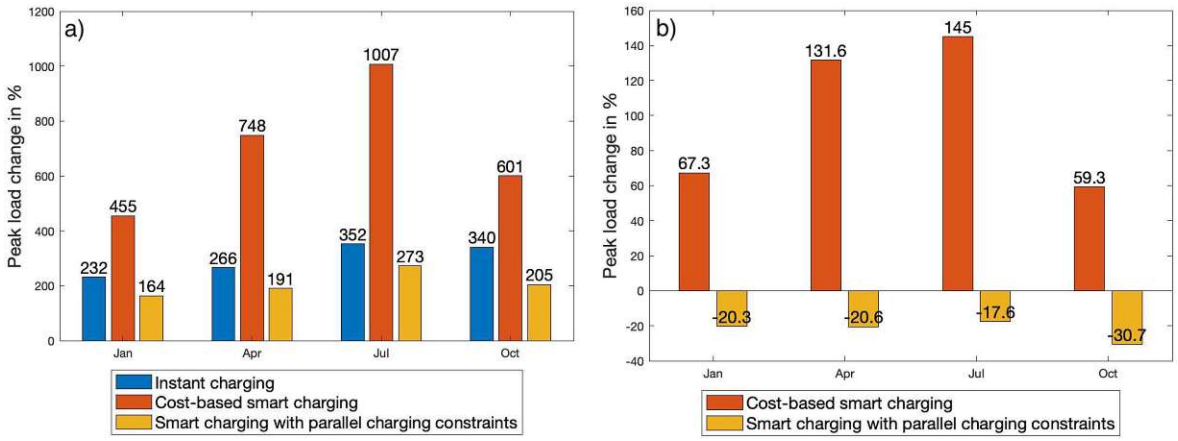

Figure 4.5: a) Comparison of the peak loads of each charging method with standard scenario and, b) comparison of the peak loads of the two smart charging methods with instant charging method in different months

In the Figure 4.5a, the comparison of the peak loads of each charging scenario with the standard scenario is shown. In the winter month, the instant charging approach delivered a peak load 232 % higher than the standard scenario, while the two other charging approches provided an increased peak load of 455 % and 164 % respectively. In seasons with higher outdoor temperatures such as in spring and summer months when the residential load is lower, the impact of the mobility load in the load profile is much higher. Thus, the smart charging approach delivered up to 1007 % higher peak loads compared to the standard scenario. On the other hand, the smart charging with parallel charging constraints provides the best results among the other options, as it can be seen in Figure 4.5b.

Scenario 3 - 50% EV penetration

In the third scenario, the electric vehicle penetration is higher, reaching 50 % as previously discussed in Section 3.3. Like the previous scenarios, Figure 4.6 illustrates the monthly peak loads for each charging method throughout the year. The results show an ongoing pattern similar to previous scenarios, where the smart charging approach leads to the highest peak loads, followed by the instant charging method and smart charging scenario with parallel charging constraints. The very high peak loads of more than 400 MW in smart charging approach continue to be sparse with only 13 quarter-hour timeslots in the month of April as shown in Figure 4.7. This month was chosen because it is also the month with the highest peak load overall. Furthermore, the highest peak load is zoomed in in Figure 4.8, in order to show the overlap of electric vehicle charging in the time frames with the lowest electricity prices. The smart charging method with parallel charging constraints shows the lowest peak loads among the charging methods. In comparison to the second scenario, the peak loads experience an increase of 43 % with the smart charging method with parallel charging constraints and up to 77 % with the smart charging method, as EV penetration doubles from 25 % to 50 %.

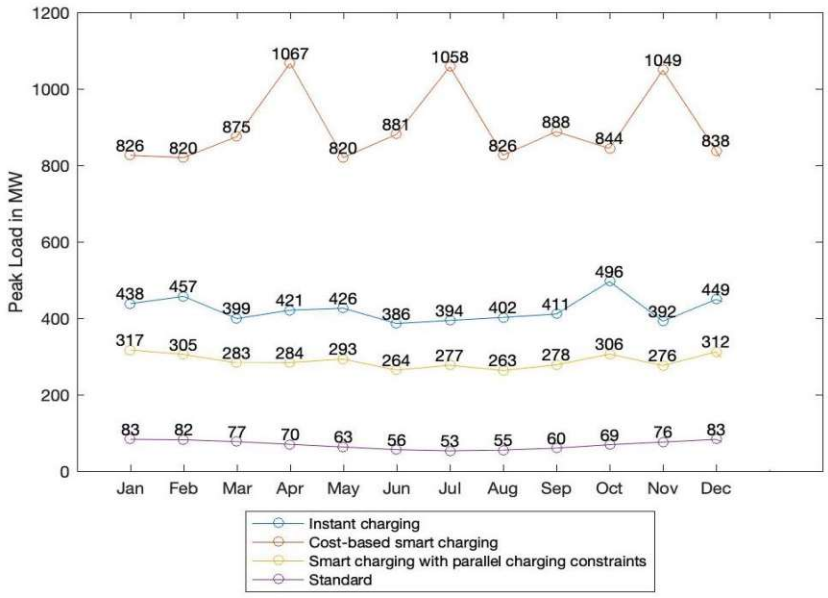

Figure 4.6: Monthly peak loads of all charging methods in scenario 3

The graph in Figure 4.9a illustrates the difference in peak loads between different charging approaches and a standard scenario. During January as a winter month representative, the instant charging method resulted in a peak load that was 423 % higher than the standard scenario. Meanwhile, the other two charging methods led to peak loads that were 886 % and 279 % higher, respectively. During warmer months, such as April and July, when residential load is lower, the impact of mobility load on

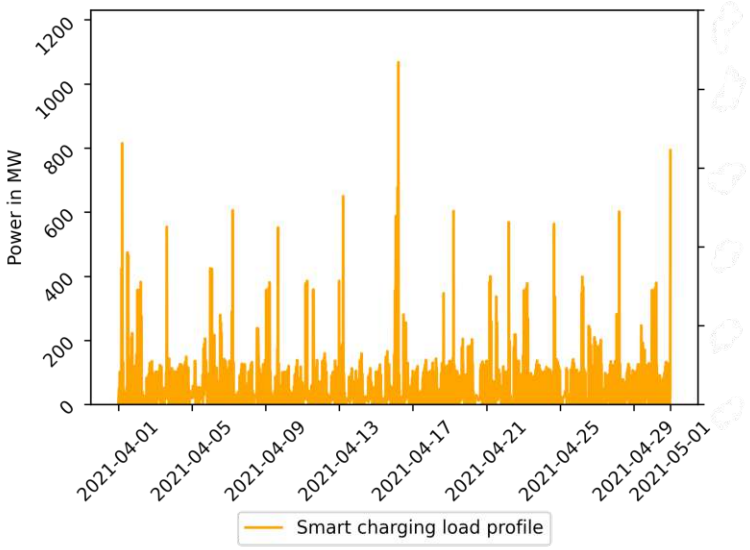

Figure 4.7: Load profile in the month of April

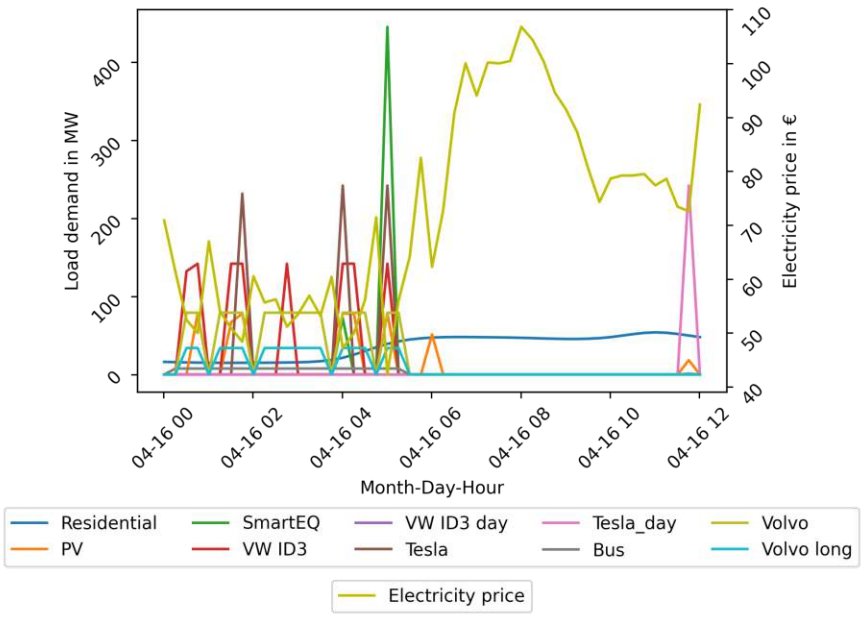

Figure 4.8: Load profile in a 12 hour timeframe in April

the load profile is more significant. As a result, the smart charging approach resulted in extremely large peak loads that were up to approximately 1900 % higher than the standard scenario. However, the smart charging with parallel charging constraints still performed the best, consistently delivering 27 - 38 % lower peak loads than the instant charging approach, as shown in Figure 4.9b.

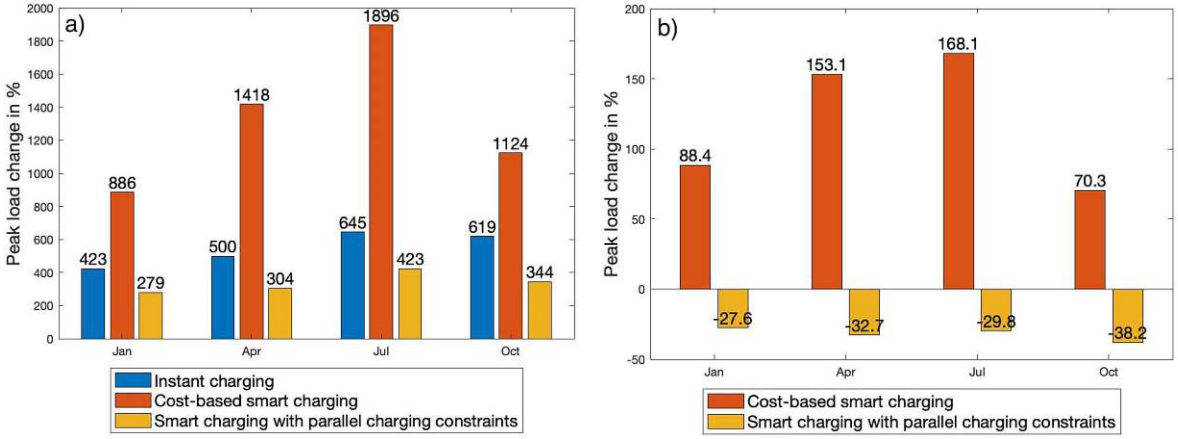

Figure 4.9: a) Comparison of the peak loads of each charging method with standard scenario and, b) comparison of the peak loads of the two smart charging methods with instant charging method in different months

Scenario 4 - 10 % BEV & FCEV penetration

In the fourth scenario, the mobility load is comprised of 10 % battery electric vehicles for passenger cars, 10 % fuel cell electric vehicles for light-to-medium trucks and 100 % fuel cell electric buses as discussed in Section 3.3. Figure 4.10 shows the monthly peak loads for the standard scenario and the two smart charging approaches. There is no instant charging method included in these scenarios because of the nature of hydrogen preparation and refuelling. The results show a pattern like the first scenario, with the smart charging approach resulting in the highest peak loads, followed by the smart charging scenario with parallel charging constraints with approximately 41 % lower peak loads than smart charging approach. It is important to note that the parallel charging constraint applies only to the battery electric vehicles serving as passenger cars. In comparison to the first scenario with solely battery electric vehicles, the peak loads decrease by 3,2 % with the smart charging method and by 1,7 % with the smart charging method with parallel charging constraints.

In the Figure 4.11a, the comparison of the peak loads of each charging scenario with the standard scenario is displayed. In the winter month, the smart charging approach delivered peak loads 197 % higher than the standard scenario, while the smart charging with parallel charging constraint provided 116 % higher peak loads. In warmer months, the smart charging approach delivered up to 444 % higher peak loads compared to the standard scenario such as in July. On the other hand, the smart charging with parallel charging constraints provides consistent increases in the range of 115-170 % compared to standard scenario throughout the year.

The graph in the Figure 4.11b shows the comparison between each charging approach with the respective charging method in the first scenario. The charging approaches in the fourth scenario delivers generally lower peak loads with peak load reductions of up to 5 % in the summer months. In the month of October, the smart charging of the fourth scenario with fuel cell trucks and buses delivered 0,91 % higher peak loads

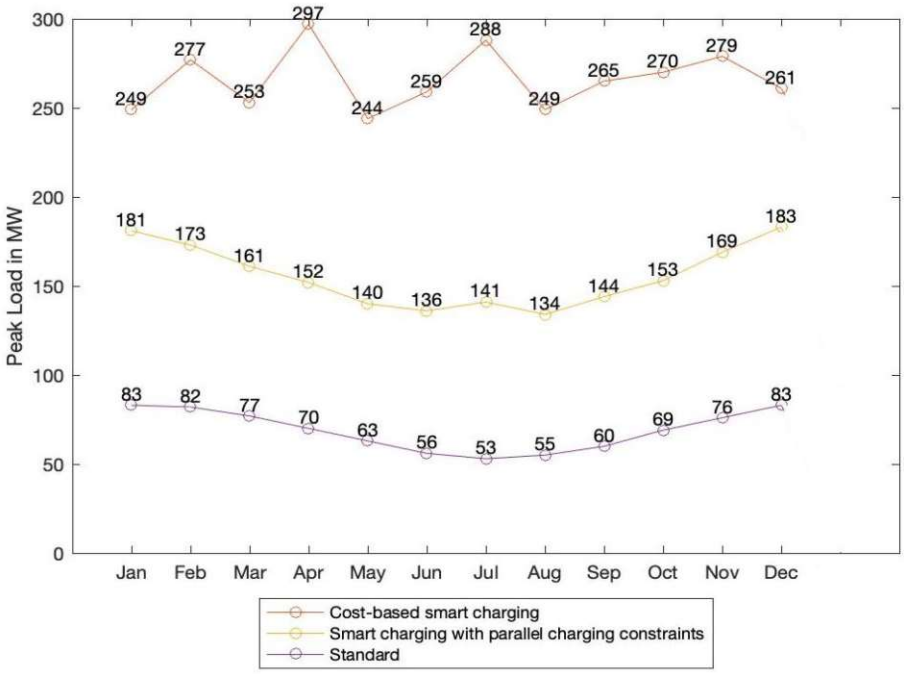

Figure 4.10: Monthly peak loads of all charging methods in scenario 4

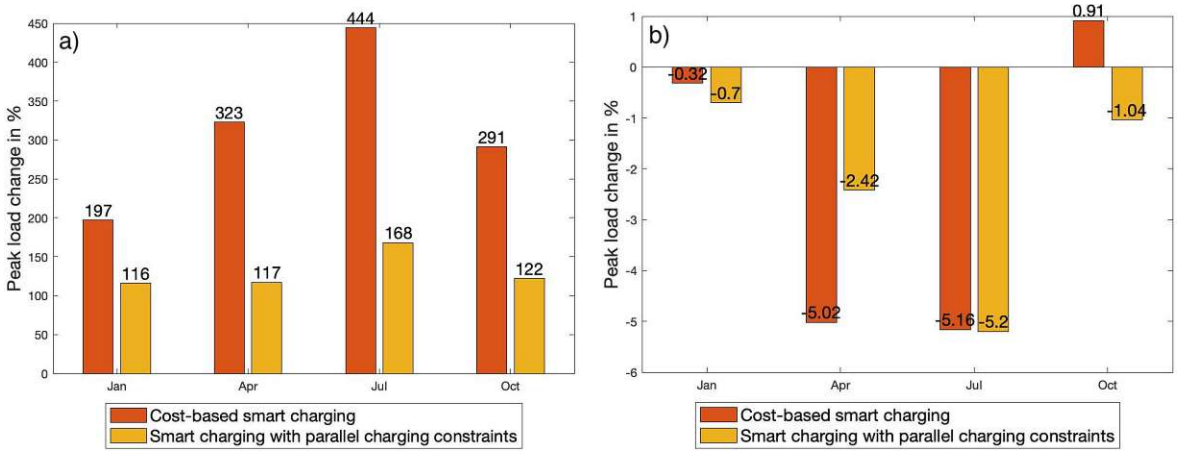

Figure 4.11: a) Comparison of the peak loads of the two smart charging methods with standard scenario and, b) comparison of the peak loads of the charging methods with the first scenario in different months

compared to the first scenario with solely battery EVs.

Scenario 5 - 25 % BEV & FCEV penetration

In the fifth scenario, the electric and fuel cell vehicle penetration rate rises from 10 % to 25 %, as detailed in Section 3.3. Like the previous scenarios, Figure 4.12 displays the monthly peak loads for each charging method throughout the year. The results indicate that the smart charging approach results in the highest peak loads. It is worth noting that peak loads above 300 MW occur infrequently, only 11 times in

the month of April as shown in Figure 4.13, during periods of low electricity prices. The smart charging method with parallel charging constraints delivers on average 59 % lower peak loads compared to solely cost-based smart charging. Compared to Scenario 2 with solely battery electric vehicles, the peak loads decrease on average by 2,13 % with the smart charging method and increase by 0,3 % with the smart charging with parallel charging constraints method.

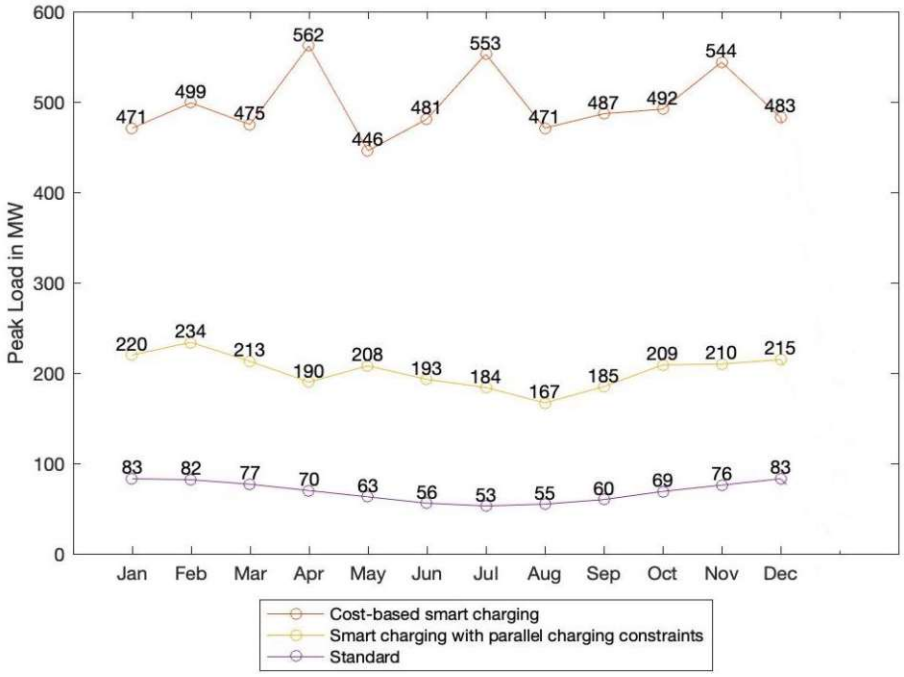

Figure 4.12: Monthly peak loads of all charging methods in scenario 5

The peak loads of each charging scenario in relation to the standard scenario are displayed in Figure 4.14a. In the winter months, the smart charging approach resulted in peak loads that are 462 % higher than the standard scenario, while the smart charging with parallel charging constraints approach resulted in peak loads that were 163 % higher. In warmer months, such as July, the smart charging approach resulted in peak loads that were up to 943 % higher than the standard scenario. In contrast, the smart charging with parallel charging constraints approach consistently delivered peak loads that were 160 - 250 % higher than the standard scenario throughout the year.

Figure 4.14b shows the comparison between each charging approach in the fifth scenario and the respective charging method in the second scenario. The charging approaches in this scenario generally produced lower peak loads, with peak load reductions of up to 7 % in the April. In January and October, the smart charging approach in this scenario, which includes fuel cell trucks and buses, resulted in peak loads that were 1,21 % and 1,64 % higher than the second scenario, which only includes battery EVs.

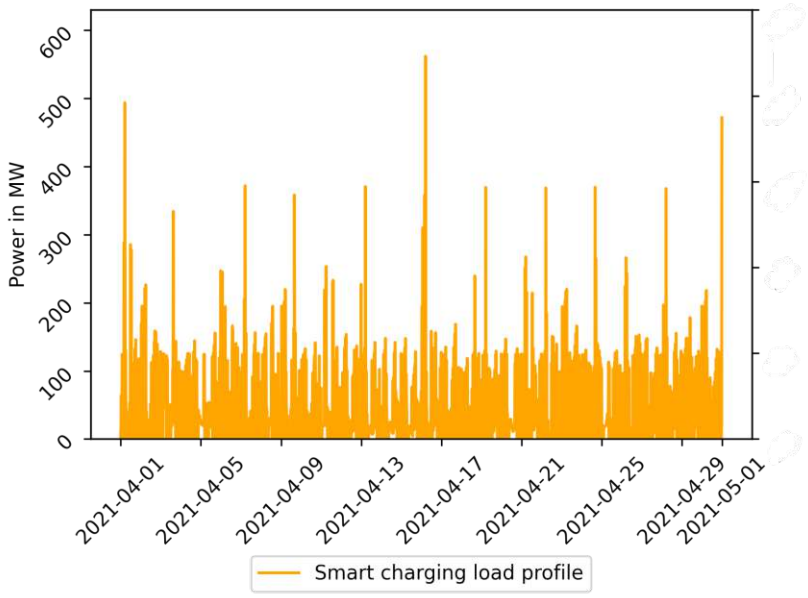

Figure 4.13: Load profile in the month of April

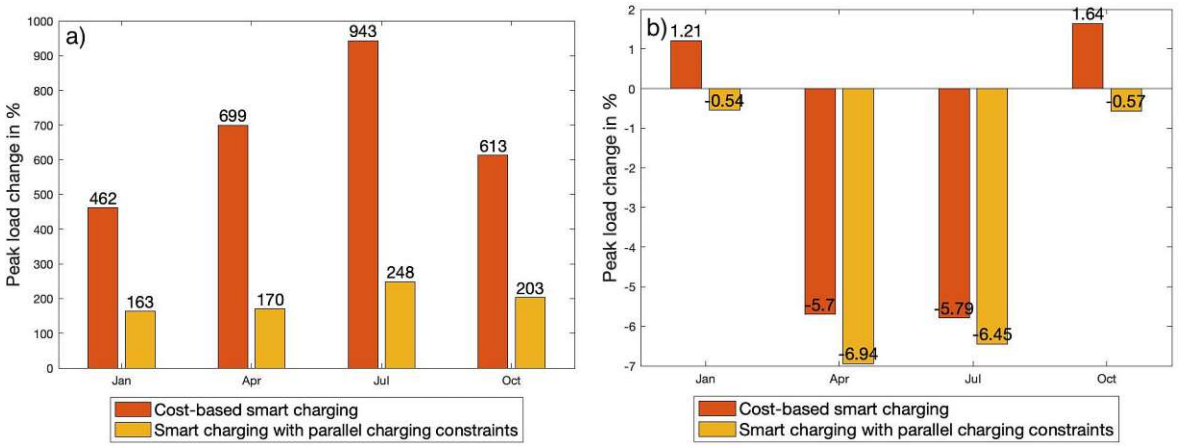

Figure 4.14: a) Comparison of the peak loads of the two smart charging methods with standard scenario and, b) comparison of the peak loads of the charging methods with the second scenario in different months

Scenario 6 - 50% BEV & FCEV penetration

In the last scenario, the electric and fuel cell vehicle penetration rate double from 25 % to 50 %, as detailed in Section 3.3. As in the previous scenarios, Figure 4.15 displays the monthly peak loads for each charging method throughout the year. The results continue to show a consistent pattern where the smart charging approach leads to the highest peak loads, followed by the smart charging scenario with parallel charging constraints with 65 % lower peak loads on average throughout the year. The very high peak loads of over 400 MW in the smart charging approach remain infrequent, with only 12 quarter-hour timeslots in April. Compared to the third scenario, peak loads decrease by 1,9 % with the smart charging method and increase by 5 % with the smart

charging with parallel charging constraints method.

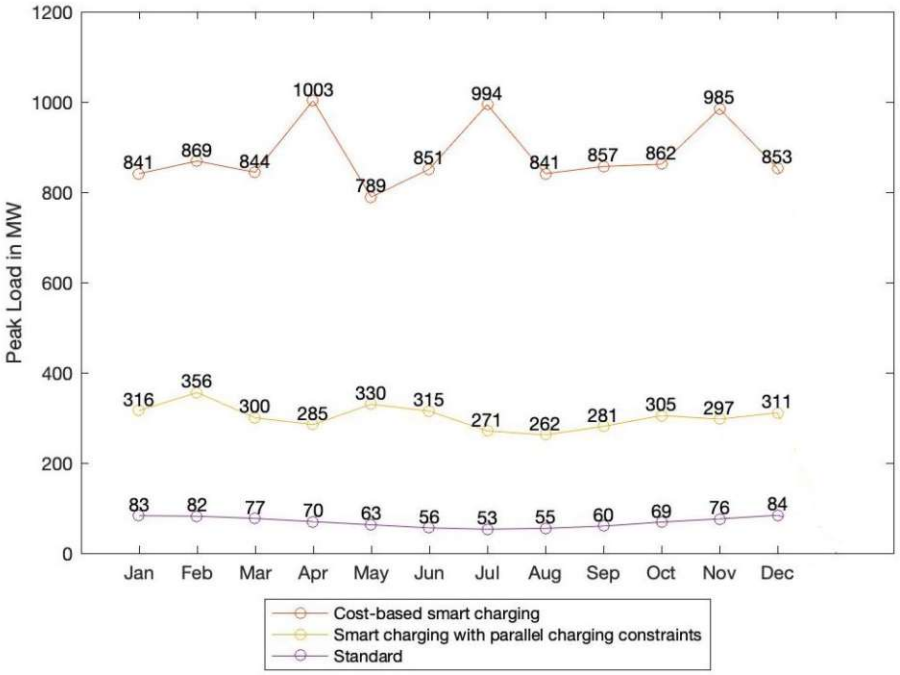

Figure 4.15: Monthly peak loads of all charging methods in scenario 6

Figure 4.16a displays the peak loads of each charging scenario in relation to the standard scenario. In January, the smart charging approach resulted in peak loads that were 903% higher than the standard scenario, whereas the smart charging with parallel charging constraints approach resulted in peak loads that were 278 % higher. During warmer months, such as July, the smart charging approach resulted in extremely high peak loads that were up to 1775 % higher than the standard scenario. In contrast,

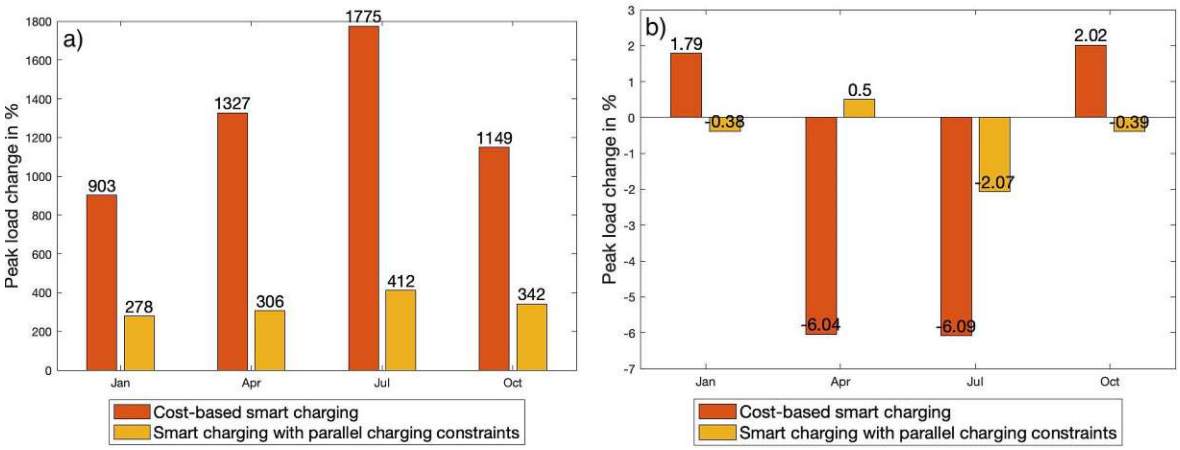

Figure 4.16: a) Comparison of the peak loads of the two smart charging methods with standard scenario and, b) comparison of the peak loads of the charging methods with the third scenario in different months

the smart charging with parallel charging constraints approach consistently delivered peak loads that were approximately 280 - 410 % higher than the standard scenario throughout the year.

Figure 4.16b compares each charging approach in the sixth scenario with the respective charging method in the third scenario. The charging approaches in this scenario generally resulted in lower peak loads, with peak load reductions of up to 6 % in April and July. In January and October, the smart charging approach in this scenario which includes fuel cell trucks and buses, resulted in peak loads that were 1,79 % and 2,02 % higher than the third scenario.

4.1.2 Energy procurement costs

In this section, the energy procurement costs for the previous scenarios are demonstrated. Starting with the first three scenarios that include only battery electric vehicles in the mobility load, Figure 4.17a shows the comparison of each charging scenario with the standard scenario. The month of January and July was chosen as they have the same amount of days and it represent the best difference in the electricity costs' behavior between summer and winter months.

Beginning with January in the first scenario, with the inclusion of PV generation, battery reserve and mobility load, the energy procurement costs in the instant charging approach amounted to 4 057 458 EUR and are 26,21 % higher than the standard scenario which came up to 3 214 919 EUR. By switching to cost-based smart charging, the energy procurement costs increase by only 24,3% compared to standard scenario, with a 1,51 % decrease compared to instant charging. The third charging approach, that delivered better load profiles as shown in the previous section, is slightly more expensive than the cost-based smart charging with a 0,15 % increase in energy costs. Overall, with the added mobility load of 10 % battery EV penetration, the energy costs increased by an average of 24 - 26 % among different charging approaches.

In the second scenario where battery electric vehicle penetration increases to 25 %, energy costs have risen by an average of 44 - 48 % across various charging methods in comparison to the baseline scenario. The instant charging approach remains the most cost-prohibitive, with expenses totalling up to 4,77 million EUR or 48,38 % higher than the baseline scenario. The smart charging method, however, reduces costs by 116 807 EUR or 2,45% in comparison to instant charging. Additionally, the implementation of parallel charging constraints with smart charging results in a marginal 0,31% increase in costs in relation to solely utilizing smart charging.

As battery electric vehicle adoption increases to 50 % in the third scenario, energy procurement costs are observed to have risen by an average of 78 - 85 % across different charging methods as compared to the baseline scenario. The instant charging approach is found to be still the most expensive, with costs reaching up to 5 957 737 EUR or 85,32 % higher than the standard scenario. On the other hand, the utilization of smart charging method has resulted to a reduction of energy costs by 208 814 EUR or 3,5 % as

compared to instant charging. Additionally, incorporating parallel charging constraints in the smart charging method results in a minimal 0,45 % increase in costs in relation to utilizing smart charging alone. The analysis of the same charging methods during

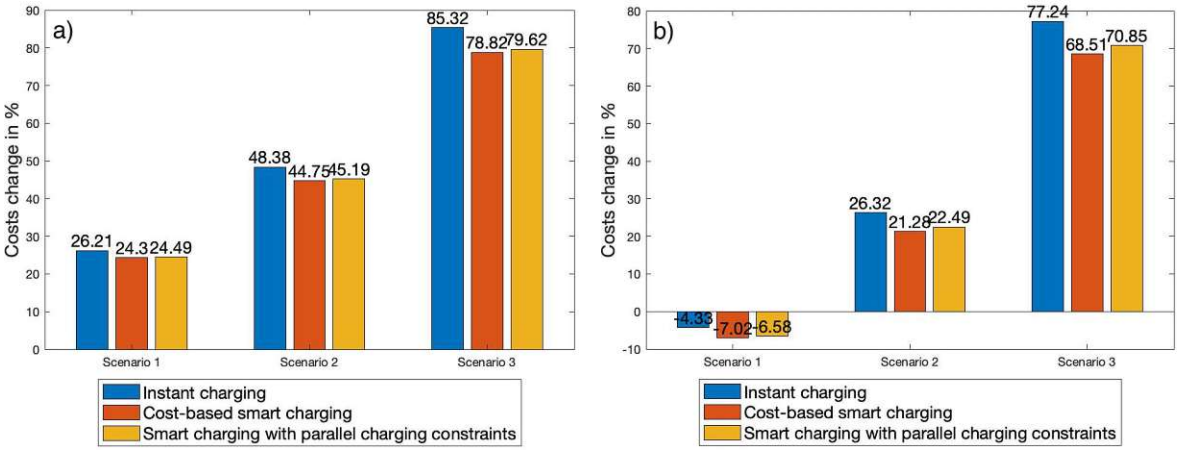

Figure 4.17: Comparison of the energy procurement costs of the charging methods with standard scenario in a) January and b) July

the month of July yielded distinct results, largely due to the increased photovoltaic generation. As illustrated in Figure 4.17b , in the first scenario where battery electric vehicle penetration is at 10 %, total energy costs on average are observed to decrease by 4 - 7 % in comparison to the baseline scenario. Specifically, the instant charging approach resulted in 2 654 844 EUR, a cost reduction of 4,3 % compared to the baseline scenario which totalled at 2 774 963 EUR. Additionally, a comparison of energy costs between July and January in the baseline scenario revealed a 14 % decrease. The instant charging approach demonstrated an even greater reduction of 35 % for this same comparison. The implementation of a cost-based smart charging approach alone resulted in a 2,81 % decrease in energy costs in comparison to instant charging. However, the inclusion of parallel charging constraints, as in the third charging method, resulted in a slight increase of 0,48 % in energy costs, totalling 2 592 483 EUR.

In the second and third scenario with a battery EV penetration of 25 % and 50 % respectively, the total energy costs increase by an average of 21 - 26% in scenario 2 and by 68 - 77 % in the third scenario. Instant charging continues to be the most expensive charging method among the rest while the cost-based smart charging gives the best results.

As previously discussed in Chapter 3, energy procurement costs encompass spot-market electricity costs, grid tariffs, and fast DC charging tariffs. Figure 4.18 provides a more detailed separation of the proportion of each cost component for the third scenario in the month of July. The first column represents the energy costs associated with instant charging, with electricity costs accounting for 47,7 % of the total, followed by DC charging tariffs and grid tariffs at 36 % and 16,3 %, respectively. The utilization of smart charging results in a decrease of 9,3 % in electricity costs due to the scheduling of EV charging during periods of low electricity prices. However, reductions in tariffs are relatively small, with only a 1,1 % decrease in DC charging tariffs and a 0,6 % decrease

in grid tariffs. Additionally, the implementation of parallel charging constraints results in a slight 2,6 % increase in electricity costs and a marginal increase in tariffs of less than 0,5 %.

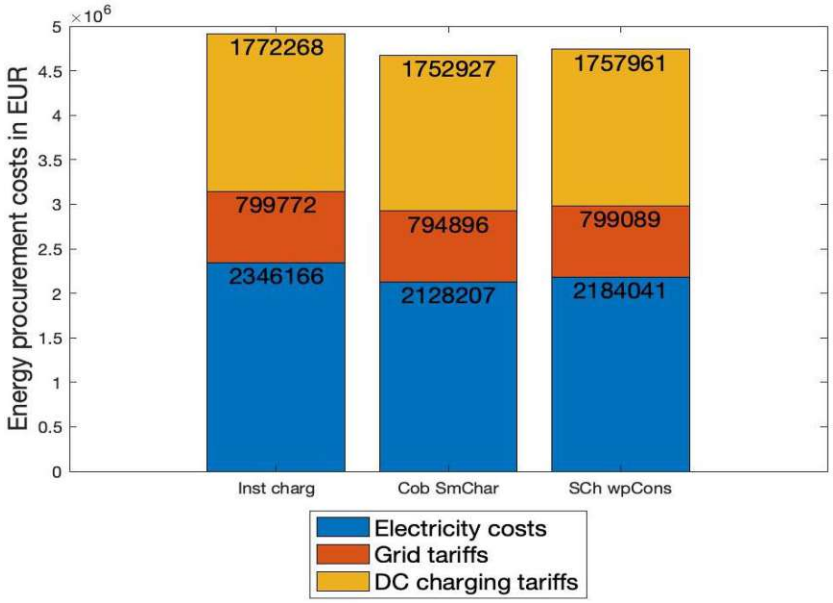

Figure 4.18: Energy procurement costs of each charging method separated into each cost category

The fourth, fifth, and sixth scenarios deviate from the initial three in that they incorporate the utilization of fuel cell electric vehicles in public transit and light-to-medium commercial trucks. As depicted in Figure 4.19a, the energy procurement costs of each scenario in the month of January are compared to the benchmark scenario, which only includes residential demand. In the fourth scenario, cost-based smart charging resulted in a 7,93 % increase in energy costs, equating to 3 469 729 EUR, with the addition of parallel charging constraints contributing an additional 0,1 % increase, or 3 252 EUR. The fifth and sixth scenarios both resulted in an average increase in costs of 20 % and 40 % respectively, averaging in 3,85 million EUR for the fifth scenario, and 4,5 million EUR for the final scenario.

By comparing the charging methods across the various scenarios, the results as depicted in Figure 4.19b indicate that the implementation of smart charging methods in the fourth scenario resulted in a 13,2 % reduction in energy costs when compared to the first scenario. This trend continues in the subsequent scenario comparisons, with the fifth scenario exhibiting a 17,2 % cost advantage over the second scenario, and the final scenario, featuring a 50 % blend of battery electric vehicles and fuel cell electric vehicles, displaying a 21,7 % reduction in energy costs when compared to the third scenario. The significant cost difference observed in these scenarios is attributed to the method of hydrogen production. As outlined in Chapter 3, the electrolyser is connected to the grid in AC mode, thus eliminating the need for DC charging tariffs for the entire fleet of buses and trucks, resulting in the substantial cost reduction of 21,7 % as previously

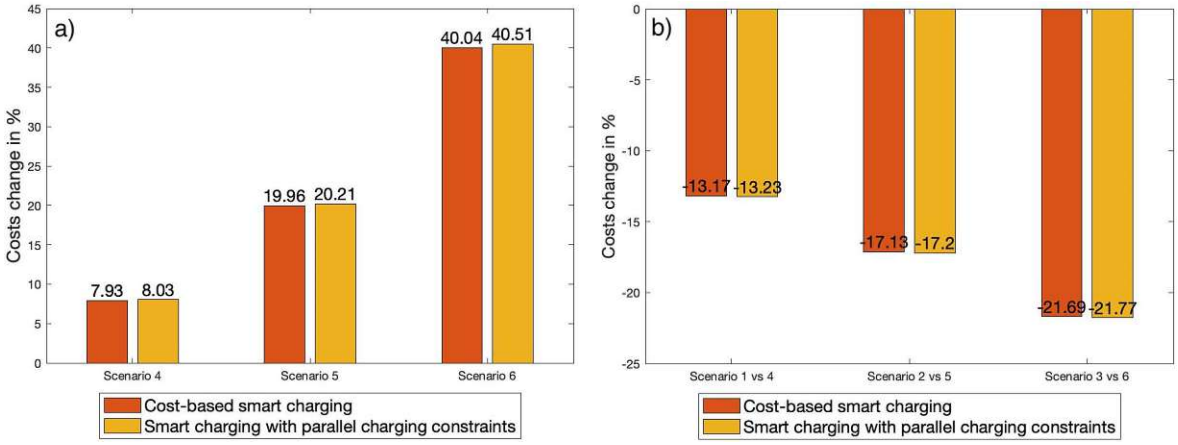

Figure 4.19: a) Comparison of the energy procurement costs of the smart charging methods with standard scenario and b) Comparison of the energy procurement costs of the smart charging methods with previous three scenarios

mentioned. In Figure 4.20, a separation of each cost component is provided, with the first column displaying the energy cost components of the cost-based smart charging method in the third scenario, and the second column showing the corresponding cost components of the sixth scenario. It is evident that while there are minor differences in electricity costs and grid tariffs, the DC charging component exhibits a significant over 75 % reduction. The remaining DC charging component in the final scenario is attributed to the fast DC charging of battery electric vehicles included in that scenario. In a hypothetical case where the electrolyser was connected in DC mode, the total energy cost reduction would be limited to 2 % on average, significantly lower than the 21,7 % reduction observed previously.

An examination of the same smart charging methods during the month of July revealed more favourable results, largely due to the increased PV generation. As illustrated in Figure 4.21a, in the fourth scenario where the penetration of battery electric vehicles and fuel cell electric vehicles is at 10 %, total energy costs on average decreased by 27 % in comparison to the baseline scenario, totalling 2 022 986 EUR. Additionally, in the fifth scenario, where the penetration of EVs is increased from 10 % to 25 %, energy costs increased to 2 524 543 EUR, representing a 24,8 % increase when compared to the fourth scenario. However, this total energy cost was still 8,13 - 9,02 % lower, depending on the charging method, when compared to the baseline scenario. In the final scenario, where the fleet is composed of 50 % battery electric vehicles and fuel cell electric vehicles, the total energy costs on average were 22 % higher than the benchmark scenario. In comparison to the fifth scenario, the total energy costs increased by only 33 % when the EV fleet was doubled. A comparative analysis of the charging methods across the various scenarios for this month, as previously done for the month of January, illustrates that the implementation of smart charging methods in the fourth scenario resulted in a 21,6 % decrease in energy costs when compared to the first scenario. Figure 4.21b shows that this trend is sustained in the subsequent scenario comparisons, with the fifth scenario demonstrating a 25 % cost advantage over the second scenario, and the final scenario, incorporating a 50 % blend of battery electric vehicles and fuel cell electric

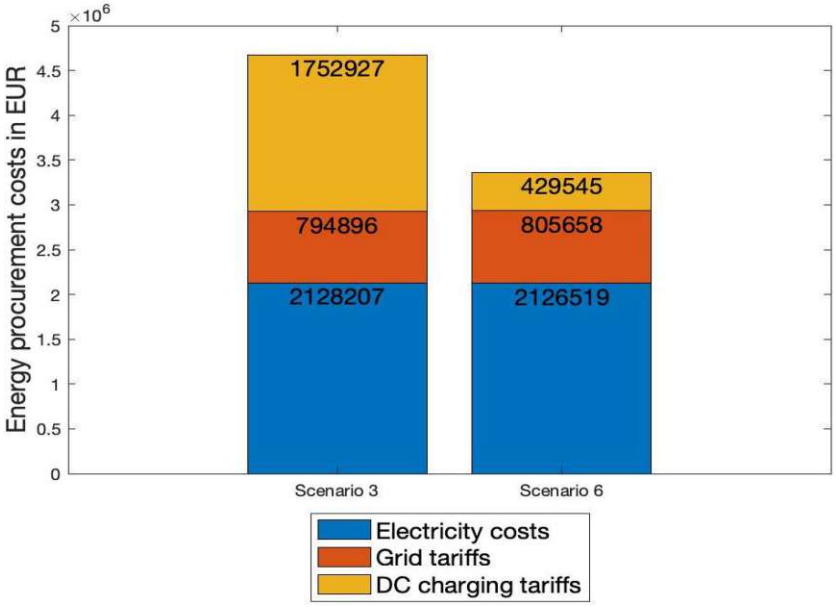

Figure 4.20: Energy procurement costs of cost-based smart charging method separated into each cost category for scenario 3 and 6

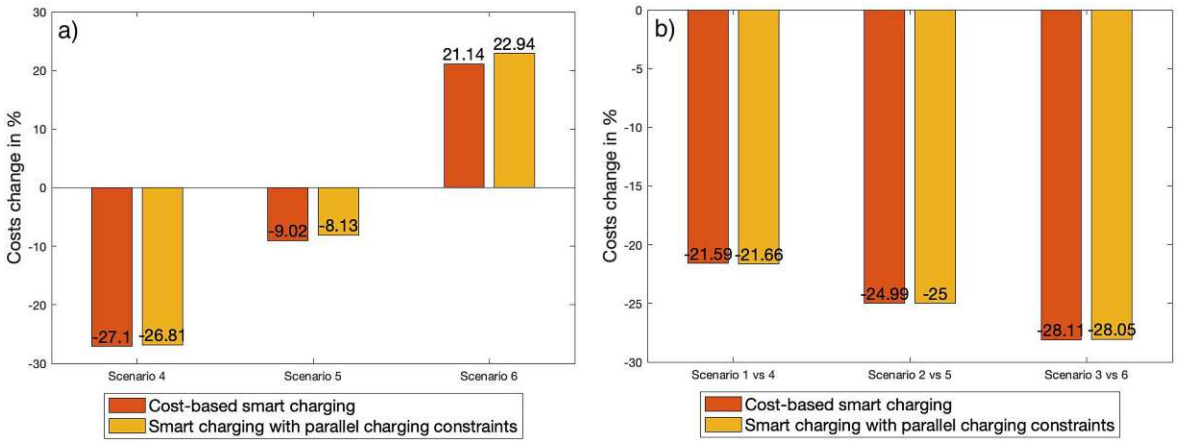

Figure 4.21: a) Comparison of the energy procurement costs of the smart charging methods with standard scenario and b) Comparison of the energy procurement costs of the smart charging methods with previous three scenarios

vehicles, displaying an average 28 % reduction in energy costs when compared to the third scenario.

4.2 Rural use case

4.2.1 Load profiles and peak loads

Scenario 1 - 10 % EV penetration

In this section, the load profiles and peak load developments resulting from differ-

ent optimization scenarios in the rural use case are analysed over various time periods. Similar to suburban use case, a comparison of the first scenario with the standard scenario is performed, using a two-day period during the wintertime as a representative sample. Figure 4.22a illustrates the residential load profile (in blue) and the load profile generated by the optimization scenario utilizing instant charging (in orange). The standard load profile exhibits a peak load of 0,57 MW during evening hours (18:45), while the peak load resulting from the instant charging load profile is 1,58 MW (19:45), representing a 177 % increase in peak load. Additionally, the electricity price (in yellow) is also included to provide insight into the correlation between charging methods and electricity prices. Due to electricity price volatility, the generated load profile displays numerous fluctuations that correspond to high load peaks when charging the battery reserve during periods of low prices, and vice versa.

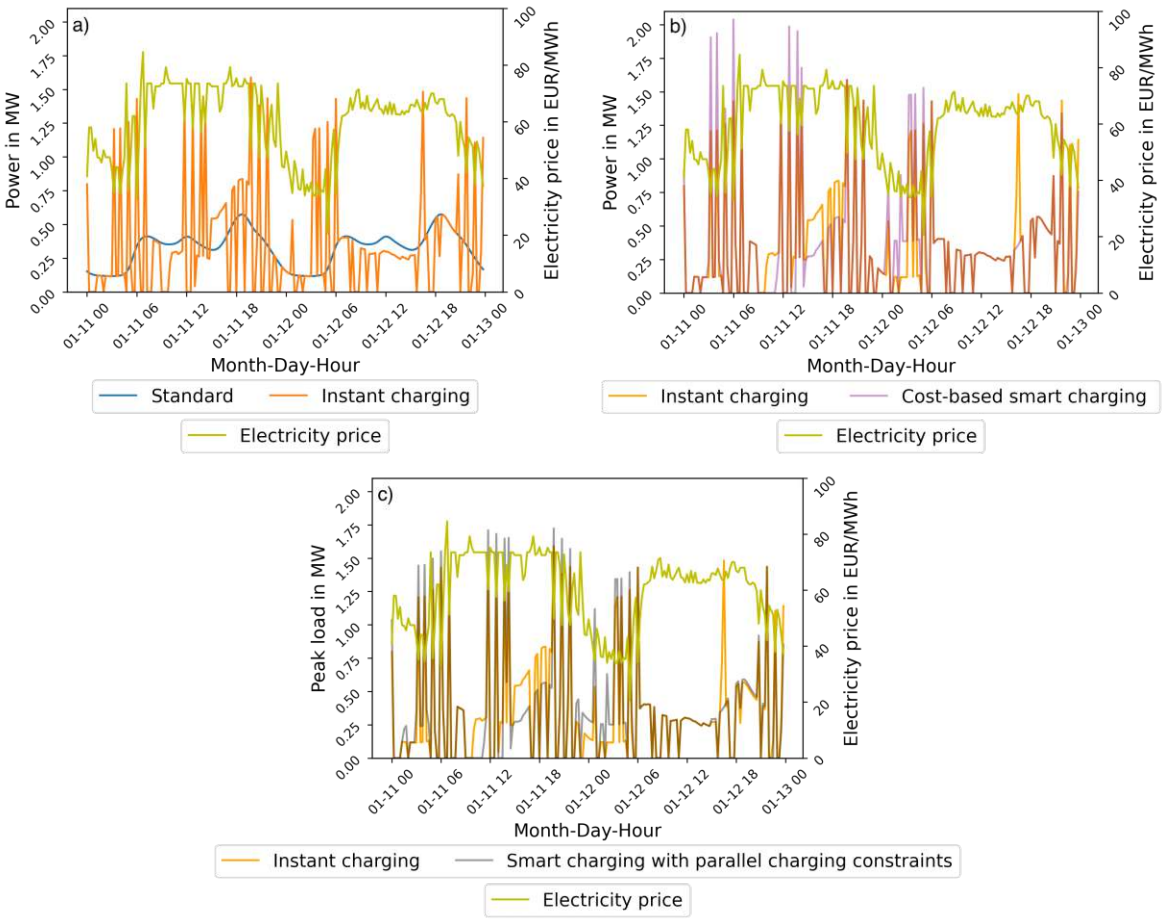

Figure 4.22: Load profiles of different charging methods; a) Standard scenario and Instant charging load profile; b) Instant charging and cost-based smart charging load profile; c) Instant charging and smart charging with parallel charging constraint method

Figure 4.22b compares the load profiles of the instant charging and smart charging methods. The graphs are plotted with a 50 % transparency to better distinguish the time periods with similar load profiles. As depicted, the smart charging approach

exhibits peak loads of up to 2,03 MW during early morning hours (06:00), representing a 256 % increase in peak load compared to the standard load profile and a 28,4 % increase compared to instant charging. Additionally, a certain level of load shifting is achieved as the highest peak loads appear during night-time hours and in time slots with high PV generation. Figure 4.22c illustrates the smart charging approach with additional technical constraints in parallel charging and its comparison to the instant charging method. This approach generates peak loads of up to 1,72 MW in evening hours (19:45), which is 8,86 % higher than instant charging. In contrast to the purely cost-based charging of smart charging, this approach delivers -15,3 % lower peak loads, particularly during nighttime hours, while also achieving load shifting.

Furthermore, the peak load developments are modeled for the whole year and Figure 4.23 shows the monthly peak loads of each charging scenario. The standard load profile with only residential load has the lowest peak loads. When including the additional mobility loads of scenario 1, all charging methods have higher peak loads compared to the standard scenario. The smart charging method has the highest peak loads throughout the year because it prioritizes cost minimization over peak load reduction. High peak loads of more than 2 MW occur sporadically only 9 times during the month of April in times of low electricity prices. The smart charging with parallel charging constraints method delivers the lowest peak loads throughout the year among all charging methods.

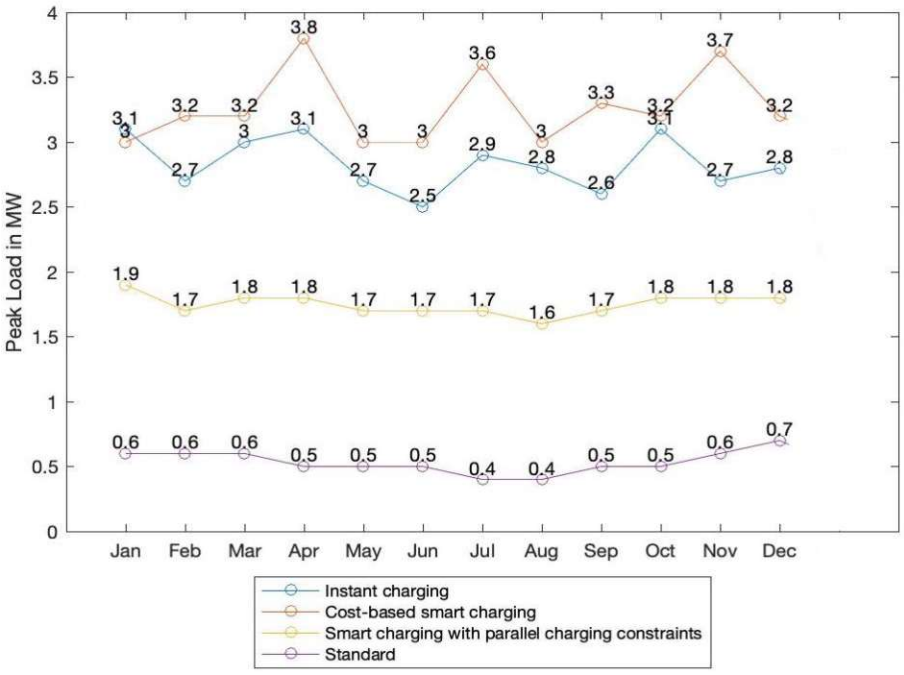

Figure 4.23: Monthly peak loads of all charging methods in scenario 1

The graph in Figure 4.24a illustrates the difference in peak loads between different charging approaches and a baseline scenario. The results show that the instant charging method delivered a peak load 369 % higher than the standard scenario in the month of January. The smart charging and smart charging with parallel charging constraint

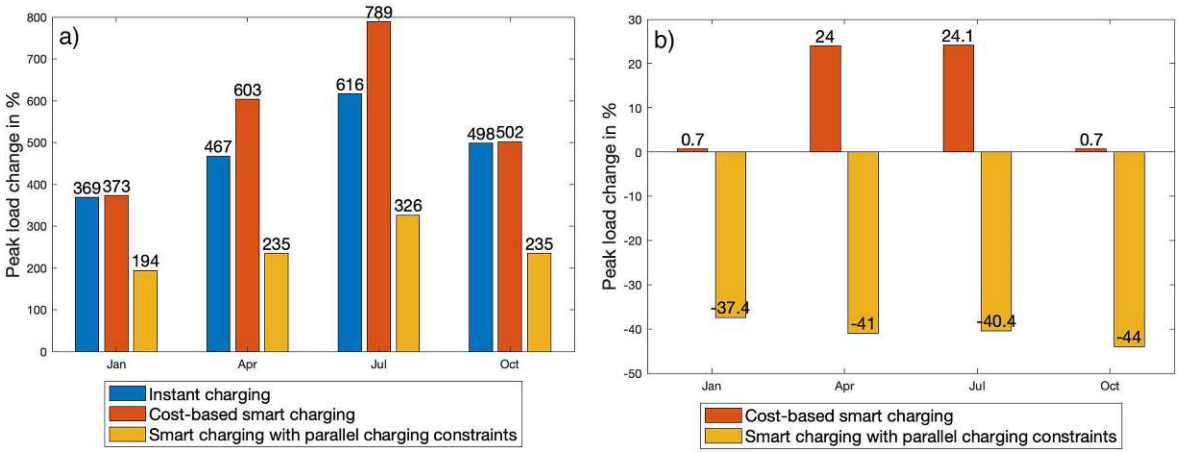

Figure 4.24: a) Comparison of the peak loads of each charging method with standard scenario and, b) comparison of the peak loads of the two smart charging methods with instant charging method in different months

methods had peak loads that were 373 % and 194 % higher compared to the standard scenario, respectively. The results for the other months and seasons also indicate similar trends with respect to the instant charging and smart charging with parallel charging constraints methods. Notably, the latter method delivers the lowest peak loads throughout the year. Conversely, the smart charging approach leads to increased peak loads of up to 789 % compared to the standard scenario.

Figure 4.24b presents a comparison of the two smart charging approaches with the instant charging approach in terms of peak load results. The results indicate that smart charging delivers peak loads that are up to 24 % higher than instant charging during the warmer months and the lowest differences, at 0,7 %, in the colder months. On the other hand, smart charging with parallel charging constraints consistently delivers lower peak loads throughout the year, with a maximum reduction of 44 % in October. These results demonstrate that the smart charging with parallel charging constraint approach provides the most optimal load profiles among the selected approaches.

Scenario 2 - 25 % EV penetration

The second scenario of the study increases the EV penetration rate from 10 % to 25 %, as described in Section 3.3. Figure 4.25 illustrates the monthly peak loads of each charging scenario throughout the year. The results reveal a similar pattern to Scenario 1, where the smart charging approach yields the highest peak loads, followed by the instant charging method. It is noteworthy that high peak loads exceeding 3 MW occur only 12 times in the month of April, the month with the highest peak load, as shown in Figure 4.26. The smart charging with parallel charging constraints approach displays the lowest peak loads among the charging approaches. In comparison to Scenario 1, the peak loads experience an average increase of 37 % in the case of the smart charging with parallel charging constraints approach, and an increase of up to 95 % in the case of the smart charging method, as the EV penetration rate increases from 10 % to 25 %.

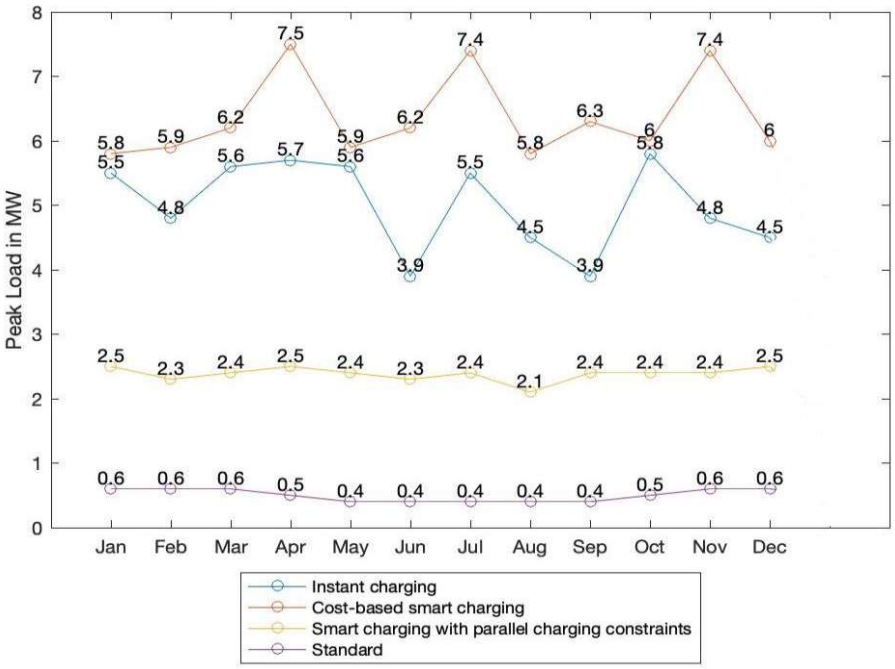

Figure 4.25: Monthly peak loads of all charging methods in scenario 2

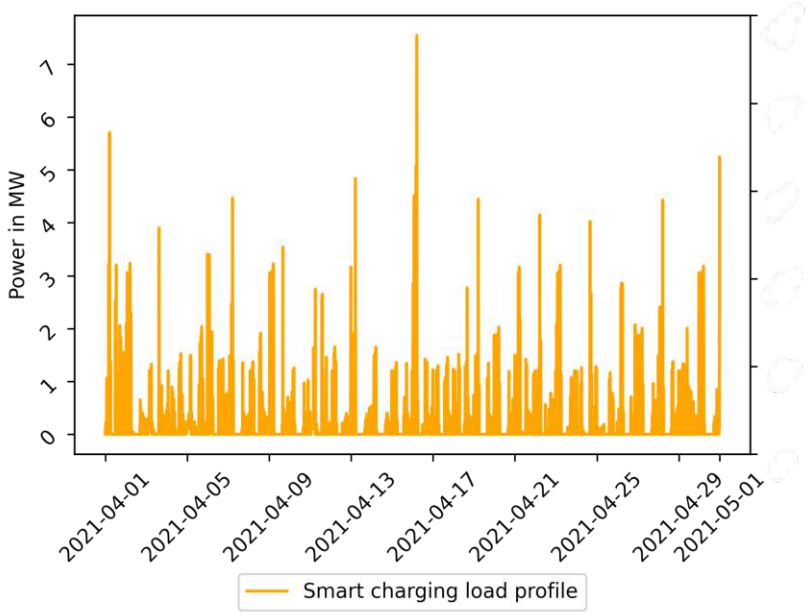

Figure 4.26: Load profile in the month of April

Figure 4.27a illustrates the comparison of the peak loads of each charging scenario with the standard scenario. In the winter month of January, the instant charging approach resulted in a peak load that was 748 % higher than the standard scenario, while the smart charging and smart charging with parallel charging constraint approaches resulted in peak loads that were 804 % and 293 % higher, respectively. In seasons with higher outdoor temperatures such as spring and summer, when the residential load is lower,

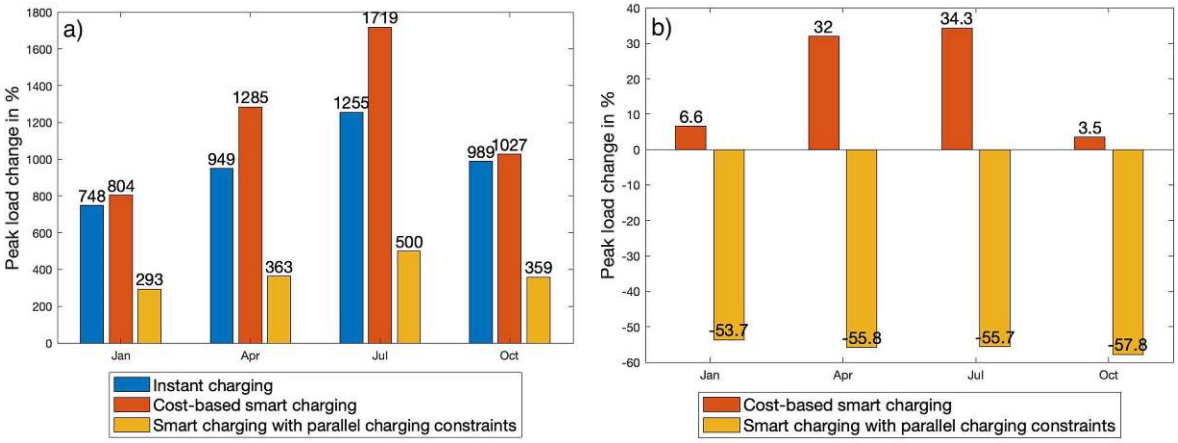

Figure 4.27: a) Comparison of the peak loads of each charging method with standard scenario and, b) comparison of the peak loads of the two smart charging methods with instant charging method in different months

the impact of the mobility load on the load profile is more pronounced. As a result, the smart charging approach leads to peak loads that are up to 1719 % higher than the standard scenario. In contrast, the smart charging with parallel charging constraints approach delivers the most optimal results among the other options, as depicted in Figure 4.27b. This approach consistently yields peak loads that are 53 - 58 % lower than the instant charging approach.

Scenario 3 - 50 % EV penetration

The third scenario increases the EV penetration rate to 50 %, as previously discussed in Section 3.3. Figure 4.28 illustrates the monthly peak loads for each charging method throughout the year. The smart charging approach continues to yield the highest peak loads, followed by the instant charging method and the smart charging with parallel charging constraints approach. The very high peak loads of more than 6 MW in the smart charging approach continue to be infrequent, with only 10 quarter-hour timeslots in the month of April. This month was chosen as it also has the highest peak load overall. The smart charging with parallel charging constraints approach displays the lowest peak loads among the charging methods. In comparison to the second scenario, the peak loads experience an increase of 47 % with the smart charging with parallel charging constraints approach, and up to 80 % with the smart charging method, as the EV penetration rate doubles from 25 % to 50 %.

The graph in Figure 4.29a presents an analysis of the difference in peak loads between the various charging approaches and a standard scenario. Specifically, during the month of January, which serves as a representative of winter months, the instant charging method yielded a very high peak load that was 1466 % higher than the standard scenario. Additionally, the smart charging and smart charging with parallel charging constraint methods resulted in peak loads that were 1522 % and 479 % higher, respectively. During warmer months, the smart charging approach resulted in peak loads that were substantially higher, reaching up to 3225 % higher than the standard scenario.

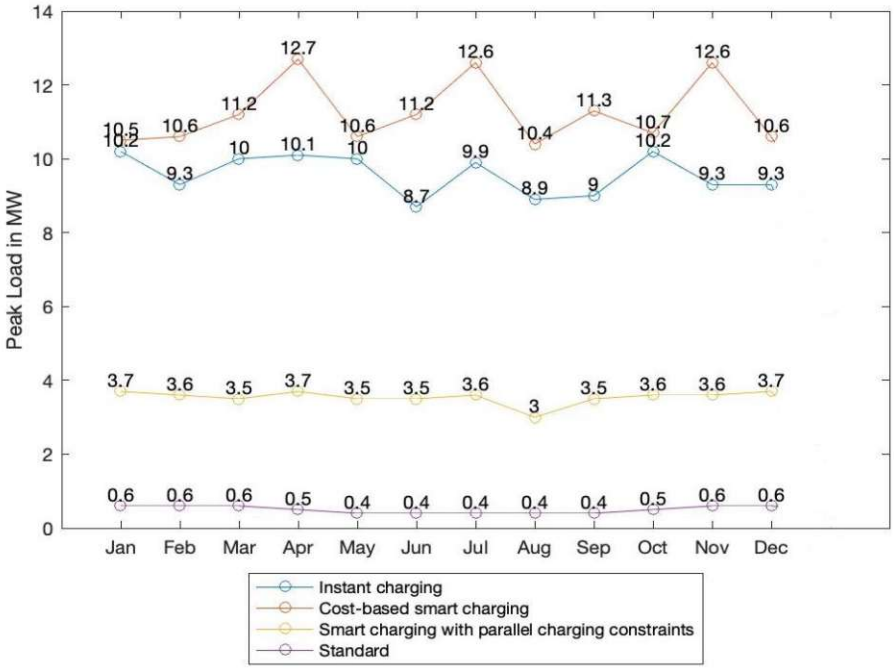

Figure 4.28: Monthly peak loads of all charging methods in scenario 3

However, the smart charging with parallel charging constraints approach performed the best, consistently delivering peak loads that were 63 - 64 % lower than the instant charging approach, as illustrated in Figure 4.29b.

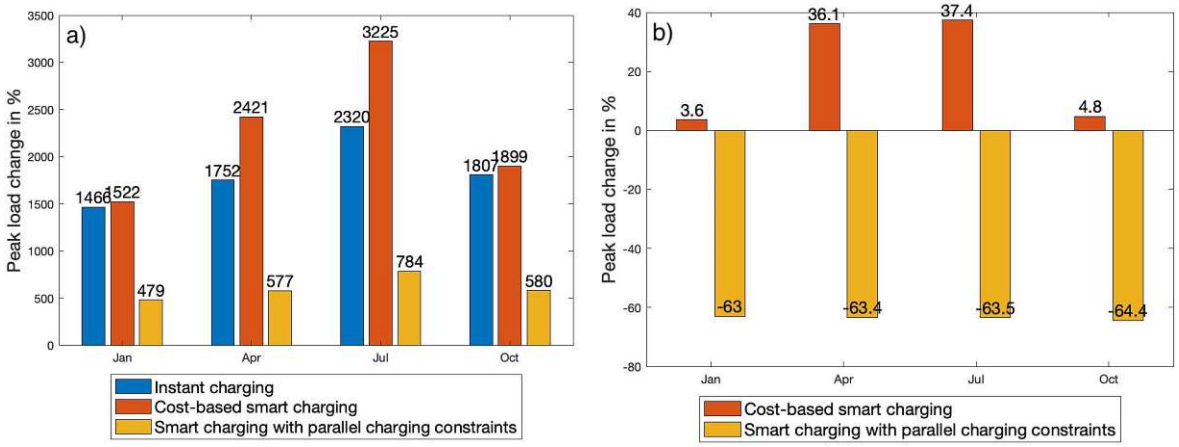

Figure 4.29: a) Comparison of the peak loads of each charging method with standard scenario and, b) comparison of the peak loads of the two smart charging methods with instant charging method in different months

Scenario 4 - 10 % BEV & FCEV penetration

In the fourth scenario, the mobility load is composed of 10 % battery electric vehicles for passenger cars, 10 % fuel cell electric vehicles for light-to-medium trucks,

and 100 % fuel cell electric buses, as shown in Table 3.4 . Figure 4.30 illustrates the monthly peak loads for the standard scenario and the two smart charging approaches. Similar to the suburban use case, the instant charging method is not included in these scenario. The results show a pattern similar to the first scenario, with the smart charging approach resulting in the highest peak loads, followed by the smart charging with parallel charging constraint approach, which yields peak loads that are 38 % lower compared to the smart charging approach. It is noteworthy that the parallel charging constraint applies only to the battery electric vehicles serving as passenger cars. In comparison to the first scenario, where solely battery electric vehicles were considered, the peak loads increase by 12,9 % with the smart charging method and by 30,8 % with the smart charging with parallel charging constraint approach.

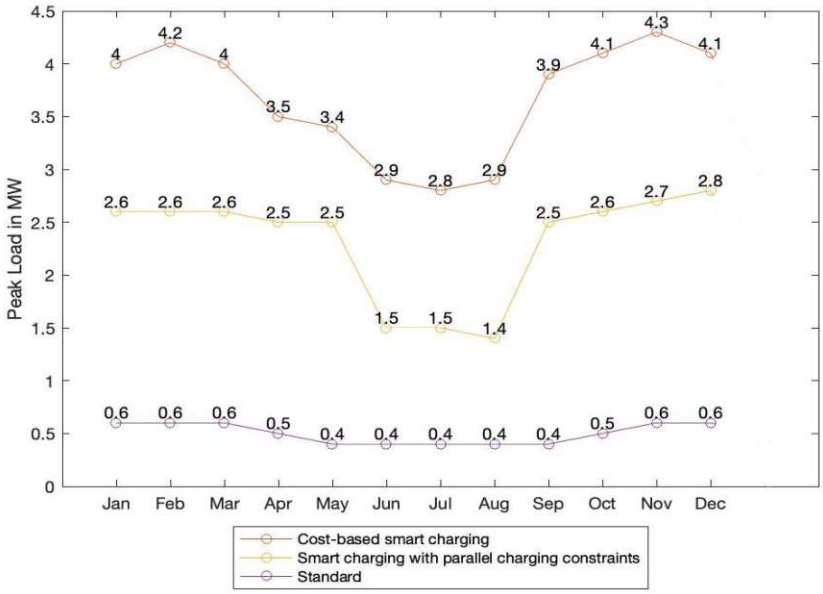

Figure 4.30: Monthly peak loads of all charging methods in scenario 4

Figure 4.31a illustrates the comparison of the peak loads of each charging scenario with the baseline scenario. In January, the smart charging approach delivered peak loads that were 516 % higher than the standard scenario, while the smart charging with parallel charging constraint approach resulted in peak loads that were 300 % higher. During the rest of the year, the smart charging approach reached peak loads up to 672 % higher than the standard scenario. On the other hand, the smart charging with parallel charging constraint approach consistently resulted in peak loads that were within the range of 265 - 385 % higher compared to the baseline scenario throughout the year.

Figure 4.31b presents a comparison of each charging approach with the respective charging method in the first scenario. In January and October, both smart charging methods deliver higher peak loads compared to the first scenario with solely battery electric vehicles. Interestingly, the smart charging approach yields a lower peak load in April and July, which also corresponds to the months with the highest peak loads in the first scenario. The main reason is the increasing PV generation during summer months, that matches with better optimization of hydrogen production. The same behavior is shown

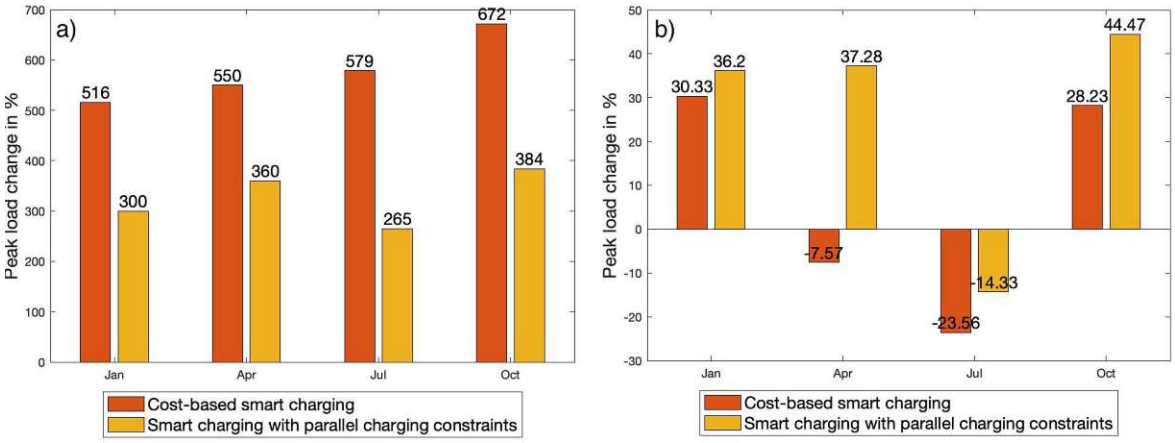

Figure 4.31: a) Comparison of the peak loads of the two smart charging methods with standard scenario and, b) comparison of the peak loads of the charging methods with the first scenario in different months

in July as well, where both smart charging methods deliver significant lower peak loads.

Scenario 5 - 25 % BEV & FCEV penetration

In the fifth scenario presented, the impact of an increase in the penetration rate of electric and fuel cell vehicles from 10 % to 25 % on peak loads is examined. Results from the model are shown in Figure 4.32 and they indicate that the smart charging approach results in the highest peak loads, though it should be noted that peak loads above 4 MW occur infrequently. Results also show that implementing parallel charging constraints in the smart charging approach results in an average reduction of 57 % in peak loads. Additionally, the peak loads were found to increase on average by 6,17 % with the smart charging method and increase by 19,22 % with the smart charging with parallel charging constraints method, when compared to scenario 2 with only battery electric vehicles.

Furthermore, the model compares the peak loads of different charging scenarios with a baseline scenario as shown in Figure 4.33a. In January, the smart charging approach results in peak loads that are 916 % higher than the standard scenario, while the smart charging with parallel charging constraint approach results in peak loads that are 328 % higher. During the rest of the year, the smart charging approach reaches extremely high peak loads up to 1739 % higher than the standard scenario. On the other hand, the smart charging with parallel charging constraint approach reaches a maximum peak load on July with approximately 600 % higher peak load than the baseline scenario. The study also compares each charging approach with the respective charging method in the first scenario using Figure 4.33b. The smart charging approach delivered on average 12 % higher peak loads in January and October while having very similar peak loads in warmer months such as April or July (around 1 % peak load increase). As for the smart charging with parallel charging constraint, it has consistently yielded higher peak loads in the range of 9 - 17 % throughout the year.

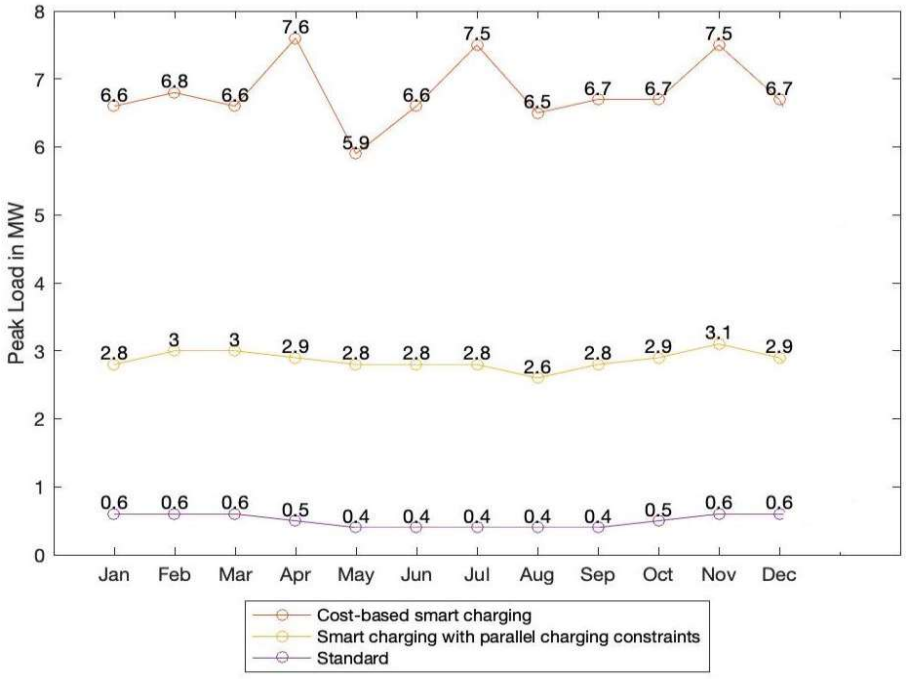

Figure 4.32: Monthly peak loads of all charging methods in scenario 5

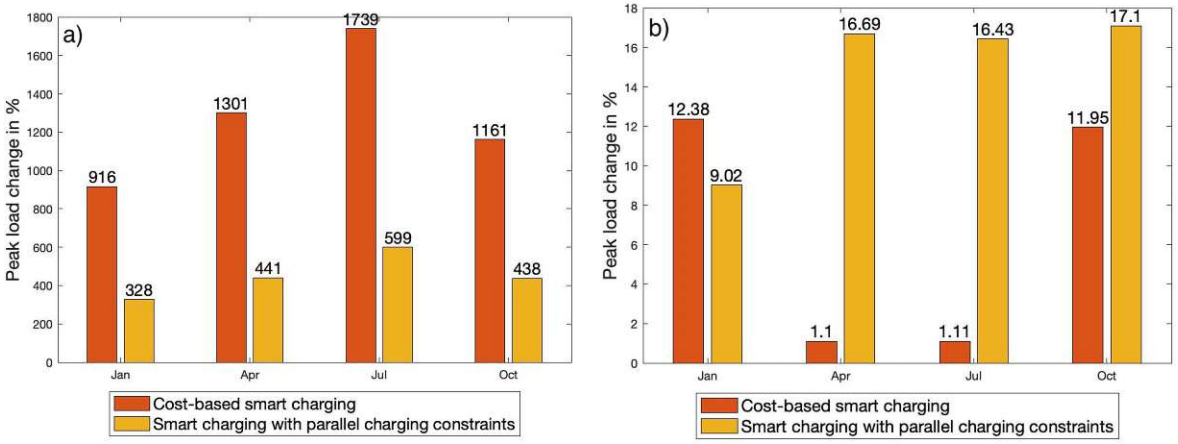

Figure 4.33: a) Comparison of the peak loads of the two smart charging methods with standard scenario and, b) comparison of the peak loads of the charging methods with the second scenario in different months

Scenario 6 - 50 % BEV & FCEV penetration

In the last scenario presented, the thesis examines the impact of doubling the penetration rate of electric and fuel cell vehicles from 25 % to 50 % on peak loads. Results from the study continue to show a consistent pattern, where the smart charging approach leads to extremely high peak loads as in Figure 4.34. However, the difference to the smart charging scenario with parallel charging constraints gets larger as the latter method results in peak loads that are 67 % lower on average throughout the year. The very high peak loads of over 6 MW in the smart charging approach remain infrequent,

with only 11 quarter-hour timeslots in April as shown in Figure 4.35a. Figure 4.35b shows the peak development of the smart charging with parallel charging constraints and it demonstrates the difference to the cost-based smart charging method. When compared to the third scenario, the peak loads decrease by 1,48 % with the smart charging method and increase by 5,31 % with the smart charging with parallel charging constraints method.

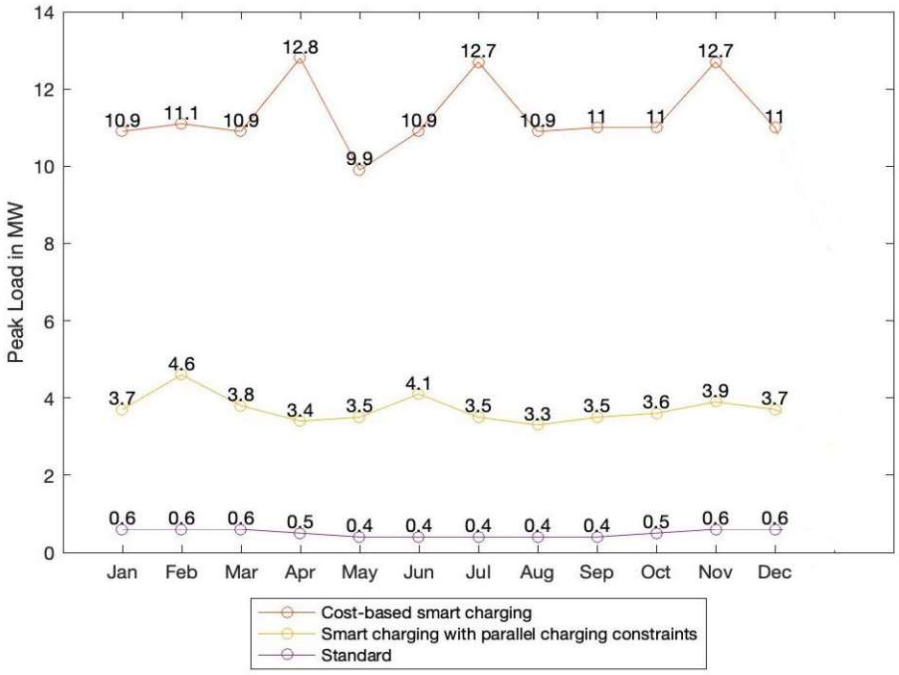

Figure 4.34: Monthly peak loads of all charging methods in scenario 6

The study compares the peak loads of different charging scenarios with a standard scenario using Figure 4.36a. Throughout the year, the smart charging approach results in extremely high peak loads that are more than 30 times higher than the standard scenario. In contrast, the smart charging with parallel charging constraint approach

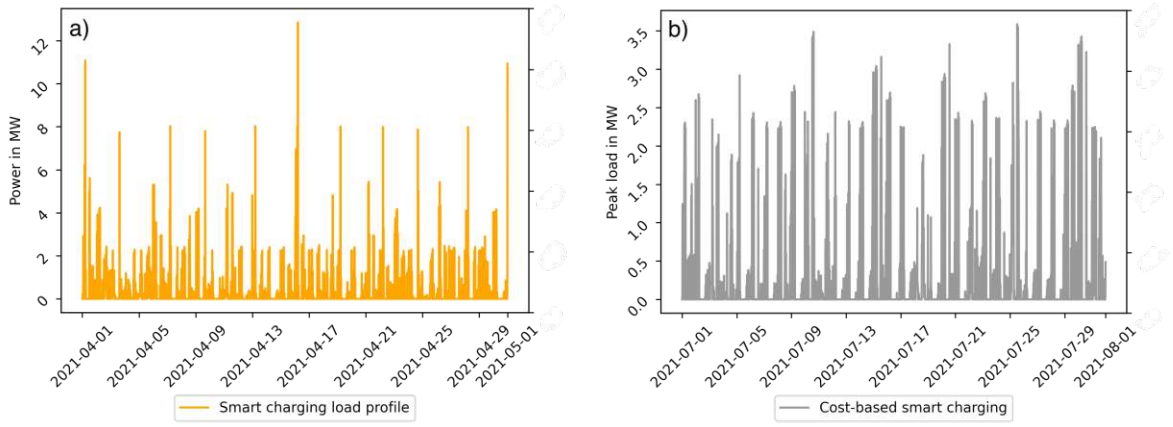

Figure 4.35: Load profile in the month of April for a) cost-based smart charging method and b) smart charging with parallel charging constraints method

consistently delivers peak loads that are in the range of 480 - 775 % higher than the baseline scenario throughout the year. The study also compares each charging approach in the sixth scenario with the respective charging method in the third scenario using Figure 4.36b. The smart charging methods delivered slightly higher peak loads in January and October, while yielding peak load reductions in warmer months.

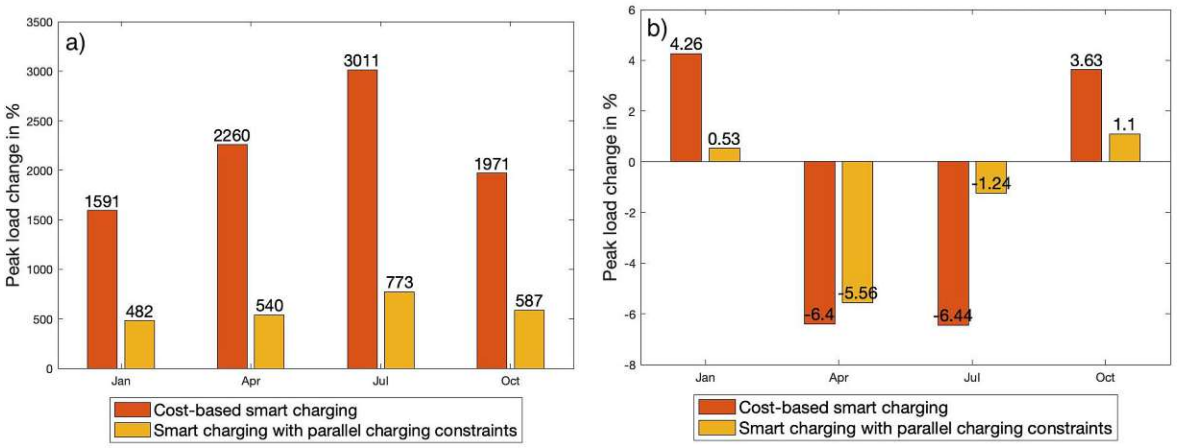

Figure 4.36: a) Comparison of the peak loads of the two smart charging methods with standard scenario and, b) comparison of the peak loads of the charging methods with the third scenario in different months

4.2.2 Energy procurement costs

In this section, the energy procurement costs for various scenarios of the rural use case are presented and analyzed. Firstly, the impact of incorporating battery EVs into the mobility load on energy costs is examined through the comparison of various charging approaches. Figure 4.37 provide a visual representation of these comparisons similar to the previous use case, with the months of January and July selected to capture the differences in electricity costs between summer and winter months. The total costs are significantly lower compared to the suburban use case due to the considerably lower residential and mobility load.

In the first scenario during the month of January, which involves a 10 % EV penetration rate, energy procurement costs for the instant charging approach were found to be 27 965 EUR, or 24,67 % higher than the total cost of 22 431 EUR coming from the standard scenario. However, by implementing a cost-based smart charging approach, energy procurement costs were found to increase by only 22,05 % compared to the standard scenario, representing a 2,1 % decrease compared to instant charging. The third charging approach, which aimed to improve load profiles as previously discussed, resulted in a slight increase in energy costs of 0,38 % when compared to cost-based smart charging. Overall, the inclusion of a 10 % EV penetration rate in the mobility load resulted in an average increase in energy costs of 22 - 25 % among the different charging approaches.

In the second scenario, where EV penetration increases to 25 %, energy procurement costs were calculated to have risen by an average of 66 - 73 % across various

charging methods when compared to the baseline scenario. The instant charging approach remained the most cost-prohibitive, with expenses totaling up to 38 787 EUR or 48,38 % higher than the baseline scenario. However, the implementation of smart charging resulted in a reduction of energy costs by 1 431 EUR or 3,69 % compared to instant charging. Additionally, incorporating parallel charging constraints with smart charging resulted in a marginal increase in costs of 0,62 % when compared to utilizing smart charging alone.

Finally, in the third scenario, where EV penetration doubles to 50 %, energy procurement costs were found to have risen significantly by an average of 140 - 153 % across different charging methods as compared to the baseline scenario. The instant charging approach was still found to be the most expensive, with costs reaching up to 57 764 EUR or 153 % higher than the standard scenario. On the other hand, the utilization of smart charging method resulted in a reduction of energy costs by 2 776 EUR or 4,89 % as compared to instant charging. Furthermore, by implementing parallel charging constraints in the smart charging method, the monthly costs increased by a minor 0,74 % when compared to smart charging alone.

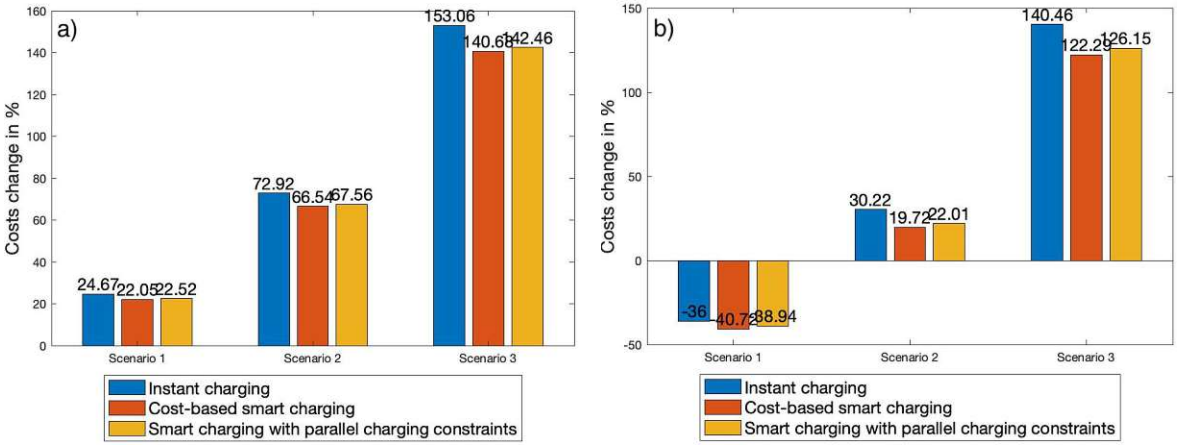

Figure 4.37: Comparison of the energy procurement costs of the charging methods with standard scenario in a) January and b) July

The analysis of various charging methods during the month of July yielded differing results, largely due to the increased photovoltaic generation. As shown in Figure 4.37b, in the first scenario where the penetration of battery electric vehicles is at 10 %, the average total energy costs were found to decrease considerably by 36 - 40 % compared to the baseline scenario which resulted to 19 362 EUR. Specifically, the instant charging method resulted in a cost reduction of 36 % in comparison to the baseline scenario, with energy costs totaling 12 391 EUR. Additionally, a comparison of energy costs between July and January in the baseline scenario revealed a 14 % decrease, while the instant charging method demonstrated an even greater reduction of 55 %. The implementation of a cost-based smart charging approach alone resulted in energy costs of 11 477 EUR, a further 7,38 % reduction compared to instant charging. However, the inclusion of parallel charging constraints, as in the third charging method, resulted in a slight increase of 3 % in energy costs, totaling 11 822 EUR.

In the second and third scenario, with a battery EV penetration of 25 % and 50 % respectively, the total energy costs increase by an average of 19 - 30 % in scenario 2 and by 122 - 140 % in the third scenario. Instant charging continues to be the most expensive charging method among the others, while the cost-based smart charging method yields the best results.

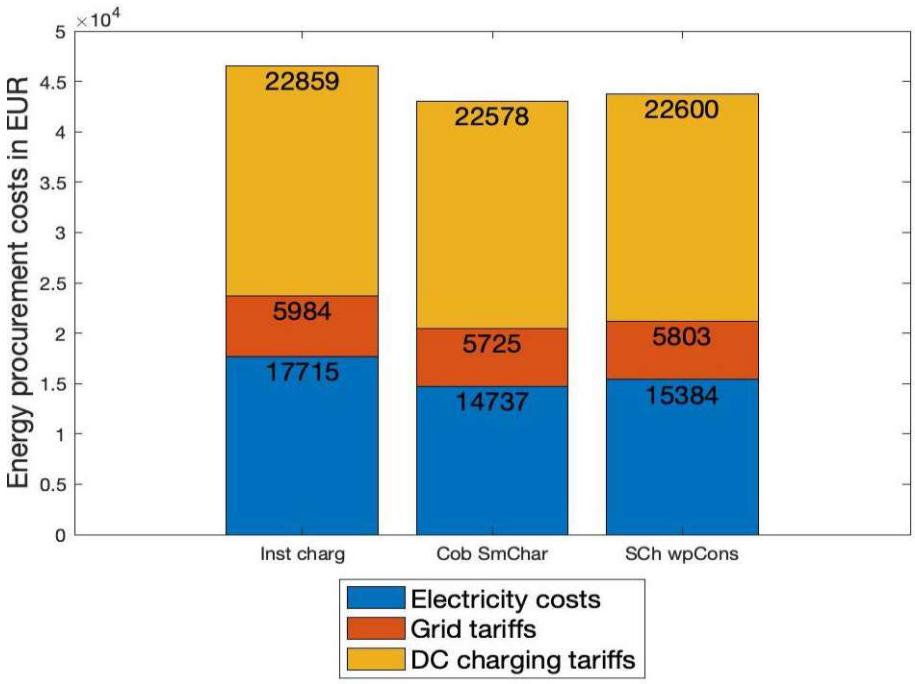

Figure 4.38: Energy procurement costs of each charging method separated into each cost category

Figure 4.38 illustrates a more detailed split of the proportion of each cost component for the third scenario in the month of July. The energy costs associated with instant charging are represented in the first column, with electricity costs comprising 38 % of the total, followed by grid tariffs and DC charging tariffs at 12,8 % and 49,2 % respectively. The implementation of smart charging leads to a decrease of 16,8 % in electricity costs due to the scheduling of EV charging during periods of low electricity prices. Furthermore, reductions in tariffs are relatively small, with only a 4,3 % decrease in grid tariffs and a 1,2 % decrease in DC charging tariffs. Additionally, the inclusion of parallel charging constraints results in a slight 4,4 % increase in electricity costs and a marginal increase of 1 % in tariffs.

Scenarios four through six diverge from the initial three by incorporating the use of fuel cell electric vehicles in public transportation and light to medium commercial trucks. As shown in Figure 4.39a, the energy procurement costs of each scenario are compared to a benchmark scenario that only includes residential demand. In scenario four, the implementation of cost-based smart charging resulted in a 6,08 % increase in energy costs, equating to 23 794 EUR. The addition of parallel charging constraints resulted in an additional 0,2 % increase, which totaled at 23 848 EUR. The fifth and sixth scenarios both resulted in an average increase in costs of 30 % and 72 %, respectively, averaging in 37 500 EUR for the fifth scenario and 54 000 EUR for the

final scenario.

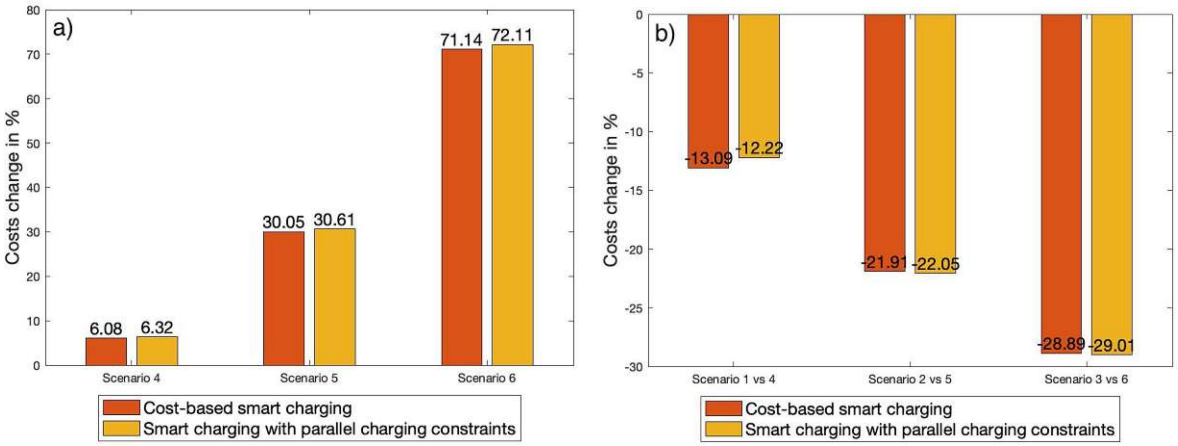

Figure 4.39: a) Comparison of the energy procurement costs of the smart charging methods with standard scenario and b) Comparison of the energy procurement costs of the smart charging methods with previous three scenarios

An analysis of the charging methods across the various scenarios, as shown in Figure 4.39b, reveals that the implementation of smart charging methods in scenario four led to an average reduction of 13,1 % in energy costs when compared to scenario one. This trend becomes more evident in the subsequent scenario comparisons, with scenario five displaying a 22 % cost advantage over scenario two, and scenario six, which features a 50 % blend of battery electric vehicles and fuel cell electric vehicles, showing a 29 % reduction in energy costs when compared to scenario three.

The significant cost difference observed in these scenarios is attributed to the lack of direct current (DC) charging tariffs for the electrolyzer. As seen in Figure 4.40, a separation of each cost component for the month of July is provided, where the first column displays the energy cost components of the smart charging method in the third scenario, and the second column shows the corresponding cost components of the sixth scenario. It is evident that while there are minor differences in electricity costs and grid tariffs, the DC charging component exhibits a significant reduction of over 75 %. The remaining DC charging component in the final scenario is attributed to the fast DC charging of battery electric vehicles (approx. 120 BEVs) included in that scenario. In a hypothetical case where the electrolyzer was connected in DC mode, the total energy cost would be increasing by 6 % on average, much higher than the 21,7 % reduction previously observed.

An analysis of the same smart charging methods during the month of July yielded more favorable results, primarily due to the higher photovoltaic generation. As depicted in Figure 4.41a, in the fourth scenario where the penetration of battery electric vehicles and fuel cell electric vehicles is at 10 %, total energy costs decreased significantly by an average of 65 % when compared to the baseline scenario, totaling 6 493 EUR. Furthermore, in the fifth scenario, where the penetration of electric vehicles is increased from 10 % to 25 %, energy costs amounted to 13 338 EUR, representing a 31 % reduction on

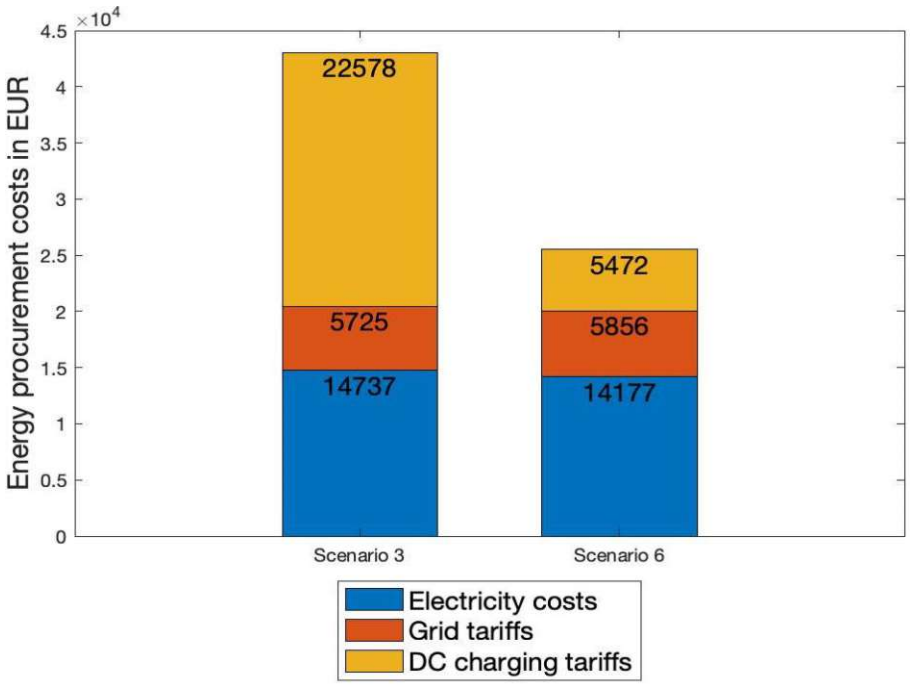

Figure 4.40: Energy procurement costs of cost-based smart charging method separated into each cost category for scenario 3 and 6

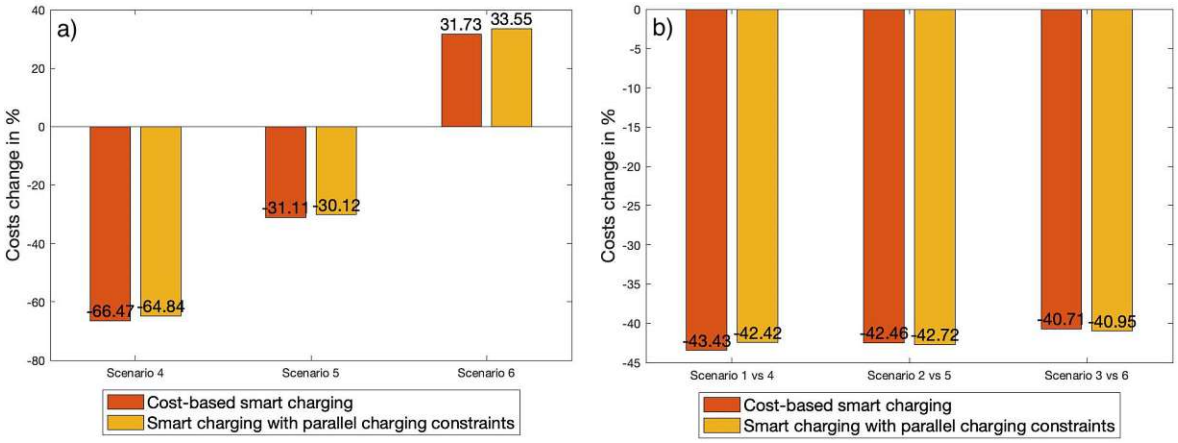

Figure 4.41: a) Comparison of the energy procurement costs of the smart charging methods with standard scenario and b) Comparison of the energy procurement costs of the smart charging methods with previous three scenarios

average when compared to the baseline scenario. In the final scenario, where the fleet is composed of 50 % battery electric vehicles and fuel cell electric vehicles, the total energy costs on average were 32 % higher than the benchmark scenario. In comparison to the fifth scenario, the total energy costs increased by 91 % when the electric vehicle fleet was doubled.

The implementation of smart charging methods in the fourth scenario resulted in a 43 % decrease in energy costs when compared to the first scenario. Figure 4.41b shows that this trend is quite consistent in the subsequent scenario comparisons, with the fifth

scenario demonstrating a 42,6 % cost advantage over the second scenario, and the final scenario, having a 50 % mix of battery electric vehicles and fuel cell electric vehicles, displaying an average 40,85 % reduction in energy costs when compared to the third scenario.

CHAPTER 5

Discussion

Suburban use case

This chapter delves deeper into the examination of the results presented earlier. The work compares the utilization and optimization scenarios of two different use cases and investigates the impact of various electric vehicle (EV) charging methods. Starting with the suburban use case, the standard scenario serves as a benchmark, representing the oldmoded configuration of solely residential loads and centralised power supply. This scenario yielded the lowest peak loads throughout the year due to the absence of EV mobility, which typically results in high peak loads in a short period of time. However, it did not produce the most favourable results in terms of energy procurement costs, as there were limited alternative power sources (such as PV and wind) and battery reserves. The comparison with subsequent EV penetration scenarios illustrates the influence of EV charging on load development and energy procurement costs.

The instant charging method, which represents the current state of EV charging, where vehicles begin charging as soon as they are plugged in, was evaluated. The results revealed that most driving profiles indicate that this charging process typically begins between 3:00 PM and 7:00 PM, when drivers return home and plug in their EVs. As a result, peak loads occur during the afternoon and evening hours, coinciding with the peak load of residential demand. The results also showed that due to the additional storage, new peak loads occur during the night hours, particularly during the winter months when electricity prices are lower and PV generation is reduced. The load profile of the instant charging method converges more closely to the standard scenario, although it remains highly fluctuating due to the optimization model's objective of reducing costs. On average, the instant charging method yielded 178 % and 523 % higher peak loads in scenarios 1 and 3, respectively, compared to the standard scenario. However, the energy obtained from the grid due to the added mobility load decreased by -7,7 % in scenario 1 and increased by 22,6 % in scenario 3, compared to the baseline scenario. This decrease in energy obtained from the grid was primarily due to the additional PV generation in

the suburban use case. Thus, the energy deriving from the PV capacity installed in the roofs of residential housing based on the current environmental goals can offset up to approximately 20 % of the energy demanded by the battery electric vehicles.

The energy procurement costs also varied depending on the season, with the two-month samples of January and July representing winter and summer months respectively. In January, the energy costs increased by 26,2 % in scenario 1 with 10 % EV penetration and by 85,3 % in scenario 3. In contrast, the energy costs decreased by 4,3 % in scenario 1 during July, primarily due to increased PV generation and added flexibility through the battery reserve. It is important to note that these added costs are still considered high, due to the charging of EVs in evening time where the electricity prices are the highest throughout the day. Furthermore, it was observed that in the month of July, the proportion of total costs attributed to DC charging tariffs increased from 23 % in the first scenario to a notable 36 % in the third scenario, which featured a 50 % penetration of battery electric vehicles in the suburban use case. Conversely, in the rural use case, the share of total costs represented by DC charging tariffs exceeded 50 % in the third scenario, highlighting the growing significance of these tariffs as electric vehicle adoption increases. Thus, the proposed fixed power-based premium tariff of 20 cents/kWh for battery electric vehicles charging using 50 kW DC charging in this thesis has the potential to impose a significant financial burden, particularly for electric trucks or buses with larger battery capacities that necessitate charging at higher power levels. An alternative solution would be a dynamic power-based tariff that adjusts to current electric vehicle charging demand and grid stability requirements.

The second charging method, cost-based smart charging, prioritizes minimizing energy procurement costs, disregarding potential impacts on the load profile. In other words, it assumes a scenario in which all electric vehicle drivers have the capability to charge their vehicles at the lowest cost based on their driving patterns. This presents an optimal scenario in terms of energy procurement costs, however, it could result in unfeasible technical outcomes in terms of peak load. It is important to note that this is a theoretical scenario, as such a high load demand in a short period of time would also alter spot market prices. Consequently, with a large penetration of battery electric vehicles, they would eventually evolve from being mere price takers to price-makers, owing to their substantial load demands. The cost-based smart charging approach delivered the highest peak loads, with the first scenario having an average of 308 % higher peak loads than standard scenario over the course of the year. This is further amplified in scenarios with increased EV penetration such as in scenario 3, where the peak loads totalled up to 1237 % higher than the benchmark scenario. However, it is important to state that these peak loads happen sporadically during a month as shown in Figure 4.7, in times of high EV charging correlated with very low electricity prices. This further reinfornces the previous argument that, this charging method cannot be considered technically viable with such extreme peak loads. The daily peak loads continue to be at approximately 15 - 20 % of the value of these very high peak loads, and such extensive peak loads can be considered as outliers throughout the year. There are also some months with amplified peak loads such as April or July, however this derives due to a coincidence of many vehicle bundles charging at the same

time as shown in Figure 4.8. Furthermore, load shifting is achieved as the majority of EV charging is done during night hours and during time periods with high PV generation.

The cost-based smart charging method, which prioritizes minimizing energy procurement costs, demonstrated significant reductions compared to the instant charging method. Specifically, cost savings ranging from 1,5 - 3,5 % were observed among different scenarios in the month of January and 2,8 - 5 % in the month of July. These savings were attributed to higher photovoltaic generation and increased flexibility through battery reserve during summer months. An analysis of the energy cost separation revealed that the electricity price was the primary contributor to cost reduction due to its volatility, while grid and DC charging tariffs had a minor impact as they are fixed costs.

The inclusion of fuel cell electric vehicles in the other three scenarios yielded rather unsignificant results in terms of peak load development, particularly in regard to energy procurement costs. The cost-based smart charging method resulted in lower peak loads compared to scenarios that only included battery electric vehicles. Additionally, peak loads were on average 5 - 6 % lower during warmer months in the fuel cell electric vehicle scenarios compared to battery electric vehicle scenarios. However, peak loads increased up to 2 % higher in months with colder weather, such as January or October, due to a lack of photovoltaic generation. The hydrogen production aims to take place during times of low electricity prices such as in high PV generation time periods. Thus, the combination of the electrolyser, compressor and cooler does not cause an increased peak load as their load is properly distributed throughout the day, given that there is an adequate hydrogen storage capacity.

In terms of energy procurement costs, the cost-based smart charging method in the fuel cell electric vehicle scenarios demonstrated significant reductions compared to the first three scenarios, such as 21 % in the month of January and up to 28 % in the month of July. Furthermore, in July, the energy costs were 9 % lower even with 25 % EV penetration compared to the standard scenario without any mobility load. Thereby, the addition of PV supply and battery capabilities according to regional environmental goals can offset energy costs up to 30 % penetration of BEV and FCEV. The main cost difference between scenarios with only battery electric vehicles and those with the inclusion of fuel cell electric vehicles was attributed to the electrolysers. As the electrolysers are not connected in DC mode within the grid, there are no DC charging tariffs applied for hydrogen production. This results in a cost advantage for hydrogen buses and trucks in terms of refuelling infrastructure. In a hypothetical scenario where the electrolyser was connected in DC mode, the total energy cost reduction would be limited to 2 % on average. Therefore, it is suggested that a tariff be considered that reflects the investment costs of hydrogen refuelling stations.

The last charging method evaluated is smart charging with parallel charging constraints, which aims to minimize costs while also respecting certain technical restrictions. To make this method more technically feasible, parallel charging constraints of 20 % and 50 % are imposed for different vehicle bundles. This means that only 20 % or 50 % of drivers in each driving profile can charge their EVs at the same time. This approach is

more representative of real-world use cases, as not all EV owners have the ability to charge their vehicles at the lowest costs.

Based on these additional constraints, this charging approach resulted in significant reductions in peak load compared to the cost-based smart charging method. Specifically, peak loads were 42 % and up to 67 % lower on average for the first and third scenarios, respectively. Furthermore, when compared to the instant charging method, average yearly reductions were 16,3 % for the first scenario and 31 % for the third scenario with 50 % EV penetration. Additionally, as electricity prices rose in Q4 2021, this charging approach could deliver even higher peak load reductions up to 38 % for the third scenario. To achieve even more substantial peak load reductions, more driving profiles should be considered, with the optimal scenario being that each vehicle is distinct and optimized based on its driving profile. However, the energy procurement costs have slightly increased by 0,15 - 0,45 % in the three scenarios during January and by 0,5 - 1,4 % during the month of July compared to the cost-based smart charging method. This minor increase in costs is due to limited charging during the time frames with the lowest electricity prices, resulting in charging being postponed to more expensive time frames. Overall, this charging approach delivers the best combination of results, representing a compromise between peak loads and energy procurement costs.

The inclusion of fuel cell electric vehicles in the smart charging with parallel charging constraints approach generally resulted in lower peak loads compared to the first three scenarios, however, the effects were limited. In the last three scenarios, the passenger cars remained battery electric vehicles and the parallel charging constraint only impacted this portion of the EV fleet, without having any effect on the fuel cell buses and trucks. The best results were observed in the fifth scenario with an EV penetration of 25 %, with a peak load reduction of up to 7 % compared to the second scenario in the month of April. In terms of energy procurement costs, the approach demonstrated a similar behaviour to the cost-based smart charging method, with no significant differences observed.

Rural use case

In this section, an analysis is conducted to compare the results of the rural use case to the suburban use case in order to understand the distinctions between the two with regard to peak load development and energy procurement costs. The input variables for this use case are based on the unique characteristics of each area. For example, in the rural area, the PV generation has more than doubled from 0,95 kWp to 2 kWp per household, in alignment with the regional goal of increasing renewable energy usage in Lower Austria in year 2030. Additionally, as is typical in a rural region, the car ownership rate has increased by 70 % compared to the suburban use case, resulting in a much greater impact on the overall load profile from mobility load. In terms of hydrogen production, the smallest industrial electrolyser from a big manufacturer was selected for this use case due to the low number of fuel cell electric vehicles in the area. The electrolyser has the capability of producing 450 kg of H_2 at nominal power per day, which is sufficient to refuel up to 15 fuel cell trucks. However, it is still over-dimensioned for the selected scenarios as there is a low number of registered trucks

in the town and thus has a larger impact on the load profile than desired. Thus, such investments in hydrogen refuelling stations should be seen as a common solution for numerous neighbouring towns in order to reach a good utilization rate for the electrolyser.

The instant charging method resulted in significantly higher peak loads compared to the standard scenario, due to the higher share of mobility load in the overall load profile. This is also evidenced in the comparison of the average peak load growth of the rural use case with the suburban use case, with the average peak load growth in the rural use case being tripled in relation to the suburban use case in the benchmark scenario. In terms of energy procurement costs, the instant charging method delivered the highest spending as expected, due to the increased demand for EV charging during the evening peak when electricity prices are at their highest. This charging method proved to be the worst combination in terms of peak load results and energy procurement costs.

The cost-based smart charging approach resulted in the highest peak loads among the first three scenarios, similar to the previous use case. The peak loads were notably high, particularly in the third scenario with 50 % EV penetration, making this hypothetical charging approach less viable. However, it should be noted that these high peak loads occur infrequently throughout the months and are primarily concentrated during time frames of high EV charging activity in conjunction with low electricity prices. In terms of energy procurement costs, the cost-based smart charging approach demonstrated a reduction in total monthly costs by 7-8 % among different EV penetration scenarios in the month of July and by 2,1 - 4,9 % in the month of January. The utilization of smart charging methods thus appears to be more financially beneficial in warmer months, as the PV generation is higher, and the battery reserves can be more effectively utilized.

When incorporating fuel cell trucks, the cost-based smart charging approach aims to produce the required hydrogen at the lowest energy costs. Results in the month of July showed that even with a BEV & FCEV penetration of 25 %, the total energy costs were 31 % lower than the standard scenario that did not include any mobility load. Additionally, these costs were up to 42 % lower compared to the second scenario that included only battery electric vehicles for passenger cars and trucks. However, similar to the argument presented in the suburban use case, the main cost difference was derived from the fact that DC charging tariffs are not applied to the electrolysers, which accounts for 95 % of the total difference.

The smart charging approach with parallel charging constraints resulted in the most favourable outcomes in terms of both peak load and energy procurement costs among the various charging methods evaluated. The peak load reduction amounted to 44 % in the first scenario and up to 64 % in the third scenario when compared to the cost-based smart charging approach. This reduction was achieved solely through the implementation of 20 % and 50 % parallel charging constraints. Thus, the smart charging methods demonstrated that they have a higher impact in rural areas where the car ownership rate is higher and the mobility load share is more significant. Furthermore, there is significant potential for further peak load reduction through the incorporation of additional driving profiles and vehicle bundles, as well as by adapting the charging

profiles to consider plug-in timeframes and charger types. This further reduction is needed as the peak load results of this charging approach remain relatively high, more than 500 % higher than the standard scenario without any mobility load. The energy procurement costs increased by a maximum of 3 % among all scenarios in comparison to the cost-based smart charging approach, which is a relatively insignificant increase in light of the substantial peak load reduction achieved.

When incorporating fuel cell trucks, the impact of parallel charging constraints is less pronounced, thus the results do not show a significant improvement in energy procurement costs compared to the first three scenarios. On the other hand, this charging method delivered higher peak load results compared to the first three scenarios, which reinforces the notion that parallel charging constraints are not a viable option for fuel cell vehicle refuelling optimization.

CHAPTER 6

Conclusion

In this thesis, a comprehensive analysis of various electric vehicle (EV) charging methods and penetration scenarios is conducted. The study utilizes the local residential load and the mobility load originating from BEVs and FCEVs, as seen from the perspective of the grid operator. The model is structured through the implementation of various scenarios, utilizing grid connection, photovoltaic systems, and battery storage as energy sources. A mixed integer linear optimization model is proposed to find the optimal energy procurement costs for the grid operator. In particular, this also includes a second objective of maintaining grid stability. The results of the two analysed use cases show how the pre-defined load scenarios and charging methods influence the energy procurement costs and the load profile. Furthermore, the energy procurement costs are separated into the different cost components and the specific impact of DC charging tariffs is analyzed.

As a benchmark, the standard scenario was used to represent the old configuration of residential loads and centralized power supply. This scenario is not applicable anymore, as distributed renewable generation such as PV supply as well as additional mobility load are being connected into the grid. The instant charging method, which represents the current state of EV charging, was evaluated and the results revealed that most driving profiles indicate that this charging process typically begins between 15:00 - 19:00, when drivers return home and plug in their EVs. As a result, peak loads occur during the afternoon and evening hours, coinciding with the peak load of residential demand. The results also showed that due to the additional storage, new peak loads occur during the night hours, particularly during the winter months when electricity prices are lower and PV generation is reduced. This charging method was found to be the least favourable in terms of peak load results and energy procurement costs.

Cost-based smart charging was next charging method evaluated in this study, which only prioritizes minimizing energy procurement costs without taking into account the impact on the load profile. This approach resulted in the most favourable scenario in

terms of energy procurement costs, however, it was found to be the least beneficial in terms of the peak load. The analysis revealed that energy costs can be significantly reduced by shifting EV charging to off-peak hours when electricity prices are lower. However, this load shifting towards the cheapest timeframes results in extremely high peak loads, making this charging method technically infeasible. It is important to note that this is a hypothetical scenario, as such a large load in a short amount of time would also alter spot-market prices in the future. Additionally, the DC charging tariffs constitute a significant portion of the total energy costs. The implementation of any smart charging methods is more beneficial in a rural region, as the car ownership rate is higher, and the mobility load constitutes a higher share of the total load.

Smart charging with parallel charging constraints was lastly evaluated in this thesis, which represents a balance between peak loads and energy costs. This approach was found to be the most favorable overall solution as it significantly reduced peak loads compared to other charging methods, while only slightly increasing energy costs compared to cost-based smart charging. These results also indicate that peak loads can be reduced without negatively impacting the EV driver's behavior. This approach converges more to the real-world use cases, as not all EV owners have the ability to charge their vehicles at the lowest costs. A more detailed optimization model that takes into account more detailed driving profiles, plug-in times and charger types can further decrease the peak load, which is crucial for the stability of the grid.

In addition, the inclusion of fuel cell electric vehicles was also found to be noteworthy, particularly in significantly reducing the energy procurement costs. The hydrogen production aims to take place during times of low electricity prices such as in high PV generation time periods. The primary cost differential between scenarios comprising solely battery electric vehicles and those incorporating fuel cell electric vehicles is attributed to the electrolysers. The absence of DC charging tariffs for hydrogen production due to the electrolysers being connected in AC mode within the grid results in a cost advantage for fuel cell electric vehicles in terms of refuelling infrastructure. Furthermore, the process of hydrogen production does not cause higher peak loads as the load demand is distributed throughout the day.

In conclusion, the analysis of EV charging strategies is of high importance for stakeholders in the realm of energy policy, grid management, and electric vehicle ownership. It is imperative that the insights taken from this thesis need to be taken into account in order to facilitate a sustainable and economically viable transition to electric mobility.

Further research in this area should aim to encompass a wider range of driving profiles in order to improve forecasting of mobility load and enhance the precision of optimization models. Additionally, the implementation of dynamic power-based tariffs at charging stations may serve to optimize the utilization of DC fast charging infrastructure. The inclusion of vehicle-to-grid capabilities to the model would further evolve to a more accurate overall solution. Lastly, an incentive scheme that better matches the driving profiles of the EV drivers to the current grid demands would provide a more sustainable solution and accelerate to a higher adoption rate.

Bibliography

[1] P. Siobhan, C. G. Vianna, L. Min, I. M. L. Azevedo, and R. Rajapogal, "Charging infrastructure access and operation to reduce the grid impacts of deep electric vehicle adoption," *Nature Energy*, 2022. [Online]. Available: https://doi.org/10.1038/s41560-022-01105-7

[2] G. Van Rossum and F. L. Drake Jr, *Python reference manual*. Centrum voor Wiskunde en Informatica Amsterdam, 1995. [Online]. Available: https://dl.acm.org/doi/book/10.5555/1593511

[3] W. E. Hart, J.-P. Watson, and D. L. Woodruff, "Pyomo: modeling and solving mathematical programs in python„" 2011. [Online]. Available: https://doi.org/10.1007/s12532-011-0026-8

[4] Gurobi Optimization, LLC, "Gurobi Optimizer Reference Manual," 2023. [Online]. Available: https://www.gurobi.com

[5] The Mathworks, Inc., "MATLAB version 9.10.0.1613233 (R2021a)," Natick, Massachusetts, 2021. [Online]. Available: https://www.mathworks.com/

[6] International Electrotechnical Commission, "Iec 62196-1:2011; plugs, socket-outlets, vehicle connectors and vehicle inlets - conductive charging of electric vehicles - part 1: General requirements," 2011. [Online]. Available: https://iec.ch/homepage

[7] A. Bahrami, "Ev charging definitions, modes, levels, communication protocols and applied standards," 01 2020. [Online]. Available: https://doi.org/10.13140/RG.2.2.15844.53123/11

[8] S. Khemakhem, M. Rekik, and L. Krichen, "Double layer home energy supervision strategies based on demand response and plug-in electric vehicle control for flattening power load curves in a smart grid," *Energy*, vol. 167, pp. 312–324, 2019. [Online]. Available: https://doi.org/10.1016/j.energy.2018.10.187

[9] M. Muratori, "Impact of uncoordinated plug-in electric vehicle charging on residential power demand," 03 2018. [Online]. Available: https://doi.org/10.1038/s41560-017-0074-z

[10] N. Brinkel, W. Schram, T. AlSkaif, I. Lampropoulos, and W. van Sark, "Should we reinforce the grid? cost and emission optimization of electric vehicle charging under different transformer limits," *Applied Energy*, vol. 276, p. 115285, 2020. [Online]. Available: https://doi.org/10.1016/j.apenergy.2020.115285

[11] H. Das, M. Rahman, S. Li, and C. Tan, "Electric vehicles standards, charging infrastructure, and impact on grid integration: A technological review," *Renewable and Sustainable Energy Reviews*, vol. 120, p. 109618, 2020. [Online]. Available: https://doi.org/10.1016/j.rser.2019.109618

[12] M. K. Gerritsma, T. A. AlSkaif, H. A. Fidder, and W. G. J. H. M. van Sark, "Flexibility of electric vehicle demand: Analysis of measured charging data and simulation for the future," *World Electric Vehicle Journal*, vol. 10, no. 1, 2019. [Online]. Available: https://doi.org/10.3390/wevj10010014

[13] N. Daina, A. Sivakumar, and J. W. Polak, "Modelling electric vehicles use: a survey on the methods," *Renewable and Sustainable Energy Reviews*, vol. 68, pp. 447–460, 2017. [Online]. Available: https://doi.org/10.1016/j.rser.2016.10.005

[14] E. Akhavan-Rezai, M. F. Shaaban, E. F. El-Saadany, and F. Karray, "Managing demand for plug-in electric vehicles in unbalanced lv systems with photovoltaics," *IEEE Transactions on Industrial Informatics*, vol. 13, no. 3, pp. 1057–1067, 2017. [Online]. Available: https://doi.org/10.1109/TII.2017.2675481

[15] C. G. Hoehne and M. V. Chester, "Optimizing plug-in electric vehicle and vehicle-to-grid charge scheduling to minimize carbon emissions," *Energy*, vol. 115, pp. 646–657, 2016. [Online]. Available: https://doi.org/10.1016/j.energy.2016.09.057

[16] M. van der Kam and W. van Sark, "Smart charging of electric vehicles with photovoltaic power and vehicle-to-grid technology in a microgrid; a case study," *Applied Energy*, vol. 152, pp. 20–30, 2015. [Online]. Available: https://doi.org/10.1016/j.apenergy.2015.04.092

[17] D. B. Richardson, "Electric vehicles and the electric grid: A review of modeling approaches, impacts, and renewable energy integration," *Renewable and Sustainable Energy Reviews*, vol. 19, pp. 247–254, 2013. [Online]. Available: https://doi.org/10.1016/j.rser.2012.11.042

[18] A. Schuller, B. Dietz, C. M. Flath, and C. Weinhardt, "Charging strategies for battery electric vehicles: Economic benchmark and v2g potential," *IEEE Transactions on Power Systems*, vol. 29, no. 5, pp. 2014–2022, 2014. [Online]. Available: https://doi.org/10.1109/TPWRS.2014.2301024

[19] R. Gough, C. Dickerson, P. Rowley, and C. Walsh, "Vehicle-to-grid feasibility: A techno-economic analysis of ev-based energy storage," *Applied Energy*, vol. 192, pp. 12–23, 2017. [Online]. Available: https://doi.org/10.1016/j.apenergy.2017.01.102

[20] W. Wu and B. Lin, "Benefits of electric vehicles integrating into power grid," *Energy*, vol. 224, p. 120108, 2021. [Online]. Available: https://doi.org/10.1016/j.energy.2021.120108

[21] K. Zhan, Z. Hu, Y. Song, N. Lu, Z. Xu, and L. Jia, "A probability transition matrix based decentralized electric vehicle charging method for load valley filling," *Electric Power Systems Research*, vol. 125, pp. 1–7, 2015. [Online]. Available: https://doi.org/10.1016/j.epsr.2015.03.013

[22] X. Ma, Y. Sato, T. Yoshikane, M. Hara, F. Kimura, and Y. Fukushima, *Hydrological Analysis of the Yellow River Basin, China*. John Wiley Sons, Ltd, 2012, ch. 4, pp. 67–78. [Online]. Available: https://doi.org/10.1002/9781118470596.ch4

[23] K. Zhou, L. Cheng, L. Wen, X. Lu, and T. Ding, "A coordinated charging scheduling method for electric vehicles considering different charging demands," *Energy*, vol. 213, p. 118882, 2020. [Online]. Available: https://doi.org/10.1016/j.energy.2020.118882

[24] Y. Zheng, Y. Shang, Z. Shao, and L. Jian, "A novel real-time scheduling strategy with near-linear complexity for integrating large-scale electric vehicles into smart grid," *Applied Energy*, vol. 217, pp. 1–13, 2018. [Online]. Available: https://doi.org/10.1016/j.apenergy.2018.02.084

[25] A. Ajanovic and R. Haas, "Economic prospects and policy framework for hydrogen as fuel in the transport sector," *Energy Policy*, vol. 123, pp. 280–288, 2018. [Online]. Available: https://doi.org/10.1016/j.enpol.2018.08.063

[26] X. Liu, K. Reddi, A. Elgowainy, H. Lohse-Busch, M. Wang, and N. Rustagi, "Comparison of well-to-wheels energy use and emissions of a hydrogen fuel cell electric vehicle relative to a conventional gasoline-powered internal combustion engine vehicle," *International Journal of Hydrogen Energy*, vol. 45, no. 1, pp. 972–983, 2020. [Online]. Available: https://doi.org/10.1016/j.ijhydene.2019.10.192

[27] C. Zhang, J. B. Greenblatt, M. Wei, J. Eichman, S. Saxena, M. Muratori, and O. J. Guerra, "Flexible grid-based electrolysis hydrogen production for fuel cell vehicles reduces costs and greenhouse gas emissions," *Applied Energy*, vol. 278, p. 115651, 2020. [Online]. Available: https://doi.org/10.1016/j.apenergy.2020.115651

[28] S. M. Saba, M. Müller, M. Robinius, and D. Stolten, "The investment costs of electrolysis – a comparison of cost studies from the past 30 years," *International Journal of Hydrogen Energy*, vol. 43, no. 3, pp. 1209–1223, 2018. [Online]. Available: https://doi.org/10.1016/j.ijhydene.2017.11.115

[29] T. Nguyen, Z. Abdin, T. Holm, and W. Mérida, "Grid-connected hydrogen production via large-scale water electrolysis," *Energy Conversion and Management*, vol. 200, p. 112108, 2019. [Online]. Available: https://doi.org/10.1016/j.enconman.2019.112108

[30] P. Yang, X. Yu, and G. Liu, "Research on optimal operation strategy of fuel cell vehicle charging-discharging-storage integrated station," *IOP Conference Series: Earth and Environmental Science*, vol. 675, no. 1, p. 012139, feb 2021. [Online]. Available: https://dx.doi.org/10.1088/1755-1315/675/1/012139

[31] J. Eichman, K. Harrison, and M. Peters, "Novel electrolyzer applications: Providing more than just hydrogen." [Online]. Available: https://doi.org/10.2172/1159377

[32] D. Wang, M. Muratori, J. Eichman, M. Wei, S. Saxena, and C. Zhang, "Quantifying the flexibility of hydrogen production systems to support large-scale renewable energy integration," *Journal of Power Sources*, vol. 399, pp. 383–391, 2018. [Online]. Available: https://doi.org/10.1016/j.jpowsour.2018.07.101

[33] E. Troncoso and M. Newborough, "Electrolysers for mitigating wind curtailment and producing 'green' merchant hydrogen," *International Journal of Hydrogen Energy*, vol. 36, no. 1, pp. 120–134, 2011, 11th International Conference: "Hydrogen Materials Science Chemistry of Carbon Nanomaterials". [Online]. Available: https://doi.org/10.1016/j.ijhydene.2010.10.047

[34] A. González, E. Mckeogh, and B. O Gallachoir, "The role of hydrogen in high wind energy penetration electricity systems: The irish case," *Renewable Energy*, vol. 29, pp. 471–489, 04 2004. [Online]. Available: https://doi.org/10.1016/j.renene.2003.07.006

[35] P. Caumon, M. Lopez-Botet Zulueta, J. Louyrette, S. Albou, C. Bourasseau, and C. Mansilla, "Flexible hydrogen production implementation in the french power system: Expected impacts at the french and european levels," *Energy*, vol. 81, pp. 556–562, 2015. [Online]. Available: https://doi.org/10.1016/j.energy.2014.12.073

[36] J. D. Hunter, "Matplotlib: A 2d graphics environment," *Computing in Science & Engineering*, vol. 9, no. 3, pp. 90–95, 2007. [Online]. Available: https://doi.org/10.1109/MCSE.2007.55

[37] C. R. Harris, K. J. Millman, S. J. van der Walt, R. Gommers, P. Virtanen, D. Cournapeau, E. Wieser, J. Taylor, S. Berg, N. J. Smith, R. Kern, M. Picus, S. Hoyer, M. H. van Kerkwijk, M. Brett, A. Haldane, J. F. del Río, M. Wiebe, P. Peterson, P. Gérard-Marchant, K. Sheppard, T. Reddy, W. Weckesser, H. Abbasi, C. Gohlke, and T. E. Oliphant, "Array programming with NumPy," *Nature*, vol. 585, no. 7825, pp. 357–362, Sep. 2020. [Online]. Available: https://doi.org/10.1038/s41586-020-2649-2

[38] United European Car Carriers, "UECC Electric Vehicle Guideline," 2016.

[39] Stadt Wien, "Bewohnte Wohnungen nach Gemeindebezirken 2019," 2019. [Online]. Available: https://www.wien.gv.at/statistik/verkehr-wohnen/tabellen/wohnungen-bewohnt-bez.html

[40] Statistik Austria, "HAUSHALTSENERGIE UND EINKOMMEN MIT BESONDEREM FOKUS AUF ENERGIEARMUT," 2017. [Online]. Available: https://www.e-control.at/documents/1785851/1811582/Endbericht_Energieverbrauch_Energiearmut.pdf/

[41] Wien Energie, "Gemeinschafts-Solarkraftwerke für Wohnhäuser," accessed in 2023. [Online]. Available: https://positionen.wienenergie.at/projekte/strom/pv-gemeinschaftsanlagen/

[42] Wien Energie, "Sprechen wir über Gebäude-Photovoltaik," accessed in 2023. [Online]. Available: https://positionen.wienenergie.at/themen/stromwende/gebaeude-photovoltaik/

[43] P. D. Lund, "Capacity matching of storage to pv in a global frame with different loads profiles," *Journal of Energy Storage*, vol. 18, pp. 218–228, 2018. [Online]. Available: https://doi.org/10.1016/j.est.2018.04.030

[44] J. Weniger, T. Tjaden, and V. Quaschning, "Sizing of residential pv battery systems," *Energy Procedia*, vol. 46, p. 78–87, 12 2014. [Online]. Available: https://doi.org/10.1016/j.egypro.2014.01.160

[45] Stadt Wien, "BKraftfahrzeugbestand nach Gemeindebezirken 2019," 2019. [Online]. Available: https://www.wien.gv.at/statistik/verkehr-wohnen/tabellen/kfz-bestand-bez.html

[46] Electric Vehicle Database, "Smart EQ fortwo," 2020. [Online]. Available: https://ev-database.org/

[47] VW, "Der ID.3 Ausstattungslinien," 2022. [Online]. Available: https://www.volkswagen.at/id3/infomaterial

[48] Electric Vehicle Database, "Tesla Model 3 Standard Range," 2020. [Online]. Available: https://ev-database.org/

[49] Bundesministerium für Klimaschutz, Umwelt, Energie, Mobilität, Innovation und Technologie, "Durchschnittliche Fahrleistung eines Pkw Österreich," 2019. [Online]. Available: https://www.bmk.gv.at/themen/mobilitaet/mobilitaetsmgmt/tourismus/sanfter-tourismus/verkehrsleistungen.html#:~:text=Die%20durchschnittliche%20Fahrleistung%20eines%20Pkw,Jahresfahrleistung%20und%20daher%20auch%20einen

[50] Mercedes Benz Bus, "E-Citaro Testbericht," 2021. [Online]. Available: https://www.mercedes-benz-bus.com/de_AT/models/ecitaro.html

[51] Volvo Trucks, "Volvo FL Electric Datenblatt," 2021. [Online]. Available: https://brochures.volvotrucks.com/de/volvo-trucks/alternative-antriebe/volvo-fl-electric-datenblatt/?page=1

[52] Wiener Linien GmbH Co KG, "Zahlen, Daten, Fakten 2018," 2018. [Online]. Available: https://www.wienerlinien.at/media/files/2019/betriebsangaben_2018_310521.pdf

[53] Bundesanstalt für Straßenwesen, Deutschland, "Fahrleistungserhebung 2014," 2014. [Online]. Available: https://www.bast.de/DE/Publikationen/DaFa/2018-2017/2017-04.html#:~:text=Pkw%20erbrachten%202014%20eine%20durchschnittliche,mit%20110.600%20Kilometern%20pro%20Jahr.

[54] H-TEC SYSTEMS GmbH, "H-tec pem electrolyzer hcs," 2022. [Online]. Available: https://www.h-tec.com/en/products/detail/h-tec-pem-elektrolyseur-hcs/4-mw-hcs/

[55] NPROXX, "500 bar: the 'sweet spot' for hydrogen storage," 2019. [Online]. Available: https://www.nproxx.com/500-bar-the-sweet-spot-for-hydrogen-storage/

[56] M. Gardiner, "Energy requirements for hydrogen gas compression and liquefaction as related to vehicle storage needs," 2009. [Online]. Available: https://www.hydrogen.energy.gov/pdfs/9013_energy_requirements_for_hydrogen_gas_compression.pdf

[57] B. Heid, C. Martens, and A. Orthofer, "How hydrogen combustion engines can contribute to zero emissions," 2021. [Online]. Available: https://www.mckinsey.com/industries/automotive-and-assembly/our-insights/how-hydrogen-combustion-engines-can-contribute-to-zero-emissions

[58] SOLARIS Bus Coach sp. z o.o., "Solaris Urbino 12 hydrogen technische Daten," 2020. [Online]. Available: https://www.solarisbus.com/public/assets/Biuro_prasowe/2021_10_Transexpo_Kielce/Technische_Daten_Urbino_12_hydrogen_Transexpo_DE.pdf

[59] Hyundai Motor Company, "Hydrogen and Hyundai. Progress for the future." 2022. [Online]. Available: https://trucknbus.hyundai.com/global/en/products/truck/xcient-fuel-cell

[60] Statistik Austria, "Bevölkerung am 1.1.2022 nach Ortschaften (Gebietsstand 1.1.2022)," 2022. [Online]. Available: https://www.statistik.at/en

[61] Statistik Austria, "Zahlen, Daten und Indikatoren der Wohnstatistik," 2022. [Online]. Available: https://www.statistik.at/fileadmin/publications/Wohnen-2021.pdf

[62] Energie- und Umweltagentur des Landes NÖ, "Solarenergie," 2022. [Online]. Available: https://www.enu.at/energie

[63] Statistik Austria, "Kraftfahrzeug Bestand 2021," 2021. [Online]. Available: https://www.statistik.at/statistiken/tourismus-und-verkehr/fahrzeuge/kfz-bestand

[64] Statistik Austria and Statista, "Anzahl der Lastkraftwagen in Österreich nach Bundesländern von 2011 bis 2021." 2022. [Online]. Available: https://de.statista.com/statistik/daten/studie/1098883/umfrage/lkw-bestand-der-klasse-n1-in-oesterreich-nach-bundeslaendern/

[65] Wien Energie, "Sprechen wir über Elektroautos." accessed in 2023. [Online]. Available: https://positionen.wienenergie.at/themen/mobilitaetswende/e-autos/

[66] L. Gear and S. Siddiqi, *Electric and Fuel Cell Trucks 2023-2043*. IDTechEx, 2022. [Online]. Available: https://www.idtechex.com/en/research-report/electric-and-fuel-cell-trucks-2023-2043/877

[67] Federal Ministry Republic of Austria, Climate Action, Environment, Energy, Mobility, Innovation and Technology, "Austria's 2030 mobility master plan," 2021. [Online]. Available: https://www.bmk.gv.at/en/topics/mobility/mobilitymasterplan2030.html

Appendix A

Decision Variables

p_t^{Grid}	Grid power supply	[MW]
$p_t^{Grid,rest}$	Feed-in power supply	[MW]
$p_t^{BAT,in}$	Battery charging power	[MW]
$p_t^{BAT,out}$	Battery discharging power	[MW]
soc_t^{BAT}	State of charge (SoC) battery reserve	[MWh]
$p_{\theta,t}^{EV,AC}$	AC Level 2 mobility load	[MW]
$p_{\theta,t}^{EV,DC}$	DC fast charging mobility load	[MW]
$soc_{\theta,t}^{EV}$	State of charge (SoC) battery electric vehicle bundle	[MWh]
$p_t^{electrolysis}$	Electrolyser load	[MW]
$soc_{S,t}^{H2}$	State of charge of the hydrogen storage tank	[MWh]
$soc_{\Phi,t}^{H2}$	State of charge of the fuel cell vehicle bundle	[MWh]
$h_{\Phi,t}^{H2,charge}$	Fuel cell mobility load	[MW]
T	Number of the timesteps	[15-mins]

Sets

t	Current timestep
Θ	Amount of battery electric vehicle bundles
Φ	Amount of fuel cell electric vehicle bundles
$powerdirection_t$	bool charge/discharge battery reserve
$\sigma_{\theta,t}^{EV,conn}$	Plug-in binary variable
$\rho_{\varphi,t}^{H2,conn}$	FCEV connected to refuelling binary variable

Parameter

C^{elec}	Electricity price	[EUR/MWh]
C^{grid}	Grid tariffs	[EUR/MWh]
$C^{DC,charging}$	DC charging tariffs	[EUR/MWh]
P_t^{RL}	Residential load	[MW]
$P_{Loadprofile}$	Residential load profile (H0)	[MW]
$N_{Residences}$	Number of residences	
P_t^{PV}	PV power supply	[MW]
$P_{Profile}^{PV}$	PV profile	[%]
P_{inst}^{PV}	PV installed peak capacity	[MWp]
$E^{BAT,standby\%}$	Battery stand-by losses	[%]
$\eta^{BAT,in}$	Charging efficiency of the battery reserve	[%]
$\eta^{BAT,out}$	Discharging efficiency of the battery reserve	[%]
$E^{EV,standby\%}$	EV stand-by losses	[%]
$\eta^{EV,in}$	Charging efficiency of the EVs	[%]
$E^{EV,consumption}$	EV travel consumption	[MWh]
$H_{\varphi,t}^{H2,consumption}$	FCEV travel consumption	[MWh]
SoC_{min}^{BAT}	Minimum battery reserve SoC allowed	[MWh]
SoC_{max}^{BAT}	Maximum battery reserve SoC allowed	[MWh]
P_{max}^{BAT}	Maximum battery supply power	[MW]
SoC_{min}^{EV}	Minimum EV SoC allowed	[MWh]
SoC_{max}^{EV}	Maximum EV SoC allowed	[MWh]
$P_{\theta,max}^{EV}$	Maximum charging power for each EV bundle	[MW]
$SoC_{min}^{H2,tank}$	Minimum SoC allowed in the H2 storage tank	[MWh]
$SoC_{max}^{H2,tank}$	Maximum SoC allowed in the H2 storage tank	[MWh]
$SoC_{min}^{H2,vehicle}$	Minimum FCEV SoC allowed	[MWh]
$SoC_{max}^{H2,vehicle}$	Maximum FCEV SoC allowed	[MWh]
P_S^{Max}	Nominal power of the electrolyser	[MW]
H_Φ^{Max}	Maximum H_2 refuelling amount per FCEV bundle	[MWh]